Physics with CDF in Run II

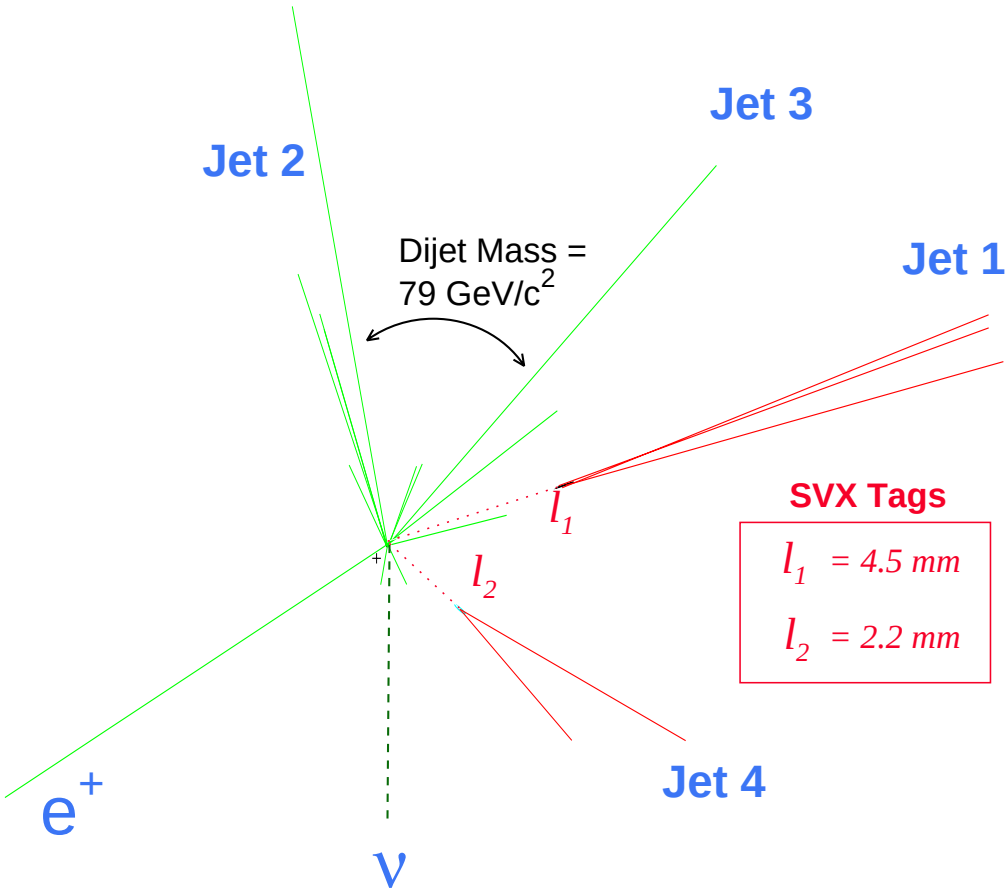

$M_{top}^{Fit} = 170 \pm 10$ GeV/c^2

$t\bar{t}$ Event
run #40758, event #44414

CDF Note 3172
Version 1.1
June 14, 1995

The CDF Collaboration

Contents

Figure 1: The number of interactions per crossing is shown as a function of instantaneous luminosity for different numbers of bunches.

1 Introduction

The recent publications of the discovery of the top quark[1, 2] and the precise measurement of the W mass[3], as well as approximately 90 other publications, have shown that the CDF detector and collaboration are extremely successful in production of fundamental physics results. In Run II the accelerator luminosity is expected to be an order of magnitude larger than the present values. For the next ten years Fermilab provides a unique opportunity to probe the fundamental parameters of the standard model, and beyond, with the highest energy collisions in the world. The CDF collaboration is planning to upgrade the current detector to take full advantage of the high luminosity available in Run II. This document describes the CDF physics program for the upgraded detector and 2 fb^{-1} of data.

In Run II, the accelerator is expected to operate at a center of mass energy of 2 TeV and initially with 36 bunches (396 ns bunch spacing) and instantaneous luminosity of 5-10x10^{31}. As the run progresses, the luminosity and bunch intensities will increase. A move to 99 bunches (132 ns bunch spacing) will keep the number of interactions per crossing at less than or equal to the current Run Ib level of ≈ 3 interactions per crossing. Figure 1 shows the number of interactions per crossing for different number of bunches as a function of instantaneous luminosity.

The CDF detector upgrades are described in detail in a separate document[4]. They include:

- A scintillating tile-fiber calorimeter in the region $1.1 < |\eta| < 3.5$. This detector will be

able to operate in the short bunch spacing (132 ns) and high radiation environment of Run II. It has better resolution and hermeticity than the current gas calorimeter system, and its compact design allows for better forward muon coverage.

- A new Silicon VerteX detector (SVX II) which is almost twice as long as the current SVX (96 cm instead of 51 cm), has 3D information and has 5 instead of 4 layers. The SVX II will use the SVX3 readout chip which allows deadtimeless triggering at Level 1.

- A fiber tracker which will fill the region between SVX II and the Central tracking chamber. The fiber tracker combined with SVX II will increase the tracking coverage out to $|\eta| = 2.0$, and will replace the functionality of the inner CTC layers at high luminosity.

- Improved muon coverage in the central region $|\eta| < 1.0$. The existing forward muon system will be moved closer to the central and will cover the region $1.5 < |\eta| < 3.2$.

- Upgraded Front-End electronics which are digital and pipelined for operation at a bunch spacing of 132 ns.

- New Level 1 and Level 2 trigger systems. Both will be buffered and pipelined. Tracking from the fibers and central tracker will be available at Level 1, and SVX II impact parameter information will be available at Level 2. The system is designed to handle 50 KHz input to Level 2 and 300 Hz input to Level 3. The CPU power of the Level 3 trigger will be increased in Run II to match the input rate from Level 2.

- Increased offline computing power.

CDF has also submitted a proposal for a time-of-flight system for Run II which would significantly enhance our b-physics capabilities.

One of the primary goals for Run II is the collection and study of large samples of top quark events. The detector upgrades increase the acceptance for top $\rightarrow$ lepton + tagged b by a factor of two over the Run Ib detector. With 2 fb^{-1} of data we expect to collect $\approx$1400 $t\bar{t}$ events with a high p_T lepton from the W decay and a b-tag. With such a sample we expect to reduce the uncertainty on the top mass to 4 GeV, and measure the cross section to 7%. Section 2 describes the current top analysis and the projections for Run II. The large sample of top events available in Run II will allow many new measurements of top quark properties. For example, a measurement of the branching ratio $\frac{Br(t \rightarrow Wb)}{Br(t \rightarrow Wq)}$ to 3% is described along with the searches for new phenomena in the $t\bar{t}$ system.

Another goal of the Run II physics program at CDF is the study of electroweak physics. Direct measurement of both the top and W mass in a single experiment are unique to the Tevatron and provide fundamental information about the standard model. With the Run II detector and a 2 fb^{-1} data sample we expect to measure the W mass to 40 MeV. This,

combined with the Run II measurement of the top mass, will provide constraints on the mass of the Higgs. Section 3 describes the current CDF measurements involving the gauge bosons and, based on this experience, makes projections for the Run II analyses. With sufficient luminosity, the CDF measurements of W mass, width, leptonic branching ratios and trilinear couplings in Run II will remain competitive with the LEP2 program.

The study of QCD at the Tevatron provides fundamental information about the standard model as well as a sensitive probe for new physics. The high statistics data samples available in Run II will extend the current QCD studies to a new high energy regime. A summary of the current QCD measurements at CDF is presented in Section 4 along with the projected improvements for Run II.

Tests of the standard model will also come from the B system. In Run II CDF expects to provide sensitive tests of the unitarity of the CKM matrix and the standard model origin of CP violation. CDF results on B hadron lifetimes, rare decays, B_s mass and B_c searches are already highly competitive with the LEP and CLEO results. With the Run Ib data CDF expects to also have competitive measurements of B_s and B_d mixing, the Λ_b mass and others. For Run II, the upgraded detectors and data aquisition system will allow for greatly expanded capabilities in B physics, for example CP violation ($\delta \sin 2\beta \approx 0.07$ and $\delta \sin 2\alpha \approx 0.10$) and B_s mixing ($x_s < 20$). A summary of the recent B physics results from CDF is presented in Section 5 along with the prospects for B-physics in Run II.

The status and prospects for the search for physics beyond the standard model is described in Section 6. To summarize, the limits and discovery potential for new phenomena simply increase with increasing integrated luminosity. Run II will provide an excellent opportunity to extend the current searches and embark on quests for new particles.

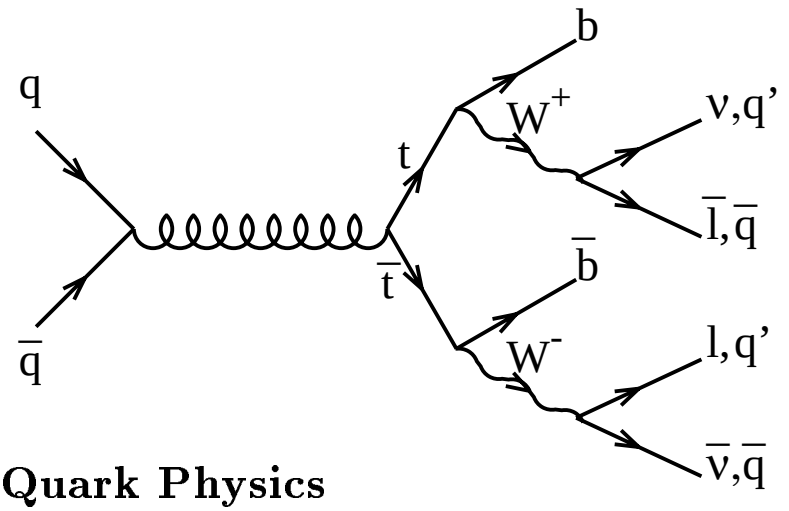

2 Top Quark Physics

For the next 10 years, the Tevatron is the only accelerator capable of producing the massive top quark. It is important to exploit fully this unique ability. Run I has brought the discovery and the first direct measure of the top quark mass and the $t\bar{t}$ production cross section[1, 2, 5]. It has also provided valuable first experience in top quark physics. For example, CDF demonstrated the importance of identifying b-quark jets in top events using a silicon-vertex detector. The ability to tag b jets provided a clear signal for the top quark discovery and important information when performing the mass reconstruction. In Run II, CDF's ability to tag b jets will be greatly enhanced with the SVX II detector system.

The primary measurement in Run II will be the precision measure of the top mass. The top mass, along with the W mass, provides important information about the electroweak symmetry breaking sector of the standard model. In addition, measurements of branching ratios, production properties, and the search for rare decays are important tests of the standard model, and may give hints to physics beyond the standard model. The Run II upgrades put CDF in an excellent position to exploit fully the large sample of $t\bar{t}$ events that will be produced by the Tevatron.

We begin by reviewing the top analysis results of Run I. Next, we discuss the impact of the upgraded components on the top analysis in Run II. The event yields are estimated in Section 2.3. The measurements that will be made with the large sample of $t\bar{t}$ events are discussed in Sections 2.4 to 2.6.

2.1 Review of Run I Analysis

The Run I top analysis has been very successful. CDF established the existence of the top quark and has begun to measure its basic production and decay properties. Using 19.3 pb^{-1} from Run Ia, CDF presented initial evidence for the top quark in the spring of 1994 [1]. A year later, with an additional 48 pb^{-1} from Run Ib, CDF confirmed its original evidence for the top quark[2].

When searching for the top quark, CDF focused on several decay channels. In the first channel, called the dilepton channel, the produced t quark and $\bar{t}$ quark both decay to a W boson and a b-quark with both W's decaying leptonically ($W \rightarrow \ell\nu$). Only leptonic W decays to an electron or a muon are considered. The nominal signature in this channel is two high P_T leptons, missing transverse energy (from the two ν's), and two jets from the b quarks. Acceptance for this channel is small, mostly due to the product branching ratio of both W's decaying leptonically (only about 5%). In the first 67 pb^{-1} from Run I, CDF observed 5 $e\mu$ events, 2 $\mu\mu$ events, and 0 ee events [6]. The background estimate for the dilepton channel is 1.3 ± 0.3 events[2]. Although not *a priori* part of the search, we test the jets in dilepton events for indications that they originated from b quarks. In the 7 dilepton events, we find 5 jets in 3 events (1 $\mu\mu$ and 2 $e\mu$) that are identified as b jets. This provides evidence for b-quarks produced in association with two W's, as expected from the decay of a $t\bar{t}$ pair.

The second decay channel is called the lepton-plus-jets channel. In this channel, one of the W's decays leptonically and the other hadronically to a pair of quarks. The nominal signature is a lepton, missing transverse energy (the neutrino from the leptonic W decay), and 4 jets from the two b quarks and two W-decay quarks. Approximately 30% of the $t\bar{t}$ events have this decay signature. To remain efficient for $t\bar{t}$ events, we require only 3 central ($|\eta| < 2.0$) jets.

In this channel, the background from W-plus-multijet production is large. However, the jets in these background events typically are gluon and light quark jets, unlike $t\bar{t}$ events which contain two b-quark jets. Therefore, in order to reduce the background, CDF utilizes b-quark tagging of jets using two techniques. The first locates a displaced vertex with the silicon-vertex detector (SVX Tag). The second locates a low P_T electron or muon primarily from the semileptonic decay of a b quark or sequential c quark (SLT Tag). The efficiency for tagging a $t\bar{t}$ event is $(42 \pm 5)\%$ and $(20 \pm 3)\%$ for the SVX and SLT algorithms, respectively. In 67 pb^{-1}, 27 SVX tags are observed in 21 events. The background is measured from a combination of data and Monte Carlo simulation to be 6.7 ± 2.1 tags. Using the SLT tagging algorithm, 23 tags are found in 22 events. The background is predicted to be 15.4 ± 2.8. The two samples have 6 events in common[2]. Figure 2 shows the jet multiplicity spectrum for the SVX b tags and the background. In the 1 and 2 jet bins, where we expect little contribution from $t\bar{t}$ events, the background and observed tags are in good agreement. In the 3 and $\geq$4 jet bins, a clear excess of tags is observed. The inset shows the proper time distribution for the b-tagged jets in the signal region ($\geq$ 3 jets). The histogram shows the expected distribution of b's from $t\bar{t}$ Monte Carlo simulation.

In addition to the search techniques based on the dilepton final state and b-quark tagging, CDF has isolated $t\bar{t}$ events based on the kinematical properties predicted from Monte Carlo simulations. These methods use the lepton-plus-jets events sample but do not rely on b-tagging to reduce the background. One technique examines the jet E_T spectra of the second and third highest E_T jets [7]. The second technique uses the total transverse energy of the event [8]. In both cases, there is a clear $t\bar{t}$ component in our data. Finally, we are

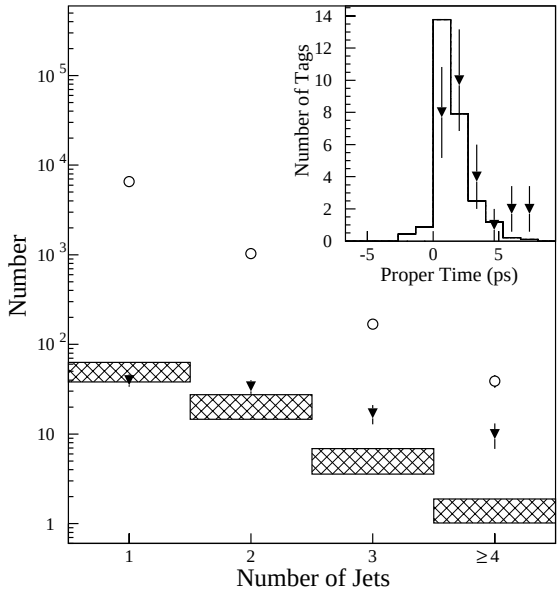

Figure 2: The jet multiplicity distribution for SVX b tags. The open circles represent the number of events before b-tagging. The dark triangles represent the observed number of b tags in each bin and the hatched areas represent the background prediction and its uncertainty. The inset shows the proper time distribution for the b tags in the W+$\geq$3 jet bins.

currently searching in the all hadronic decay channel for $t\bar{t}$ events. Achieving a reasonable signal-to-background is the challenge. Our current techniques give about a 1:1 S:N ratio.

The top mass measurement is based on reconstructing the $t\bar{t}$ system with lepton-plus-jets events. The events must contain a lepton and at least 4 jets such that each final state parton can be assigned to an observed jet or lepton. The reconstruction is performed using a constrained fitting technique which selects the best assignment of observed jets to final state partons based on a χ^2. Without any b-tagging information there are 24 combination which must be considered (12 parton assignments $\times$ 2 possible P_z^{ν}). When one or two jets are tagged as b quarks, the number of combinations is reduced to 12 and 4, respectively. The events containing a b-tagged jet provide the most precise mass measurement. Figure 3 shows the reconstructed mass distribution for 19 events with at least one b-tag. The background estimate for this sample is $6.9^{+2.5}_{-1.9}$ events. Using a maximum likelihood technique, we determine a top quark mass of $176 \pm 8\ (stat) \pm 10\ (sys)$[2]. The systematic uncertainty is dominated by the uncertainty in initial and final state gluon radiation and the detector energy scale.

In addition to measuring the top quark mass, CDF is measuring the production properties of the $t\bar{t}$ system. Figure 4 shows the measured $t\bar{t}$ production cross section compared with the theoretical prediction. The cross section is determined from the dilepton, SVX b-tagging, and SLT b-tagging counting experiments. With 67 pb^{-1} of data, we measure a cross section of $7.6^{+2.4}_{-2.0}$ pb[9]. The theoretical cross section at 176 GeV/c^2 is 4.8 pb [10].

We have also started to measure top decay branching ratios. One measurement,

$$R_1 = \frac{Br(t \to Wb)}{Br(t \to Wq)}$$

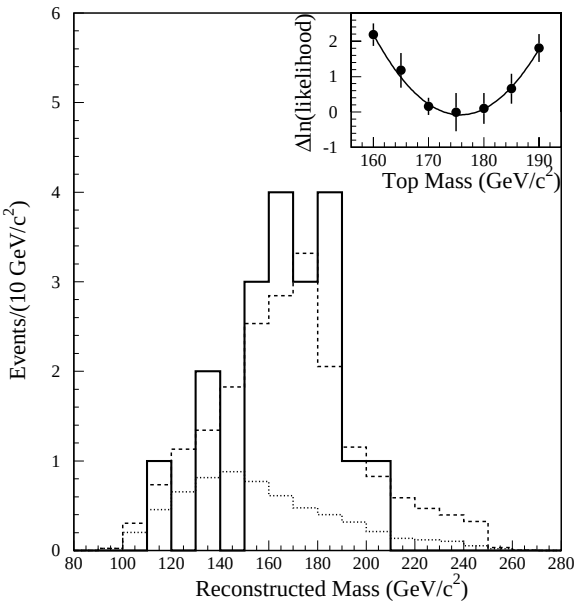

Figure 3: Mass spectrum for b-tagged events in 67 pb^{-1} of data. The dotted curve is the expectation from background. The dashed curve is from background plus top production. The likelihood fit is shown as an inset.

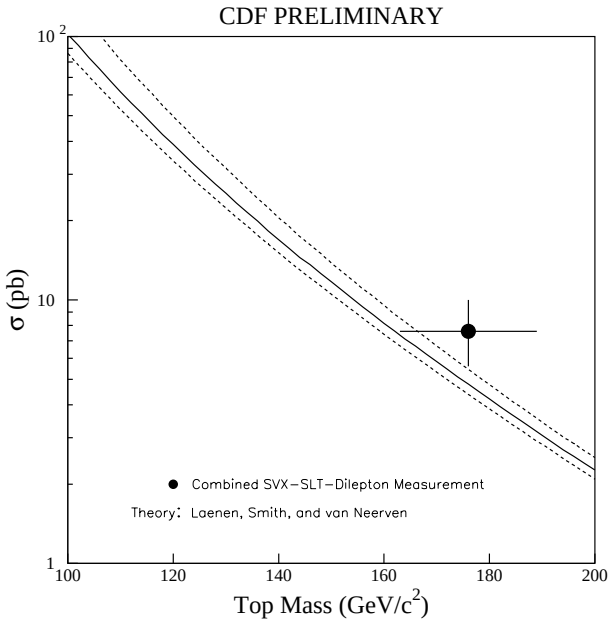

Figure 4: The measured cross section for $t\bar{t}$ production compared with a theoretical prediction. The point is plotted at our best measure of the top quark mass and the horizontal error bar represents the current uncertainty on M_{top}.

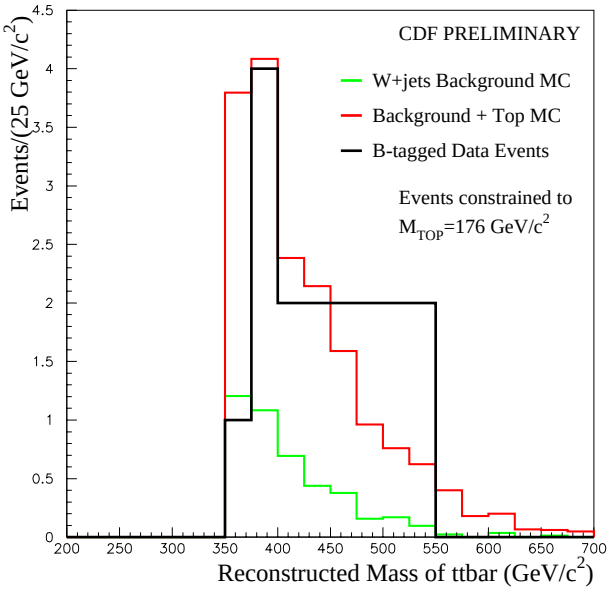

Figure 5: The $M_{t\bar{t}}$ distribution with 67 pb^{-1} of data. When calculating $M_{t\bar{t}}$, a top mass constraint ($M_{top} = 176$ GeV/c^2) is imposed. This improves the resolution for resonances by a factor of two and as a consequence produces a sharp cutoff at $M_{t\bar{t}} = 2M_{top} \simeq 350$ GeV/c^2.

is made using the number of single and double tagged lepton-plus-jets and dilepton events. The measurement of R_1 can be turned into a measure or limit on the CKM matrix element, V_{tb}. The preliminary value is found to be $R_1 = 0.87^{+0.13+0.13}_{-0.30-0.11}$[11], giving $|V_{tb}| > 0.016$ at the 95% CL. Finally, studies currently in progress include:

- Measurement of the $t\bar{t}$ invariant mass, $M_{t\bar{t}}$ (see Figure 5.)
- Measure of P_T^{top}, $P_T^{t\bar{t}}$
- $R_2 = \mathrm{Br}(t\bar{t} \to \ell\ell + X)/\mathrm{Br}(t\bar{t} \to \ell + X)$
- $\mathrm{Br}(t \to W_0 b)$ (Longitudinally Polarized W's)
- Angular distributions such as η_t, $\cos(\theta_t^*)$

Run I data collection is continuing. We expect by the end of July 1995 to approximately double the size of the dataset used for the top analysis results presented here. Therefore, we expect the statistical errors on our measurements to decrease by $1/\sqrt{2}$ (30%). Work is continuing on reducing the systematic uncertainties on all measurements. With the Run I dataset, we are beginning to use the $t\bar{t}$ system as a laboratory to understand the standard model. The experience gained with this dataset will help create better analysis techniques for Run II and allows us to predict our future performance.

2.2 Impact of Proposed Upgrades on Top Analysis

The CDF upgrades increase the acceptance for top events. The improvement occurs in two major areas; i) added acceptance for identifying the primary lepton from the W boson, and ii) added efficiency for identifying b-quark jets. Subsequently, each of these impacts on CDF's ability to make top quark measurements, such as the top mass.

Although all components of the upgrade [4] affect our ability to perform top physics, here we summarize only the major components and qualitatively how each impacts the analysis:

- **Silicon Vertex Detector (SVX II)**: The 5 layer double-sided device will greatly improve the acceptance for tagging b quarks from top quark decay. The double-sided silicon in all 5 layers will provide a 3 dimensional reconstruction which will improve the track-finding efficiency and reduce 'fake' tracks. This will be important in the high luminosity environment of Run II.

- **Intermediate Fiber Tracker (IFT)**: Because of the stand alone tracking capability of the IFT-SVX combination, b tagging of top events will be possible out to $|\eta| = 2$.

- **Plug Calorimeter Upgrade**: The new scintillating tile-fiber calorimeter with its shower max detector will provide improved jet resolution and electron identification in the forward region. The improved electron identification will add to the acceptance for both the identification of the primary electron from W decay and the low-P_T electron from semileptonic b-quark decay.

- **Muon Detection System**: The more complete ϕ and η coverage will assist in the identification of primary muons from W decay and low-P_T muons from semileptonic b-quark decay.

2.3 Event Yield

To estimate the yield of top events, we extrapolate from our current measured acceptances and we assume the theoretical cross section (6.8 pb) at $M_{top} = 175$ GeV/c^2 and $\sqrt{s} =$ 2 TeV[12]. At $\sqrt{s}$ =2 TeV, the $t\bar{t}$ cross section is approximately 40% higher than at $\sqrt{s}$=1.8 TeV. In addition, the measured value of the cross section is larger than the theoretical prediction and therefore the actual Run II yields could be greater than predicted here. Table 1 summarizes the acceptance for various decay channels assuming the Run II configuration. The Run Ib acceptances are shown for comparison. The added acceptance is estimated based on the increased geometrical acceptance and assumes we can achieve similar signal-to-background to that achieved in the current datasets. The increase in acceptance for the primary lepton ($W \rightarrow \ell\nu$) identification is estimated to be 36% for electrons and 25% for muons[13].

The increased b-tagging efficiency is substantial. The length of the SVX II detector provides coverage over most of the interaction region. We estimate that 97% of the b-quark

Channel	Acceptance, A_{IB} (Run Ib)	Acceptance,A_{II} (Run II)	# of Events (w/ A_{Ib})	# of Events (w/ A_{II})
Produced $t\bar{t}$	-	-	13600	13600
Dileptons (ee,$\mu\mu$,$e\mu$)	0.85%	1.1%	115	140
lepton+$\geq$3j	9.5%	12%	1300	1700
lepton+$\geq$3j w/ $\geq$1 b tag	5.1%	10.5%	690	1400
lepton+$\geq$4j	8.2%	11%	1100	1500
lepton+$\geq$4j w/ $\geq$1 b tag	4.3%	9.1%	600	1200
lepton+$\geq$4j w/ 2 b tags	1.1%	4.5%	150	610
W+$\geq$1j	0.45%	0.60%	200K	270K
W+$\geq$4j	1.2×10^{-3}%	1.5×10^{-3}%	500	700
Z+$\geq$1j	0.45%	0.60%	20K	27K
Z+$\geq$4j	1.2×10^{-3}%	1.5×10^{-3}%	50	70

Table 1:
Acceptance and yield of $t\bar{t}$ events for a Run II upgraded detector. The yield is determined using the theoretical cross section (6.8 pb) at M_{top} = 175 GeV/c^2 and $\sqrt{s}$ = 2 TeV. In addition the number of expected W/Z-plus-jet events is also shown. For comparison, the acceptances for Run Ib are shown along with the expected yield with 2 fb^{-1}. The acceptances include branching ratios and leptonic and kinematic selection (*e.g.* jet counting). The efficiency for identifying a high P_T electron (muon) from W/Z decay is approximately 80% (90%).

decay products will be found in the fiducial region of the SVX II detector. The tagging efficiency for a fiducial b-jet will be approximately 60%[13]. For top events passing our kinematical selection, the probability of tagging at least one (both) b jets will be 80% (36%). The "double" tagging rate is substantially increased over Run I. In addition, CDF will still have the capability for tagging b-jets using soft leptons. If we include the efficiency of the current soft lepton tagging algorithm, the overall single (double) tagging efficiency will rise to 85% and 42%[13].

2.4 Top Quark Mass Measurement

The top quark mass measurement will be one of the most important electroweak measurements made at the Tevatron. Currently, the statistical and systematic uncertainty on CDF's top mass measurement are about equal. Therefore, in Run II we can assume that the dominant uncertainty will be systematic. We first estimate the behavior of the statistical

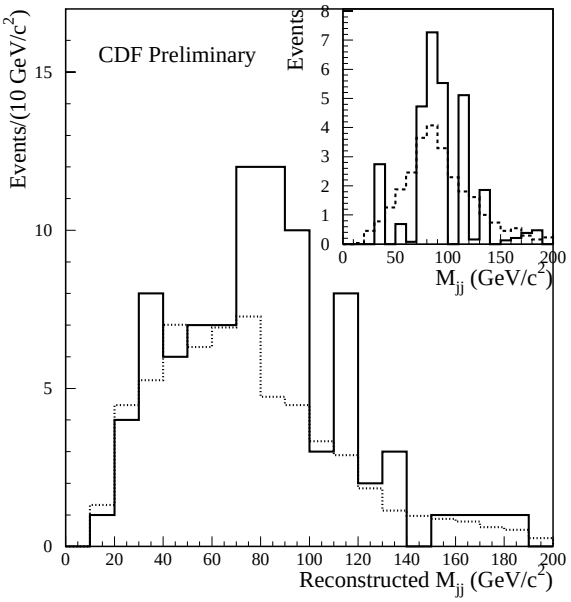

Figure 6: The M_{jj}^W distribution is shown for data (solid) and expected background (dotted). The value of M_{jj}^W is determined from the constrained mass fitting procedure *without* imposing the $M_{W\to jj} = 80.3$ GeV/c^2 constraint. The data uses 67 pb^{-1} of W+4 jets events without requiring any b tagging. The inset shows data-background compared to the prediction from a $t\bar{t}$ monte carlo (dashed). An enhancement is observed near 80 GeV/c^2.

uncertainty since it should scale as $1/\sqrt{N}$. Performing this scaling, we estimate the statistical uncertainty to be ≈ 1 GeV/c^2. This estimate uses the lepton plus four jet events with at least one b-tagged jet (see Table 1).

With the upgraded SVX II detector, the acceptance for double tagged lepton plus four jet events increases dramatically, about a factor of 4. In these double tagged events, the number of combinations for the constrained mass fitter is only 4 instead of 12. Monte Carlo studies show that the mass resolution for single tagged events is 22 GeV/c^2 and double tagged events is 18 GeV/c^2. Using only double tagged events, CDF still can achieve a statistical uncertainty of ≈ 1 GeV/c^2. Because both the b quarks are identified in the double tagged sample, the systematics ultimately may be better understood for this class of events.

The scaling of the systematic uncertainties to a 2 fb^{-1} data sample is not as straightforward. However, many systematic uncertainties do depend on samples whose statistics will scale with luminosity. For example, Z-plus-jet events are used to understand the systematic uncertainty with energy scale and gluon radiation, two of the dominant uncertainties. In 2 fb^{-1}, we expect to have 27K (70) Z's with 1 (4) or more jets. The effect of gluon radiation will also be studied in large statistical samples of W-plus-jets, γ-plus-jets, and $b\bar{b}$ events. In addition, the top sample itself, by measuring a mass peak from $W \to qq'$ (see Figure 6), can be used to understand the effects of energy scale. Scaling the systematic errors as $1/\sqrt{\mathcal{L}}$ would reduce our systematic error to ≈ 2 GeV/c^2. This is probably a lower limit. We use 4 GeV/c^2 as our goal for the total uncertainty on the top quark mass.

The top mass combined with the W mass gives information about a standard model Higgs boson mass. The W mass measurement is discussed in Section 3. Figure 9 shows how the predicted top and W mass measurements limit the Higgs mass.

2.5 Production and Decay Properties

The large Run II data sample will allow us to determine many of the fundamental production and decay properties of the top quark. The measurements include:

- Production Cross Section, $\sigma_{t\bar{t}}$
- Branching Ratios:
  - $R_1 = \mathrm{Br}(t \to Wb)/\mathrm{Br}(t \to Wq)$
  - $R_2 = \mathrm{Br}(t\bar{t} \to \ell\ell + X)/\mathrm{Br}(t\bar{t} \to \ell + X)$
  - $\mathrm{Br}(t \to W_0 b)$ (W_0 is a longitudinally polarized W.)
- Angular distributions (*e.g.* η_t, $\cos(\theta_t^*)$)
- Γ_t, Single Top Production
- Measure of $|V_{tb}|$
- A_{FB} of the t quark.
- Search for anomalously large rare decays:
  - $t \to Zc, \gamma c$
  - $t \to WZb$
  - $t \to W^+W^-c$

These measurements are the first steps in an emerging program to understand the features and implications of the top quark. The production cross section is a test of the QCD Lagrangian at large Q^2 [14]. Branching ratios are important probes of the couplings at the top quark decay vertex. Decay channels other than $t \to Wb$, such as $t \to H^+b$, will alter R_1 and R_2 from their expected standard model values. Deviations of the branching ratio of the top quark to a longitudinally polarized W, $\mathrm{Br}(t \to W_0 b)$, from the expected standard model value could indicate new non-universal weak-interaction couplings, such as a V+A coupling, at the top decay vertex[15, 16]. The cross section for single top production is proportional to $\Gamma(t \to Wb)$ and can be used to extract a measurement of the CKM matrix element $|V_{tb}|$ [17, 18]. Separating the single top production from $t\bar{t}$ production remains the challenging aspect of this analysis. In addition, we can search for rare decays. With 2 fb^{-1} of data, these searches will likely produce only limits on these decay channels. Table 2 summarizes the current and predicted precision of certain top quark physics measurements.

Measurement	Current Run Ib (67 pb^{-1})	Precision Run II
δM_{top}	13 GeV/c^2	4 GeV/c^2
$\delta\sigma_{t\bar{t}}/\sigma_{t\bar{t}}$	30%	7%
$\delta R_1/R_1$	25%	3%
$\delta R_2/R_2$	50%	10%
$\delta Br(t \to W_0 b)/\mathrm{Br}(t \to W_0 b)$	-	3%

Table 2: The current and Run II estimated precision on various top physics measurements.

2.6 Probing the Electroweak Symmetry Breaking Sector

Because of its large mass, the top quark is an excellent probe for physics beyond the standard model. New phenomena involved in symmetry breaking are expected to show up as enhancements or changes in the shape of the $t\bar{t}$ invariant mass, $M_{t\bar{t}}$, spectrum, P_T^{top}, or center-of-mass angle of the top quark[19, 20]. A color-octet vector meson associated with a top condensate[21] and multiscale technicolor[22] are two examples of processes which can enhance $t\bar{t}$ production. CDF is currently searching for resonances, $X \to t\bar{t}$, in the $M_{t\bar{t}}$ spectrum (see Figure 5). By the end of Run I, we should have sensitivity to new objects with masses as large as 500-600 GeV/c^2. In the absence of a signal, limits in Run II will be as high as 1000 GeV/c^2. New resonances with masses below the limit could be observed. For example, Figure 7 shows the $M_{t\bar{t}}$ spectrum for 2 fb^{-1} with standard model $t\bar{t}$ production plus the addition of a topcolor Z$'$ at 800 GeV/c^2 [19]. The Z$'$ is decaying to a $t\bar{t}$ pair. In this theory, the branching fraction of Z$'$ to $t\bar{t}$ pairs is potentially large (50-80%) but depends on the Z$'$ width. In the case shown in Figure 7, we would expect 17 events from standard model $t\bar{t}$ production in the range $700 < M_{t\bar{t}} < 900$ GeV/c^2 and 70 events from Z$' \to t\bar{t}$ in this range. The $M_{t\bar{t}}$ spectrum along with other $t\bar{t}$ production distributions provide an excellent means for searching for new phenomena.

2.7 Summary of Top Physics

During Run II, the Tevatron will be the only accelerator capable of studying the top quark. An upgraded CDF detector will be well-suited for the study of top physics. The increased coverage of the SVX II detector and muon systems will allow us to tag at least 1 b-quark in 85% of $t\bar{t}$ events and both b-quarks in 42% of the events. With 2 fb^{-1} of integrated luminosity, we expect 1400 single tagged $t\bar{t}$ events. From this event sample we expect to measure the top mass, one of the fundamental electroweak parameters, to approximately 4 GeV/c^2. Measurements of branching ratios, angular distributions, and the $t\bar{t}$ production cross section will be performed. In addition, searches for rare decays of the top quark along

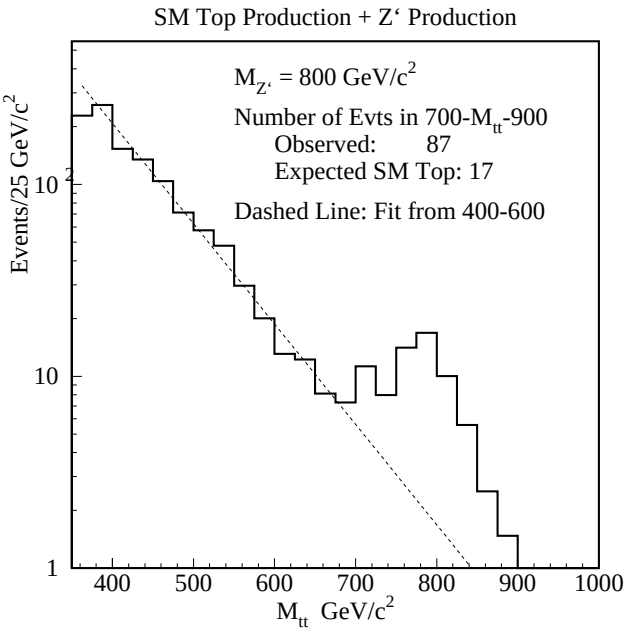

Figure 7: A hypothetical $M_{t\bar{t}}$ spectrum with an 800 GeV/c^2 Z′ topcolor boson. The rate is based on the theoretical predicted cross section for $t\bar{t}$ production and Z′ production [19] with 2 fb^{-1}.

with searches for exotic physics with the $t\bar{t}$ system will be carried out. Run II promises to be an exciting time for top physics, a newly opened area of study.

3 Electroweak Physics

3.1 Introduction

The comparison of diverse precision experimental measurements to expectations from the standard model [23] allows precise tests sensitive to new physics at scales above the electroweak scale, as well as a determination of the Higgs mass within the framework of the model. Of these measurements, that of the top mass [2] is unique to the Tevatron, and will be a significant input into global electroweak fits that have been largely dominated by LEP data, with some contribution from neutrino neutral current data, the SLAC polarization measurement, and W mass measurements in $\bar{p}p$ interactions. Measurements of the W mass, width, and leptonic branching ratio, and of the W, Z and γ trilinear couplings are currently unique to the Tevatron. With sufficient Tevatron luminosity these measurements will provide sensitive tests of new physics, and can remain competitive with the LEP2 program. A good summary, including projections into the future, has been compiled by the DPF Electroweak Working Group [24].

In this section we restrict ourselves to measurements directly involving the gauge bosons. Top quark issues are discussed in Section 2. Searches for new gauge bosons are discussed in Section 6

3.2 W Mass

The mass of the W boson is a fundamental parameter of the theory. Fits to the e^+e^- data predict the W mass to ± 60 MeV/c^2 [25]. In the coming years the direct measurement should surpass that accuracy. The 4 pb^{-1} of the 1988-89 Tevatron Collider run enabled CDF to measure the W mass to be

$$M_W = 79.91 \pm 0.39 \text{ GeV/c}^2 \text{ [26]},$$

and with 19 pb^{-1} from Run Ia CDF measured

$$M_W = 80.41 \pm 0.18 \text{ GeV/c}^2 \text{ [3]}.$$

This new measurement dominates the world average. The uncertainties in the current measurement scale rather well in detail from the previous measurement; while the difficulty of the measurement has increased, no systematic limitation is yet evident. The statistical improvement using $\sim$67 pb^{-1} of data from Run Ib is illustrated in Figure 8.

The uncertainties for the Run Ia measurement are shown in Table 3. Figure 9 (a) shows the sensitivity in the M_W-$M_{\rm top}$ plane of this result when combined with the value $M_{\rm top} = 176 \pm 13$ GeV/c^2 [2], compared to theoretical predictions based on electroweak radiative corrections [27]. We extrapolate the measurement to 2 fb^{-1} by considering the scaling of each item leading to an uncertainty estimate shown in Table 4. The biggest uncertainty

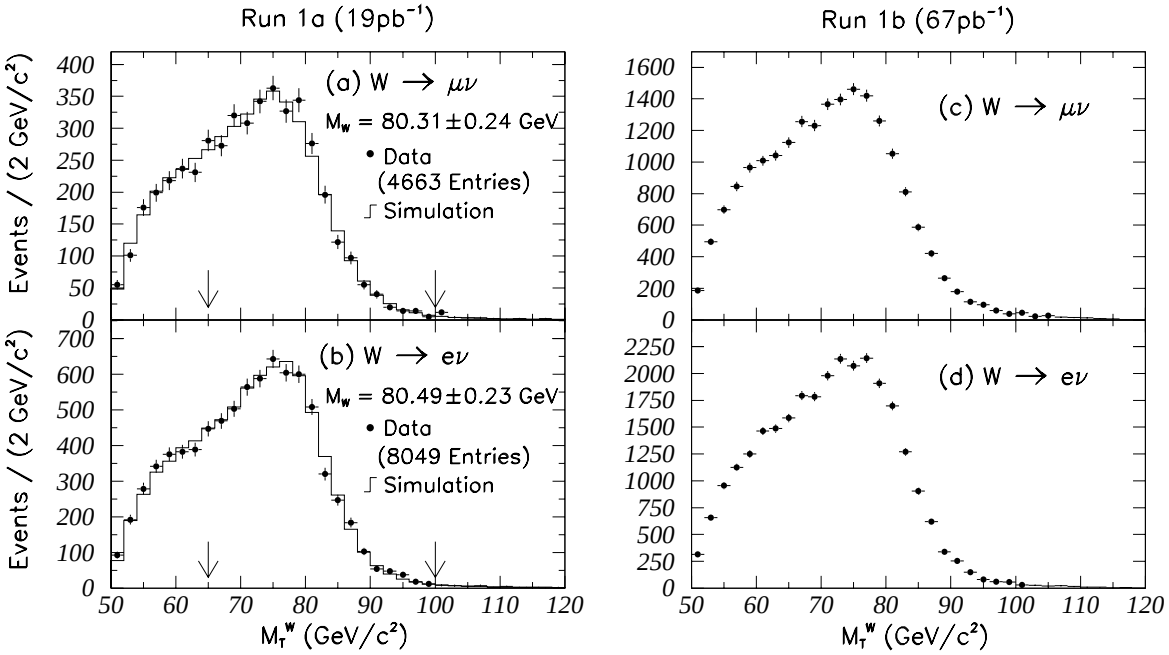

Figure 8: Transverse mass distributions for $W \to e\nu$ and $W \to \mu\nu$ from Run Ia (a and b) which gave a ± 180 MeV/c^2 measurement of the W mass, and the equivalent preliminary distributions from the first 67 pb^{-1} of Run Ib (c and d).

Source of Uncertainty	Uncertainty (MeV/c^2)		
	$W \to e\nu$	$W \to \mu\nu$	Common
Statistical	145	205	–
Lepton Energy/Momentum Scale	120	50	50
Lepton Energy/Momentum Resolution	80	60	–
Recoil modeling	60	60	60
Trigger, Event Selection	25	25	–
Backgrounds	10	25	–
Theoretical Model	75	75	65
Fitting	10	10	–
Total Uncertainty	230	240	100
e and μ Combined Uncertainty		180	

Table 3: Summary of uncertainties in the Run Ia W mass measurement.

Source of Uncertainty	Uncertainty (MeV/c^2)		
	$W \to e\nu$	$W \to \mu\nu$	Common
Statistical	14	20	–
Lepton Energy/Momentum Scale	20	15	15
Lepton Energy/Momentum Resolution	8	6	–
Recoil modeling	6	6	6
Trigger, Event Selection	10	10	–
Backgrounds	5	10	–
Theoretical Model	30	30	30
Fitting	5	5	–
Total Uncertainty	42	40	34
e and μ Combined Uncertainty		38	

Table 4: Estimate of uncertainties in the W mass measurement for 2 fb^{-1}.

comes from the theoretical model, dominated by the parton distribution functions (PDF). PDF related systematics will be discussed below. We have not included several important beneficial effects of the upgrades in making this estimate. Within the region $|\eta| < 1.1$ the muon acceptance will be 40% greater than was used in the Run Ia analysis. With the improvement in tracking in the intermediate η region by the addition of the fiber tracker and the extended SVX II acceptance, and with the improved muon toroid acceptance which will begin at $|\eta| > 1.5$, the background from $Z \to \mu\mu$ with one muon lost will be largely eliminated. In addition, the acceptance for $Z \to \mu\mu$ should be sufficiently broad that this sample can contribute at the same level as the $Z \to ee$ sample in the study of systematics, doubling the number of Z events in this critical control sample.

For high luminosity running (Run Ib) we currently average about 2 extra minimum bias events overlying W and Z events at $L \sim 1.8 \times 10^{31}\ cm^{-2}\ sec^{-1}$. We expect about a 10% loss in statistical precision due to the degraded resolution in the recoil measurement in Run Ib as opposed to Run Ia. In Run II the increased number of bunches reduces the number of extra minimum bias events back to the Run Ia level, giving us a situation which is better than at present.

For central tracks with $|\eta| < 1$ in Run Ib data the stand-alone central tracker (CTC) resolution degrades with luminosity, but using SVX points, or the SVX beam spot constraint, tracking resolution holds up reasonably well. For the upgrade, SVX II points will essentially always be available (SVX II is longer). The fiber tracker should also help retain good central track resolution as the inner CTC superlayers lose effectiveness. This works as long as the central tracker is viable ($L < 1 - 2 \times 10^{32} cm^{-2} sec^{-1}$). If we compare early Run Ib

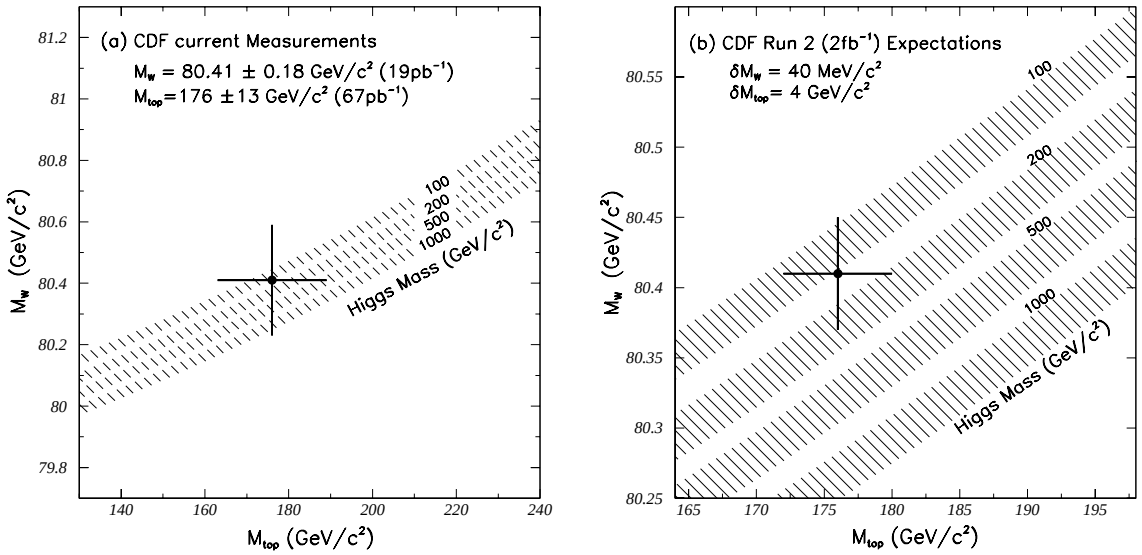

Figure 9: The data point in the left figure represents the CDF measurements of M_W and $M_{\rm top}$, and the point in the right figure represents the CDF estimate for 2 fb^{-1}. The curves are from a calculation [27] of the dependence of M_W on $M_{\rm top}$ in the minimal standard model using several Higgs masses. The bands are the uncertainties obtained by folding in quadrature uncertainties on $\alpha(M_Z^2)$, M_Z, and $\alpha_s(M_Z^2)$.

($L \sim 0.2 \times 10^{31}$) to later Run Ib ($L \sim 1 \times 10^{31}$), the CTC resolution observed in the width of the J/ψ peak worsens by 35% but using the SVX points in addition to the CTC points the resolution worsens by only 5%.

Knowledge of material in the tracking volume is of importance in determining the momentum and energy scale. The associated systematics are the uncertainties in the muon energy loss (dE/dx) for the momentum scale and in the radiative shift of the electron E/p for the energy scale. Although the amount of material in the tracking volume will be increased in the Run II upgrade, we have recently shown that photon conversions allow us to measure the amount of material quite accurately, as illustrated in Figure 10 and can reduce the uncertainties on the W mass measurement.

We make a conservative estimate that 2 fb^{-1} will allow CDF to measure the W mass to ± 40 MeV/c^2, which is comparable to the overall LEP2 expectation. Figure 9 (b) shows the sensitivity in the M_W-$M_{\rm top}$ plane of this estimate when combined with the estimate of $\delta M_{\rm top}$ for 2 fb^{-1} of data.

3.3 W Leptonic Branching Ratio, Width and Associated Measurements

The leptonic branching ratio of the W may be inferred from the ratio $R = \sigma \cdot Br(W \to l\nu)/\sigma \cdot Br(Z \to ll)$, using LEP measurements for the Z couplings and a theoretical prediction

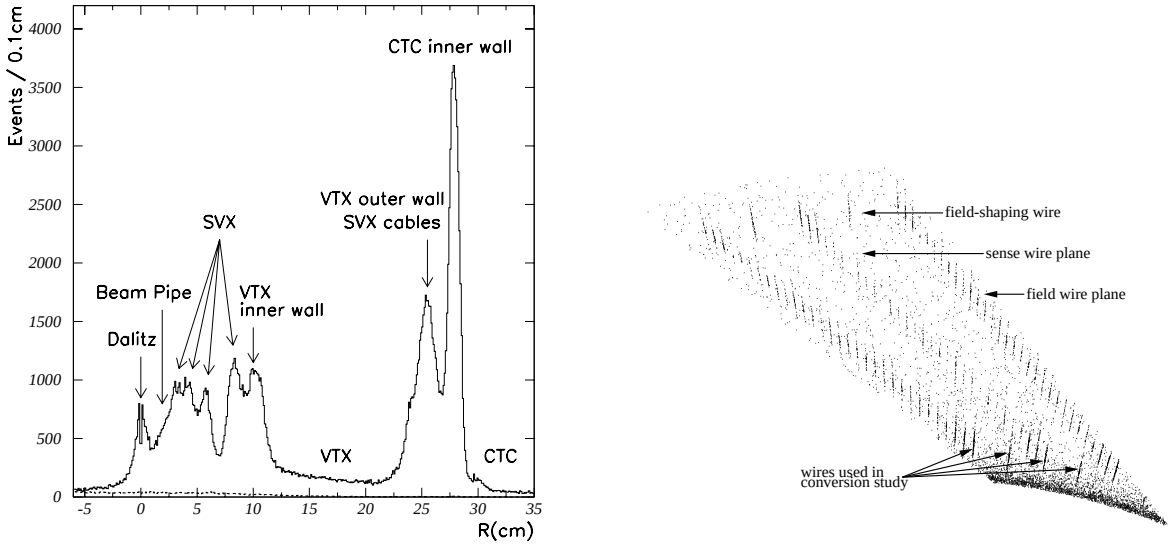

Figure 10: Left: The radial distributions for conversions (solid line) and background (dashed line). Right: Reconstructed photon conversion vertex density in the r-ϕ plane for the innermost super-layer in the CTC, folded into 1/30 of the circumference (this layer has 30-fold symmetry).

of the production cross section ratio. Before the top quark was discovered, this measurement was used to exclude hidden top scenarios. Now it is a standard model consistency check. For Run Ia [28] CDF measured $Br(W \to e\nu) = 0.109 \pm 0.005$, dominating the world average [29]. If one further assumes standard couplings for $W \to e\nu$, one can derive a value for the total width of the W, $\Gamma_W = 2.064 \pm 0.085$ GeV. The theoretical uncertainty in the cross section ratio is expected to limit precision to about $\pm 1\%$. However, the upgraded momentum measurement in the region $1 < |\eta| < 2$ should give improved acceptance systematics, lessening the dependence on the parton distribution functions.

The measurements of $\sigma \cdot Br$ themselves are not likely to improve much beyond Run Ib. For Run Ia, CDF measured $\sigma \cdot Br(W \to e\nu) = 2.51 \pm 0.12$ nb and $\sigma \cdot Br(Z \to ee) = 0.231 \pm 0.012$ nb [30]. These measurements are approaching the $\pm 3.6\%$ level of the luminosity normalization [31].

The W width can be measured directly from the shape of the transverse mass distribution (see Figure 11). For $M_T^W > 110$ GeV/c^2 resolution effects are under control and using Run Ia in the mode $W \to e\nu$, CDF measured $\Gamma_W = 2.11 \pm 0.32$ GeV [32]. The uncertainties should scale with statistics allowing a ± 30 MeV measurement for 2 fb^{-1}, much better than the LEP2 expectation of ± 200 MeV. Figure 11 summarizes indirect and direct measurements of Γ_W so far and the predicted uncertainty for 2 fb^{-1} from the direct measurement.

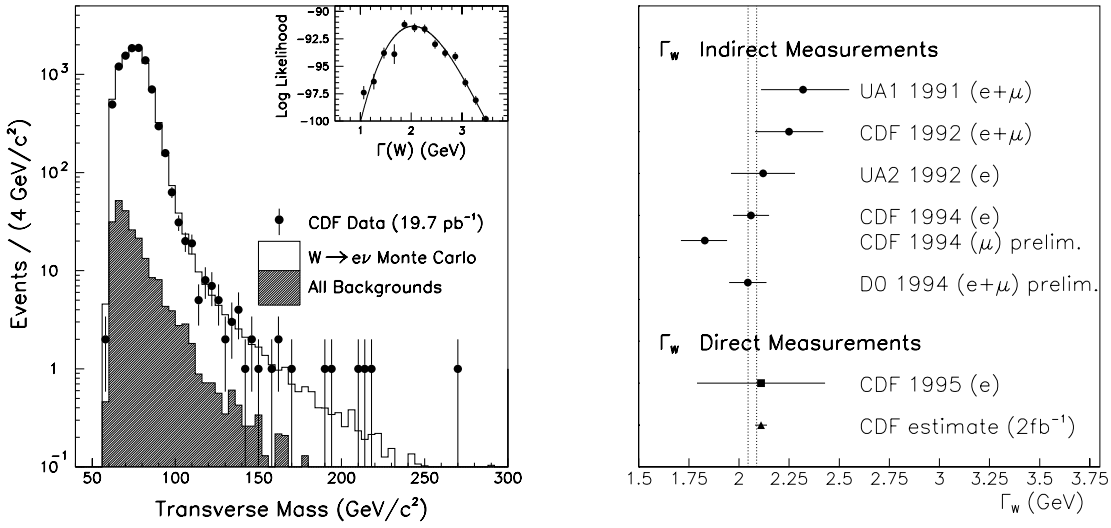

Figure 11: Left: Transverse mass distribution (M_T^W) for $W \to e\nu$ candidates along with background and signal expectation. The inset is the fit to $M_T^W > 110$ GeV/c^2. Right: Indirect and direct measurements of Γ_W and the predicted uncertainty from the direct measurement for 2 fb^{-1} of data. The dotted band represents the standard model prediction.

3.4 Gauge Boson Couplings

The standard model makes specific predictions for the trilinear couplings of the gauge bosons, W, Z, and γ. These can be studied by looking for photons produced in association with a W [33] or a Z [34] ($W\gamma$ and $Z\gamma$ production), or WW and WZ production. The major goals of the studies will be testing the standard model and searching for new physics.

From the E_T^γ distribution in $W\gamma$ and $Z\gamma$ production, limits are set on possible non-standard (anomalous) couplings, such as $-2.3 < \Delta\kappa_\gamma < 2.2$ [33]. We are attempting to include the plug region $1.1 < |\eta| < 2$ in our analysis. This should yield $\sim 30\%$ better limits. This will be much more straightforward after the calorimeter and tracking upgrade.

Stricter coupling limits come from the absence of WW and WZ production at high boson p_T [35]. One vector boson is observed by leptonic decay and the other is sought as a jet pair of appropriate mass. The boson p_T is required to be high enough to avoid W + jets background. The Run Ia data give $-0.89 < \Delta\kappa_V < 1.23$; this can be reasonably extended to Run Ib but as the p_T cut needed to avoid background rises the jet pair coalesces and the technique is no longer viable.

Figure 12 (Left) summarizes current limits on anomalous couplings. Coupling sensitivity for CDF measurements with 2 fb^{-1} should be comparable and complementary to LEP2 measurements. For example, with 2 fb^{-1} of data, limits on $|\Delta\kappa_\gamma|$ should get to about 0.3 and limits on $|\Delta\kappa_V|$ to about 0.2 [36] (see Figure 12 (Right)).

$W\gamma$ production in hadron collisions is of special interest due to the presence of amplitude zeros for the $W\gamma$ production from the $WW\gamma$ coupling. CDF has started to see this zero

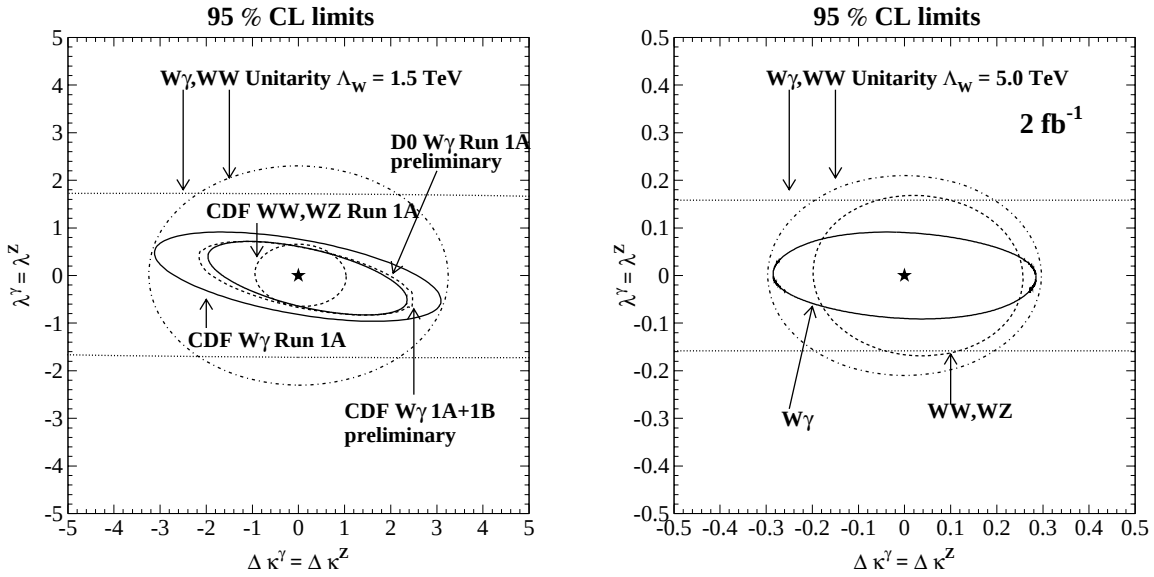

Figure 12: 95% CL limits on anomalous couplings. Left: Present limits. Right: Estimate for 2 fb^{-1} of data. The points at $\Delta\kappa = 0$ and $\Lambda = 0$ represent the standard model values.

at $\cos\theta^*_\gamma \sim 0.3$ from 44 pb^{-1} of data by requiring a large distance between the γ and the lepton, and therefore removing $W\gamma$ events from final state radiation, $W \to \gamma\ell\nu$, as illustrated in Figure 13. The results are statistically limited, and can be substantially improved with 2 fb^{-1} of data and with a wider acceptance in η.

Pairs of W bosons with both bosons decaying leptonically can be readily distinguished from top background. Using 67 pb^{-1} from Run Ia and 1b [37] CDF sees 5 candidates with an expected background of 1.3 events and an NLO[38] expected signal of 2.6 events. These events are quite central and the additional acceptance provided by the upgrades of about $30 - 40\%$ comes primarily from central muon upgrades. For 2 fb^{-1} there should be about 100 dilepton W pairs which may or may not be well described by the standard model.

3.5 PDF Measurements and Issues

At present the greatest constraint on parton distribution functions for collider measurements comes from the Run Ia CDF measurement of the W asymmetry shown in Figure 14 (Left) [39]. These data have been used as input by both the MRS and CTEQ PDF groups. The measurements should remain statistically dominated through 2 fb^{-1}.

The asymmetry measurement is of direct benefit in constraining PDF effects in measuring the W mass as is seen in Figure 15 [3]. The dotted lines indicate ± 2 standard deviations from the Run Ia W asymmetry measurement. The particular advantage of the asymmetry measurement in constraining the PDF systematic uncertainty in the W mass may soon be saturated, as may be seen in the vertical extent of the allowed regions. That is, with more

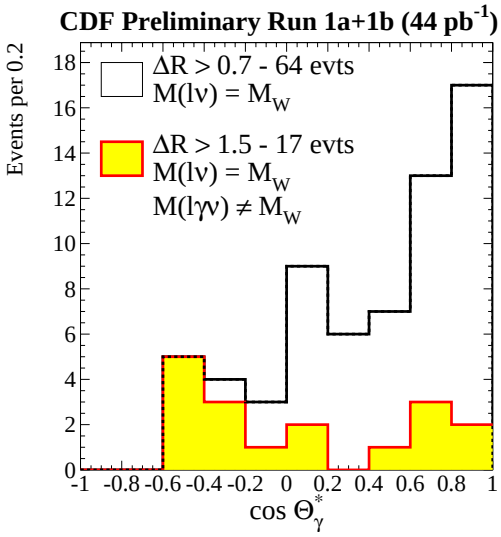

Figure 13: $\cos\theta^*_\gamma$ distribution where θ^*_γ is the angle with respect to the beam direction in the $W\gamma$ rest frame.

statistics, the dotted lines will get closer to zero, but ΔM_W won't. However, as illustrated in Figure 15 (a), (b) and (c), a higher minimum M_T^W for fitting can reduce the PDF systematic uncertainty, although it will imply a larger statistical uncertainty. The tracking upgrade and the muon toroid move will allow the extension of the asymmetry measurement to higher $|\eta|$.

Measurements of Drell-Yan production [40] can be used to get further constraints on PDFs. Upgrades to the DAQ bandwidth will be important for this program in order to preserve our ability to trigger on low p_T lepton pairs.

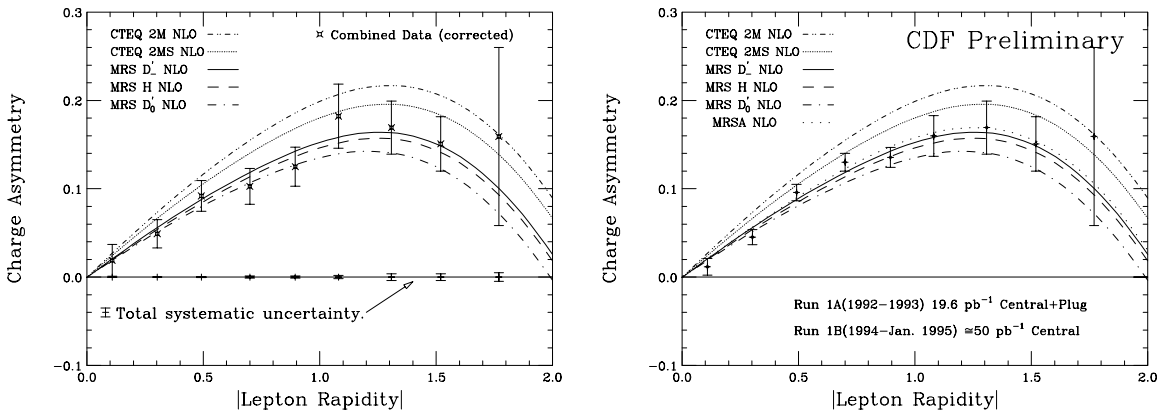

Figure 14: Left: Combined Run Ia W charge asymmetry measurement using muons and central and plug electrons. These data have been used as input in determining recent PDF sets. Right: Combined W charge asymmetry using Run Ia data and 50 pb^{-1} of Run Ib muon and central electron data.

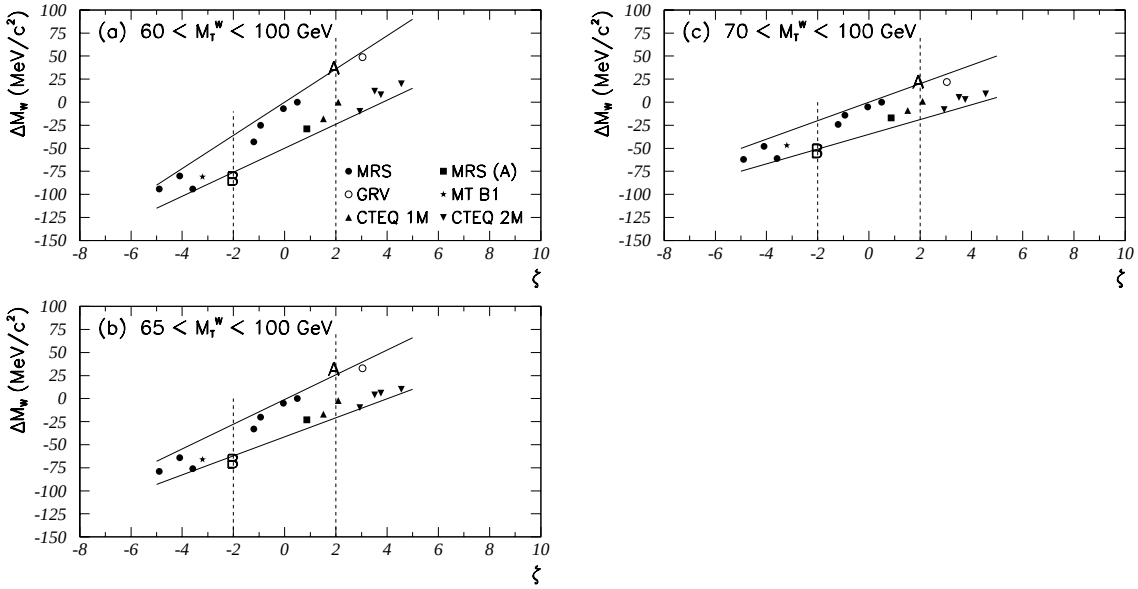

Figure 15: Change in derived $W \to e\nu$ mass (ΔM_W^e) versus the signed deviation in units of standard deviations from the average Run Ia W asymmetry measurement (ζ) for various PDFs. The lower edge of the fitting region is (a) 60, (b) 65, and (c) 70 GeV. Note that raising the lower edge of the fitting region makes the result less sensitive to PDFs, particularly for variation not correlated to the asymmetry.

4 QCD Measurements

4.1 Introduction

QCD, the theory of the strong interaction, is the least precisely tested component of the standard model. High statistics data samples at the Tevatron Collider combined with increasingly sophisticated higher order perturbative QCD calculations not only provide increasingly stringent tests of perturbative QCD, but do so at distance scales which are of the order of a few times 10^{-17} cm. These distance scales, which are an order of magnitude smaller than the weak scale, are the smallest scales currently probed in experimental particle physics. It is therefore quite plausible that new physics beyond the standard model associated with a new interaction at very small distance scales would first manifest itself as a deviation from QCD predictions at the Tevatron Collider.

The present focus of QCD analyses in CDF goes beyond the traditional comparison of observed distributions with leading-order (LO) or next-to-leading-order (NLO) QCD predictions. CDF measurements of the Drell-Yan cross-section and of the asymmetry in W production and decay have already been used to constrain parameterizations of the parton densities. It is expected that Run I data samples will enable the explicit extraction of the fundamental parameters of the theory (α_S and the parton distributions) in several different processes. The agreement or disagreement between these measured parameters and the corresponding measurements from other experiments at lower Q^2 provides a rigorous test of QCD in the same way that different measurements of $\sin^2\theta_W$ test the electroweak sector of the standard model.

The luminosity upgrades to the Tevatron, and specifically the main injector will extend the studies of QCD into a substantially higher energy regime where new high-Q^2 phenomena may be found. In addition, new calculations, higher statistics, and improvements in the understanding of detector performance will increase the precision and scope of the tests of QCD. To illustrate the reach in energy gained by the upgrade, the following topics will be discussed along with the discovery potential in each channel: a) jet cross section, b) direct photons, c) Drell-Yan and W and Z production, d) multijet events, and e) the extraction of α_S and the parton densities, f) rapidity gaps.

4.2 Jet Cross Section

Recently the inclusive jet cross section ($p\overline{p} \rightarrow$ Jet + X) has been calculated[41] to order α_s^3. This calculation greatly reduces the theoretical uncertainty characterized by the variation of the predictions with choice of renormalization scale. Figure 16 shows, as a function of jet E_t, the jet cross section measured by CDF, based on an integrated luminosity of 21 pb^{-1}. The cross-section has been measured over a range in which it varies by ≈ 9 orders of magnitude. Although the solid line, indicating the predictions of NLO QCD, appears to provide a good first description of the data, a more detailed comparison of (data - theory)/theory exhibits

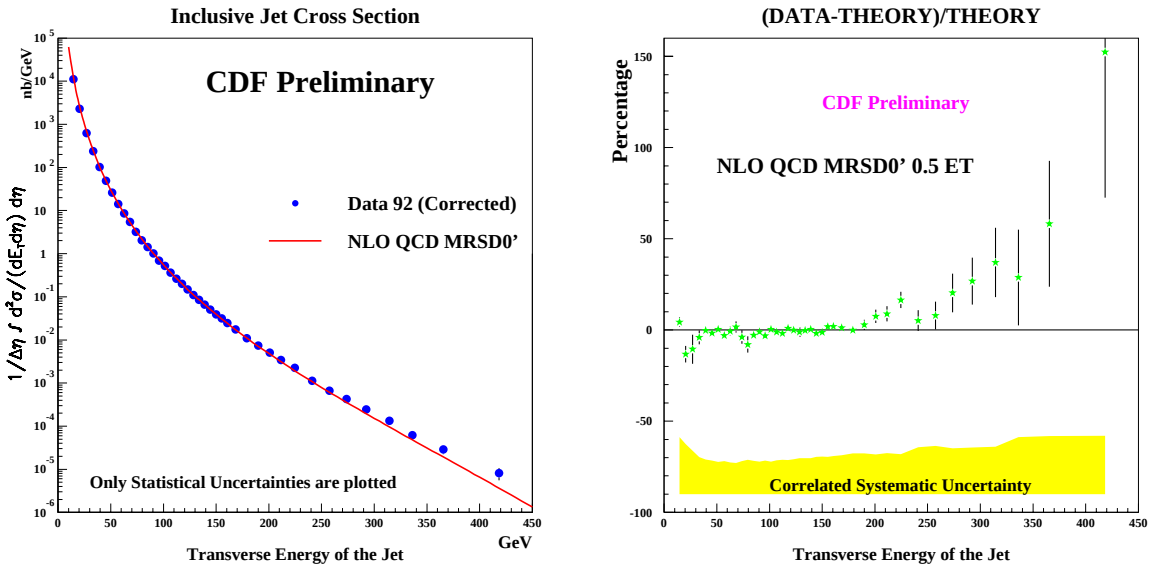

Figure 16: Comparison of the observed inclusive jet cross section measured by the CDF detector with the prediction of next to leading order QCD. The comparison is shown on a log and on a linear scale. The linear scale shows (data - theory)/theory as a function of jet transverse energy.

an intriguing excess of jets at the highest transverse energies (Figure 16). It is too early to know whether or not this excess is due to a systematic experimental effect. Higher statistics will help pin down the systematic uncertainties on this measurement.

Two other distributions that provide a sensitive test of perturbative QCD at small distance scales are the two-jet mass distribution (Figure 17) and the distribution of total transverse energies (summed over all jets in the event) shown in Figure 18. Preliminary measurements of both these distributions also show an excess of events at large energies. Since the three analyses share many events, one theoretical or experimental problem would probably explain the excesses in all three channels. If these excesses are not due to an experimental uncertainty or an error in the QCD calculations, then their resolution will be very interesting, and will either indicate (i) the need for corrections to the perturbative QCD calculations that go beyond NLO, (ii) something wrong with the world's knowledge of the parton distribution functions in the x range 0.25-0.45, or (iii) something new beyond the standard model. Whatever the solution to the apparent discrepancy is, measurements using higher statistics data samples are clearly mandatory.

One way of understanding how high statistics data samples from future Tevatron collider running will improve the sensitivity of our tests of QCD at small distances is to consider the sensitivity of the basic distributions to new physics beyond the standard model. We begin by considering the effect of quark substructure on the shape of the jet E_t spectrum at large E_t. Quark substructure would modify quark-parton scattering at short distances. This effect can be parameterized by adding a contact term to the QCD Lagrangian with an

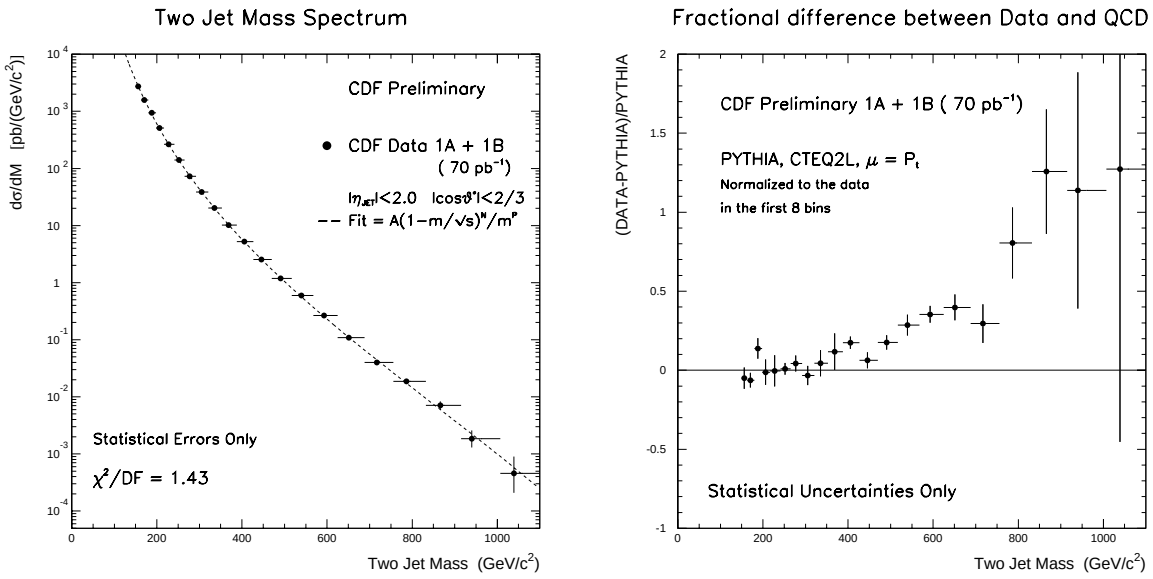

Figure 17: Two-jet mass distribution compared to a smooth parameterization on a logarithmic scale and compared to the PYTHIA QCD prediction on a linear scale.

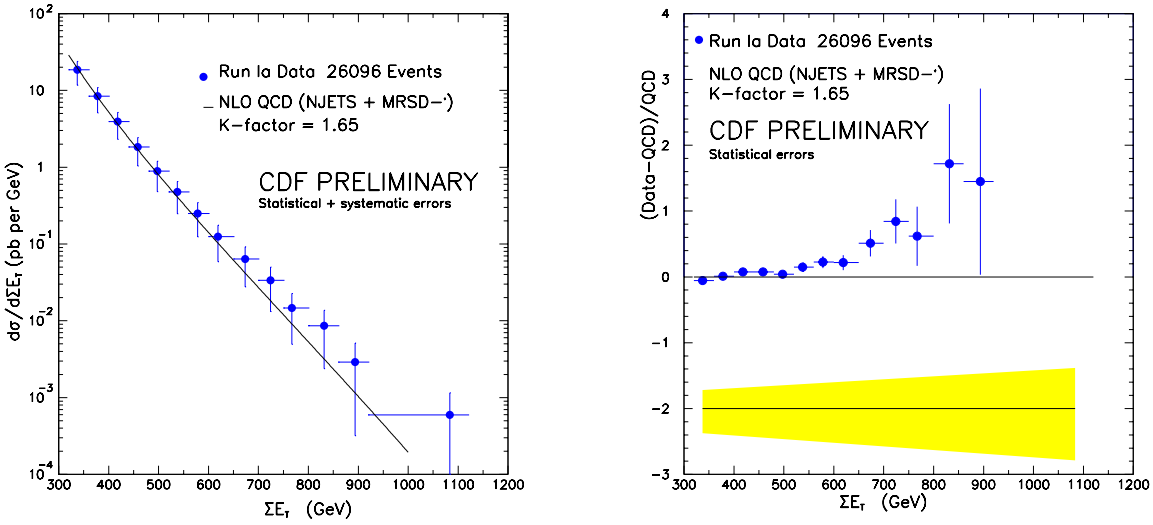

Figure 18: Total transverse energy distribution compared to an $O(\alpha_S^3)$ QCD prediction on log and linear scales. The theory is normalized to the first 3 data points.

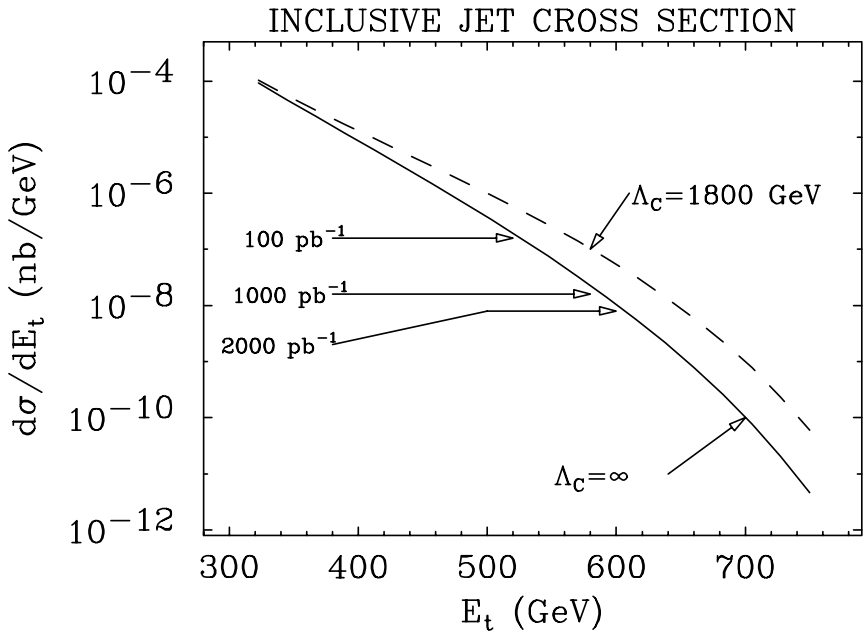

Figure 19: High energy end of the inclusive jet cross section. Arrows indicate the expected reach in jet E_t for different amounts of integrated luminosity.

effective distance scale defined by the parameter Λ_C [42]. Figure 19 shows the theoretical prediction for the high energy end of the inclusive jet cross section, and the E_t reach for different amounts of integrated luminosity. The arrows indicate the potential reach in cross section for several values of integrated luminosity. For example, a run of 2000 pb $^{-1}$ will probe the jet spectrum out to about 600 GeV, and yield a sensitivity that corresponds to Λ_C of approximately 1.8 TeV. In addition to providing a sensitive search for new small-distance interactions, the shape of the spectrum at transverse energies as large as 600 GeV is expected to be sensitive to soft gluon resummation effects associated with the approaching kinematic limit at high E_t, and therefore provide an important test of resummation techniques. The measured inclusive jet spectrum would also tie down the high x end of the parton distribution functions. Finally, let us suppose that the present apparent excess of events at high jet E_t at the Tevatron is not found to be due to an experimental or theoretical systematic effect, and an excess is eventually observed at the LHC at the high x end of the spectrum. In this case the results of the Tevatron measurement should provide the basis for understanding whether the LHC excess arises from the difficulty of reliably calculating the inclusive jet cross-section at very high E_t within the framework of perturbative QCD, or is the result of some new effective interaction.

4.3 Direct Photons

Studies of direct photon production in CDF complement jet studies, and have the advantage that photon energies are measured with greater precision than the energies of jets. So far direct photons have provided the best experimental and theoretical probe of low x parton distributions at the Tevatron. The present measurements have shown the need for additional k_t beyond that present in NLO QCD. Figure 20 shows the data compared to NLO QCD

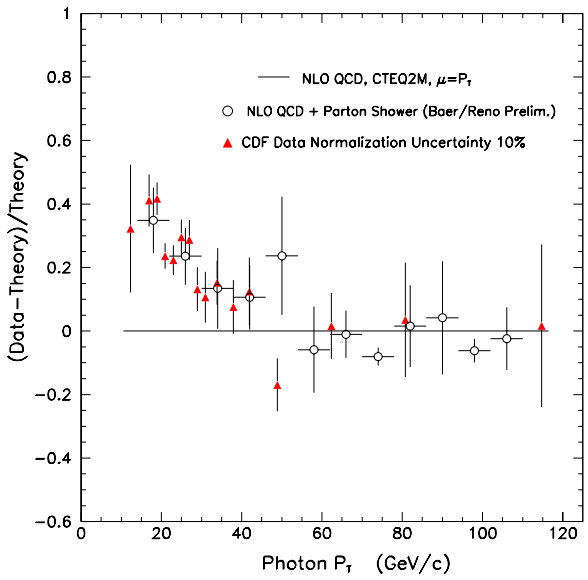

Figure 20: Comparison of the direct photon differential cross-section with NLO QCD predictions. The data (solid triangles) and NLO theory + parton shower model (open circles) which includes the effects of initial k_t are compared to NLO theory.

predictions. The normal prediction falls below the data at low p_t, while the addition of the parton shower matches the data quite well. This has implications for any hadron collision measurement using NLO QCD. It is also clear on this plot that the increased luminosities will help this measurement statistically at high p_t.

A comparison of the direct photon + jet angular distribution with the dijet angular distribution is interesting since at LO direct photon processes are mediated predominantly by quark propagators, whereas dijet production is mediated predominantly by gluon propagators. This is shown in Figure 21, where the dijet, W+jet and photon+jet angular distributions are shown along with their NLO QCD predictions. One sees the dramatic differences between jets and photon/W production. Further studies of the photon+jet measurement as well as photon + 2 jets will probe the direct photon production mechanisms.

The study of diphoton events provides important information about NLO QCD. For example, the k_t effects discussed above can be measured directly in the diphoton system. Also, diphoton production is an irreducible background for the detection of an intermediate mass Higgs at the LHC. The results from CDF on diphotons are statistically limited and will benefit enormously from the addition of more data and from the addition of the new plug calorimeter and shower max detector in the region $1.1 < |\eta| < 3.5$.

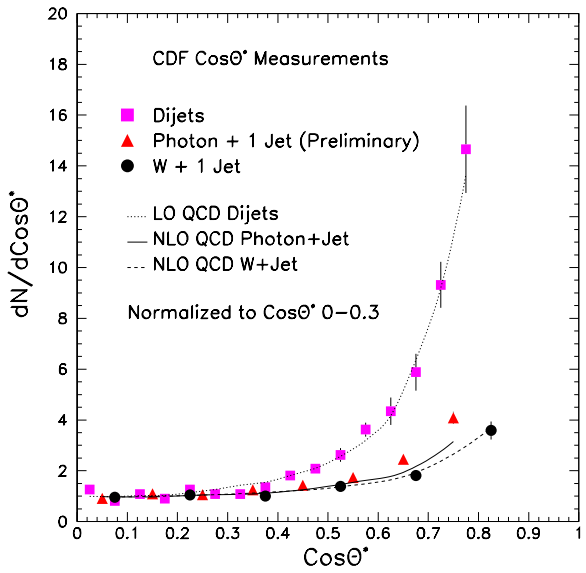

Figure 21: Angular distributions for dijet events, photon-jet events and W + 1 jet events compared to theory. Note that θ^* is defined in the two-body rest frame as the scattering angle between the average beam direction and the outgoing particles.

4.4 Drell-Yan and W and Z production

The data collected at the Tevatron Collider during the current run should provide 140000 $p\overline{p} \rightarrow$ W + X and 14000 $p\overline{p} \rightarrow$ Z + X events after all selection cuts. This estimate assumes a total Run I integrated luminosity of 120 pb^{-1}, and includes both electron and muon W/Z decays. Figure 22 shows the QCD jet multiplicity distribution associated with W and Z bosons using 73 pb^{-1} of electron decays from Run I. Of these events, 20% have associated QCD jets, with approximately 1% having 3 or more jets (jet E_t>15 GeV). An extrapolation to a 2 fb^{-1} data sample from Run II yields, for example, 2.3 million W bosons, including approximately 500000 with associated jets. These data can be used for a variety of important tests of the Standard Model, for top quark studies and to search for new phenomena. A brief discussion of the potential for these measurements is given below, based upon the assumption of a 2 fb^{-1} data sample from Run II.

The hadronic production of W and Z bosons provides the opportunity to test the Standard Model in processes which naturally occur at a high Q^2 scale, and for which the parton level scattering is identified by the presence of the bosons. Measurements of α_s can be extracted from jet multiplicity spectra. The data shown in Figure 22 would be increased by a factor of about 50 in Run II. This would allow measurements of the jet multiplicity associated with W bosons out to seven jets. A complimentary measurement of α_s can be obtained from W

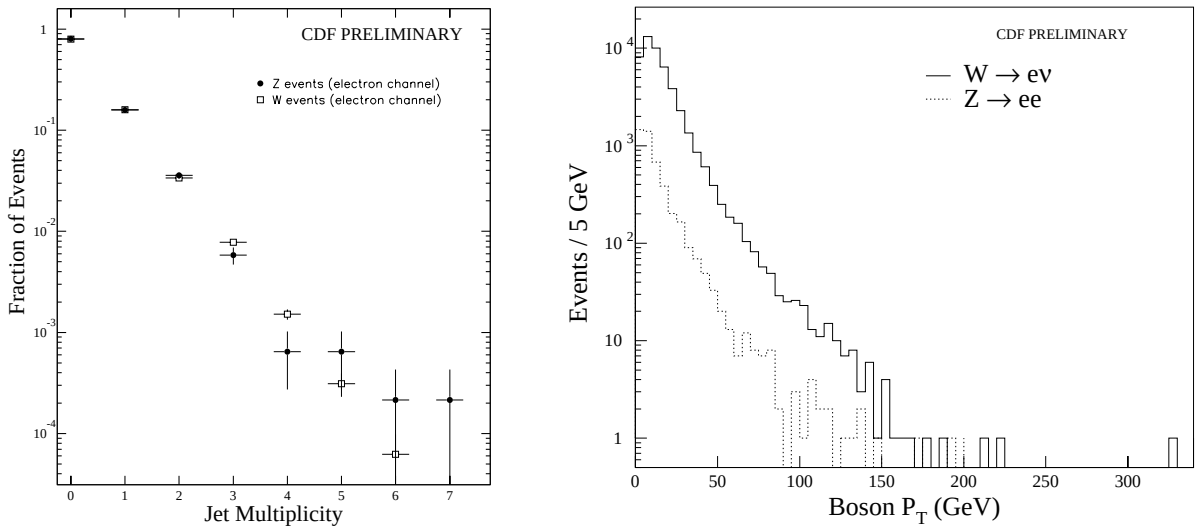

Figure 22: Multiplicity spectra (left) of jets associated with W and Z bosons, from 73 pb^{-1} of data. The jets have $E_t > 15$ GeV and $|\eta| < 2.4$. P_t spectra (right) of W and Z bosons from 73 pb^{-1} of data. No corrections for W and Z acceptance effects have been made.

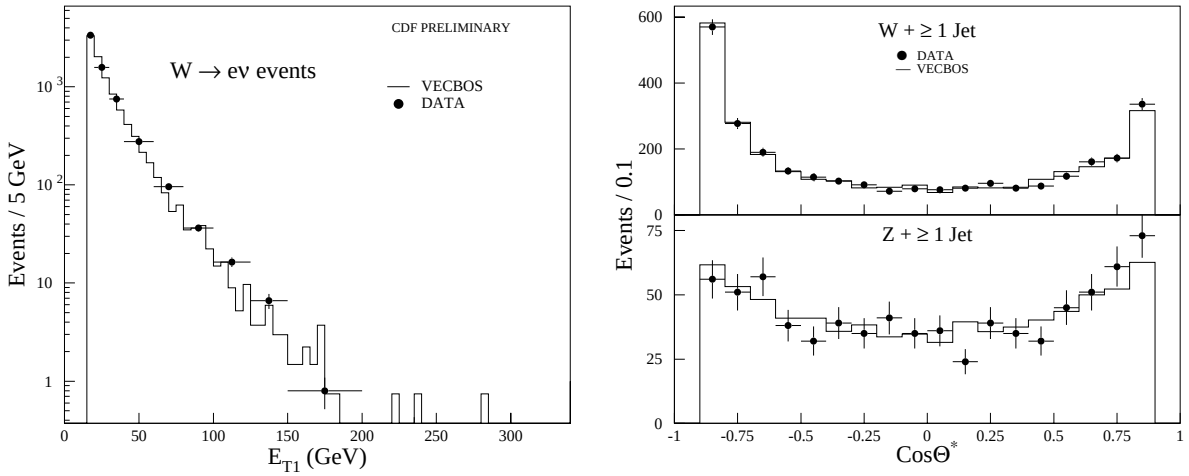

Figure 23: E_t spectrum (left) of the most energetic jet from W+jet events and the $\cos\theta^\star$ distribution (right) for W/Z boson plus most energetic jet. The data (points) are compared to a LO (VECBOS) QCD prediction with HERWIG fragmentation and detector simulation.

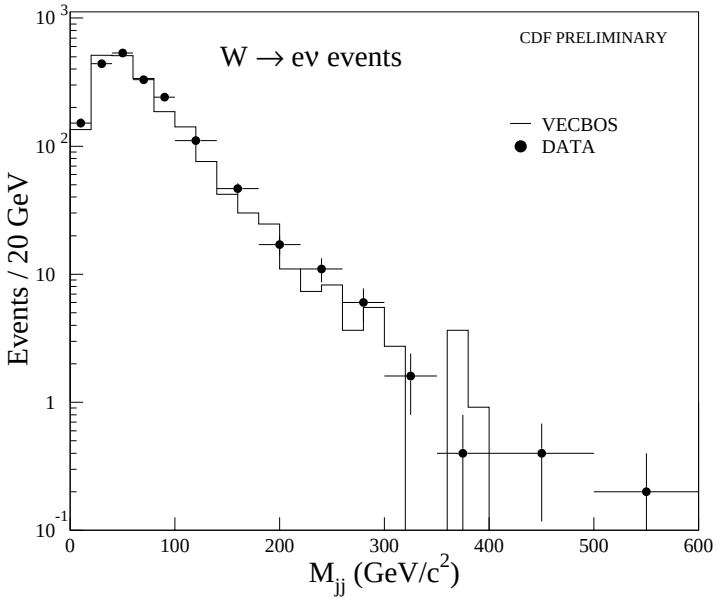

Figure 24: Dijet mass spectrum from W+ $\geq$ 2 jet events. The data (points) are compared to LO QCD with HERWIG fragmentation and detector simulation.

and Z P_t spectra of the type shown in Figure 22. Recently, calculations have been performed at order α_s^2 for the P_t spectra of the W/Z.[43] These calculations reduce the theoretical uncertainty in the cross section. With 2 fb^{-1} of data, the P_t reach for W's would allow a significant measurement out to 250 GeV. The Z P_t spectrum can be measured very cleanly. The Run II data sample would be 50 times larger than that shown in Figure 22, providing over 200000 Z bosons. The low P_t part of the W and Z spectra provide data useful for a measurement of gluon resummation effects. Non-standard processes, such as a techni-rho would appear as an enhancement in the P_t spectrum.[44]

A good understanding of the direct production of W and Z bosons with QCD jets can be made from the 500000 W+jet and 50000 Z+jet events expected from 2 fb^{-1} of data. Figure 23 illustrates measurements made from a sample of data (73 pb^{-1}) from the current Tevatron run. The E_t distribution of the highest energy jet from W events and the production angular distributions of the W/Z bosons + a high E_t jet (in the Collins-Soper reference frame) are presented in Figure 23. In both distributions the data (points) are compared to LO QCD calculations (histogram). A 50-fold increase in the statistics shown in these plots will allow a study of the QCD jet spectra out to E_t of about 250 GeV. Currently NLO predictions are available only for W/Z + 1 jet events, but calculations for higher multiplicities should be available for comparison to the Run II data.

A good understanding of direct W and Z boson production with jets is important both for an accurate measurement of the top mass and in searches for new particles which decay to W/Z's or are produced in association with them. Processes involving technicolor-type models could produce heavy particles decaying to W pairs. The exact nature of such couplings are

not certain, but do provide some impetus to examine the potential discovery limits. From different scenarios, and depending on the coupling, it may be possible to detect techni-rho's with masses up to 250 GeV. Backgrounds for Higgs bosons can be reduced by searching for production in channels with associated W/Z bosons. The jet-jet invariant mass spectrum from events with W bosons is shown in Figure 24 for a sample of Run I data. The data (points) are well reproduced by a LO QCD calculation out to jet-jet masses of 300 GeV/c^2. Scaling this up to a 2 fb^{-1} data sample predicts on the order of 600 W events with a di-jet in the invariant mass range from 260 to 300 GeV/c^2. This provides the background to any new particle with mass in this range decaying to dijets and produced in association with a W boson. The high statistics W/Z + jet sample available in Run II should permit a good understanding of the normal QCD production and allow a sensitive search for new particles out to masses of 300 GeV/c^2.

4.5 Multijet Events

The study of events with three or more jets in the final state provides a test of perturbative QCD that complements the inclusive jet and two-jet measurements. A comparison of recent CDF measurements of the mass dependent jet multiplicity distributions (Figure 25) shows that LO QCD predictions give a reasonable description of the measurements. However, at the highest energies, both the statistical uncertainties on the measurements and the systematic uncertainties on the predictions are large. With a 2 fb^{-1} data sample the statistical uncertainties on the data points will shrink by more than a factor of 5. Improvements in computing resources should yield a corresponding improvement in the statistical uncertainties on parton shower Monte Carlo predictions. Furthermore, the availability of a NLO three-jet calculation together with further understanding of the theoretical uncertainties based on analyses of current data samples may well result in substantial reductions in the estimates of these uncertainties. Hence it is likely that the precision of quantitative comparisons between predicted and observed multijet properties will improve by about a factor of 5.

4.6 The extraction of α_S and the parton densities

An important goal of QCD analyses of CDF data in the coming months is the extraction of α_S and/or the parton densities from all processes for which there are reasonable data samples and reliable predictions. Some examples are the inclusive jet differential cross-section, the two-jet mass and angular distributions, jet and photon rapidity distributions, the charge asymmetry in leptonic W decays, the direct photon differential cross-section, jet multiplicity distributions, photon + charm production cross-sections, and the W, Z, and Drell-Yan transverse momentum distributions. These measurements will provide new constraints on the parameters of the theory. The self consistency of the extracted parameters, together with their consistency with measurements from other experiments at lower energies and Q^2-scales, provides a rigorous test of perturbative QCD.

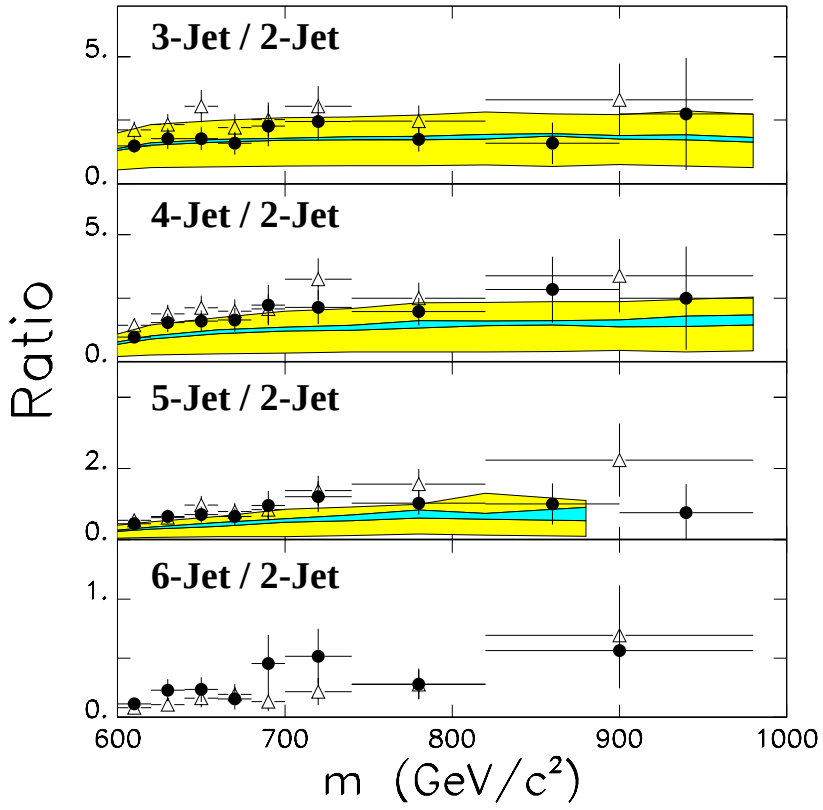

Figure 25: CDF measured ratios of N-jet to 2-jet events shown as a function of multijet mass (points) for jets with $E_t > 20$ GeV, compared to LO QCD predictions from a matrix element calculation (bands) and from the HERWIG parton shower Monte Carlo program (open triangles).

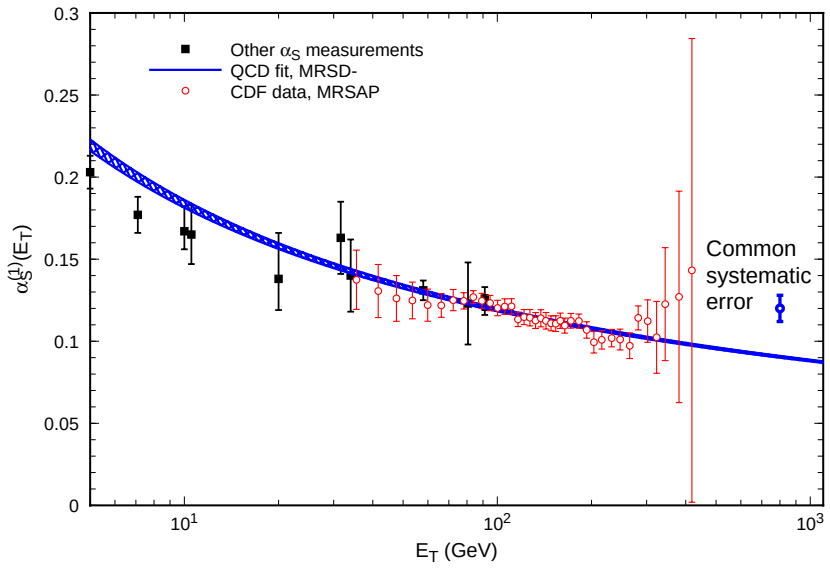

Figure 26: The value of $\alpha_S(E_T)$ extracted by Giele and Glover using published CDF data ($4\ pb^{-1}$).

The published CDF inclusive jet differential cross-section has been used to extract α_S ([45]). Preliminary results are shown in Figure 26 to not only be consistent and competitive with the world's knowledge of α_S, but also to demonstrate in a single measurement the running of the strong coupling "constant". The strength of the CDF measurement of α_S based on the jet spectrum is that it extends the Q^2 range of the worlds data by more than a factor of 4. With a data sample of 2 fb^{-1} the statistical errors will shrink by a factor of 20 with respect to those shown in the Figure, and the measurement will extend out to about 600 GeV.

In addition a 2 fb^{-1} data sample would facilitate a precise simultaneous determination of α_S and the parton distributions, which will enable systematic uncertainties associated with global structure function fits to be minimized. This is important since the global fit systematic uncertainties are difficult to quantify.

Reliable QCD predictions require a precise knowledge of the parton distributions. CDF Drell-Yan and W lepton charge asymmetry measurements are already being used to constrain these distribution functions as discussed in section 3.5. The present precision of these measurements is limited by statistics. A 2 fb^{-1} data sample will therefore provide more stringent constraints on the parton distributions.

4.7 Rapidity Gaps

Recently CDF published a discovery of rapidity gap events in events with two high p_T jets[46]. In this measurement the gap region was limited to $|\eta| < 1.0$. With the new plug upgrade it will be possible to expand the gap region and perform a more sensitive measurement of rapidity gap events.

5 B Physics

5.1 Introduction

CDF has shown that a very rich B physics program can be pursued in a hadron collider environment. CDF is currently highly competitive with LEP experiments and CLEO in the following areas:

- Individual B hadron lifetimes
- Searches for rare decays ($B_{d,s} \to \mu^+\mu^-$; $B_u \to \mu\mu K$; $B_d \to \mu\mu K^*$)
- B_s mass
- Search for B_c in the $J/\psi\pi$ and $J/\psi\ell\nu$ decay modes
- Polarization in $B_d \to J/\psi K^*$ and $B_s \to J/\psi\phi$

There are also a number of physics topics for which we have preliminary results based on Run Ia data. These ongoing analyses will also be competitive with LEP and CLEO with the inclusion of Run Ib data:

- Measurement of the B_d mixing parameter x_d
- Limits on the B_s mixing parameter x_s
- Λ_b mass

CDF has also carried out many studies of B and quarkonium production, and $b\bar{b}$ correlations. The QCD aspects of these results have generated much interest. In addition, they provide the understanding of B production necessary as input to studies of B decay.

Currently, CDF is unique in having a sample of $B \to J/\psi K_s$ events that can be tagged for a CP asymmetry analysis. We are working on several flavor tagging methods. With the full Run I data sample we expect to achieve the first non-trivial measurement of $\sin(2\beta)$, though the precision is unlikely to be adequate for a definitive observation of CP violation.

The analyses completed or in progress by CDF have shown that the mass resolution obtained with the CTC, coupled with the vertex resolution obtained with the SVX, allows us to (a) isolate fully reconstructed B decays and (b) measure the lifetime of the decaying mesons. Point (a) is best illustrated in Figure 27 where the observed signals for $B^\pm \to J/\psi K^\pm$ and $B^0 \to J/\psi K^*$ are displayed. These data samples are currently the world's largest for these decay modes. Point (b) is illustrated in Figure 28 where the lifetime distribution of these modes is used to extract the individual $B^\pm$ and B^0 meson lifetimes.

In addition, we have gained extensive experience in measuring the B decay vertex in partially reconstructed B decays, e.g. in B semileptonic decays. We have used the decays

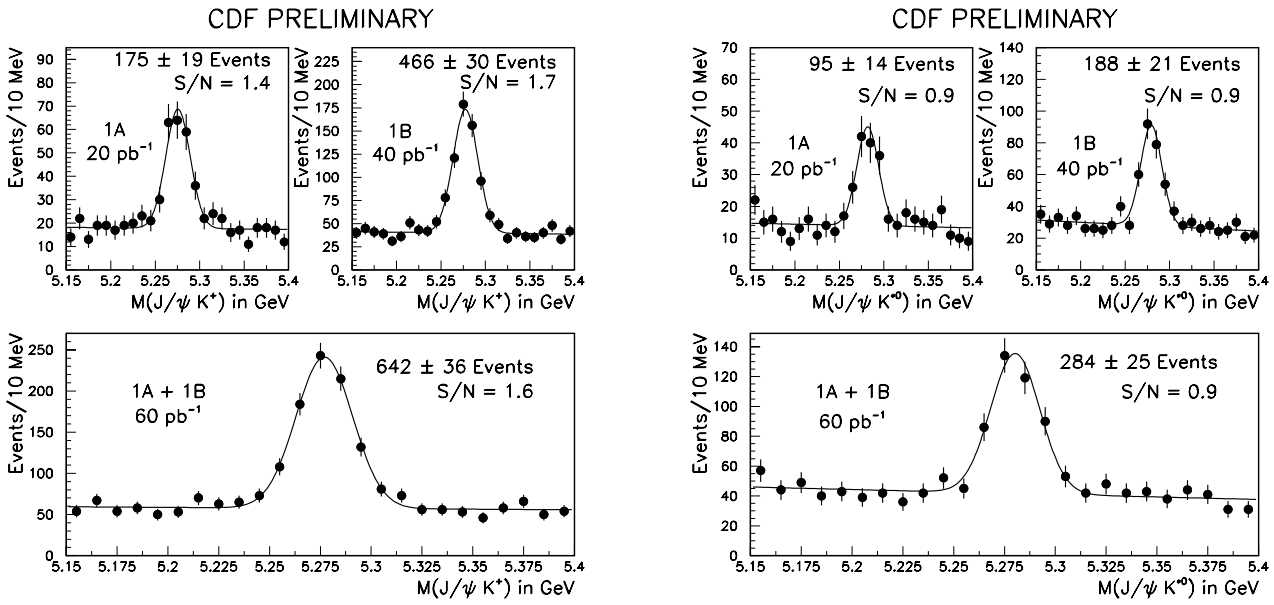

Figure 27: The invariant mass distribution of $J/\psi K^+$ and $J/\psi K^*$ combinations from the CDF experiment. The number of signal events is the result of a fit.

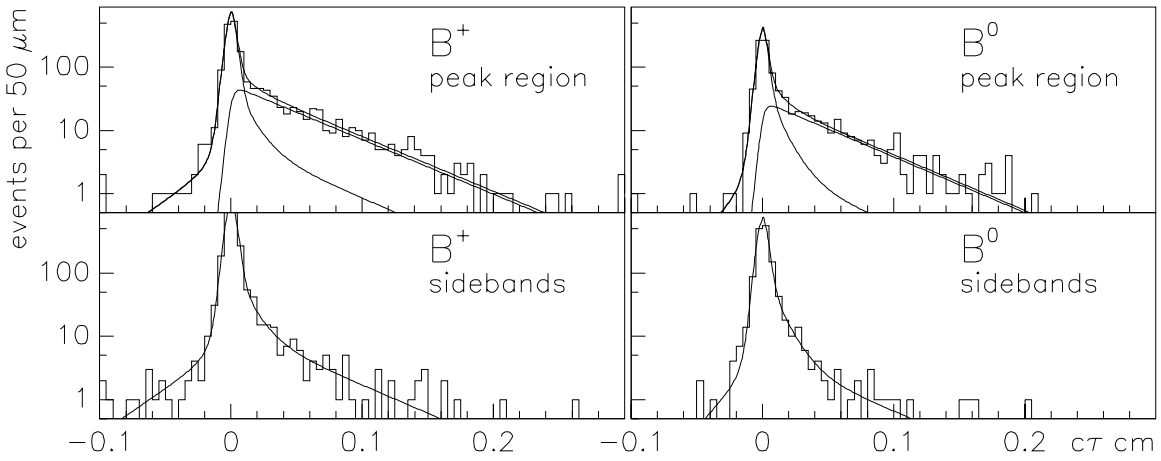

Figure 28: The proper lifetime distribution of charged and neutral B mesons reconstructed via the decay modes $B^+ \to J/\psi K^+$ and $B^0 \to J/\psi K^{*0}$.

$B^- \to \ell^- D^0 \nu$, $B^0 \to \ell^- D^{*+} \nu$ and $B^0 \to \ell^- D^+ \nu$ to measure the lifetimes of the charged and neutral B mesons. The D mesons employed were either fully or partially reconstructed using the decay modes $D^0 \to K^- \pi^+; D^0 \to K^- \pi^+ X; D^0 \to K^- \pi^+ \pi^- \pi^+; D^* \to \pi D^0; D^+ \to K^- \pi^+ \pi^+$. These D signals are displayed in Figure 29; the corresponding B lifetimes are displayed in Figure 30.

The observation of these modes shows that combinatoric backgrounds in B decays can be reduced while still maintaining high efficiency for the signals. In addition, we have shown that we can meaningfully measure B lifetimes in decays involving two secondary vertices (one due to the B decay and one due to the D decay). If we combine our results using exclusive decays from 70pb^{-1} of Run I data with our results using semileptonic decays from 20pb^{-1} of Run I data, we obtain a ratio of the B^+ to B^0 lifetimes of 1.00 ± 0.07.

The current generation of B experiments, CDF, CLEO, LEP and SLD, are already making important measurements and placing constraints on the parameters of the CKM matrix. On the time scale of Run II, there will be competition among many new or upgraded experiments. The strategy for CDF is to build on our experience in Run I, to optimize the quality of information in the central region while expanding coverage, and to exploit many additional B decay channels. The tracking upgrades will maintain the present mass resolution while the 3D Silicon tracker improves the vertexing ability. The lepton coverage will improve, and a time-of-flight system will provide for K/π separation at low P_T. Finally, the high-rate data acquisition system will enable us to handle high luminosity while lowering thresholds and keeping events in many more channels.

Thus, the CDF Run II upgrade will provide for a competitive B physics program that has unique features and addresses a wide variety of topics of fundamental importance. We discuss below the following topics:

- Observation of CP violation in both the $B_d \to J/\psi K_s$ and $B_d \to \pi^+ \pi^-$ channels, and measurement of $\sin(2\beta)$ and $\sin(2\alpha)$.
- Search for CP violation in $B_s \to J/\psi \phi$.
- Reconstruction of channels useful for measuring the angle γ.
- Measurement of the CKM matrix element ratio $|\frac{V_{td}}{V_{ts}}|$
  - B_s mixing
  - $\Delta\Gamma_s/\Gamma_s$
  - Radiative B decays
- Measurement of the CKM matrix elements V_{ub} and V_{cb} in exclusive semileptonic decays of B mesons and baryons.
- Observation of the rare decays $B_d \to \mu\mu K^*$ and $B_u \to \mu\mu K$
- Observation and study of the B_c meson.

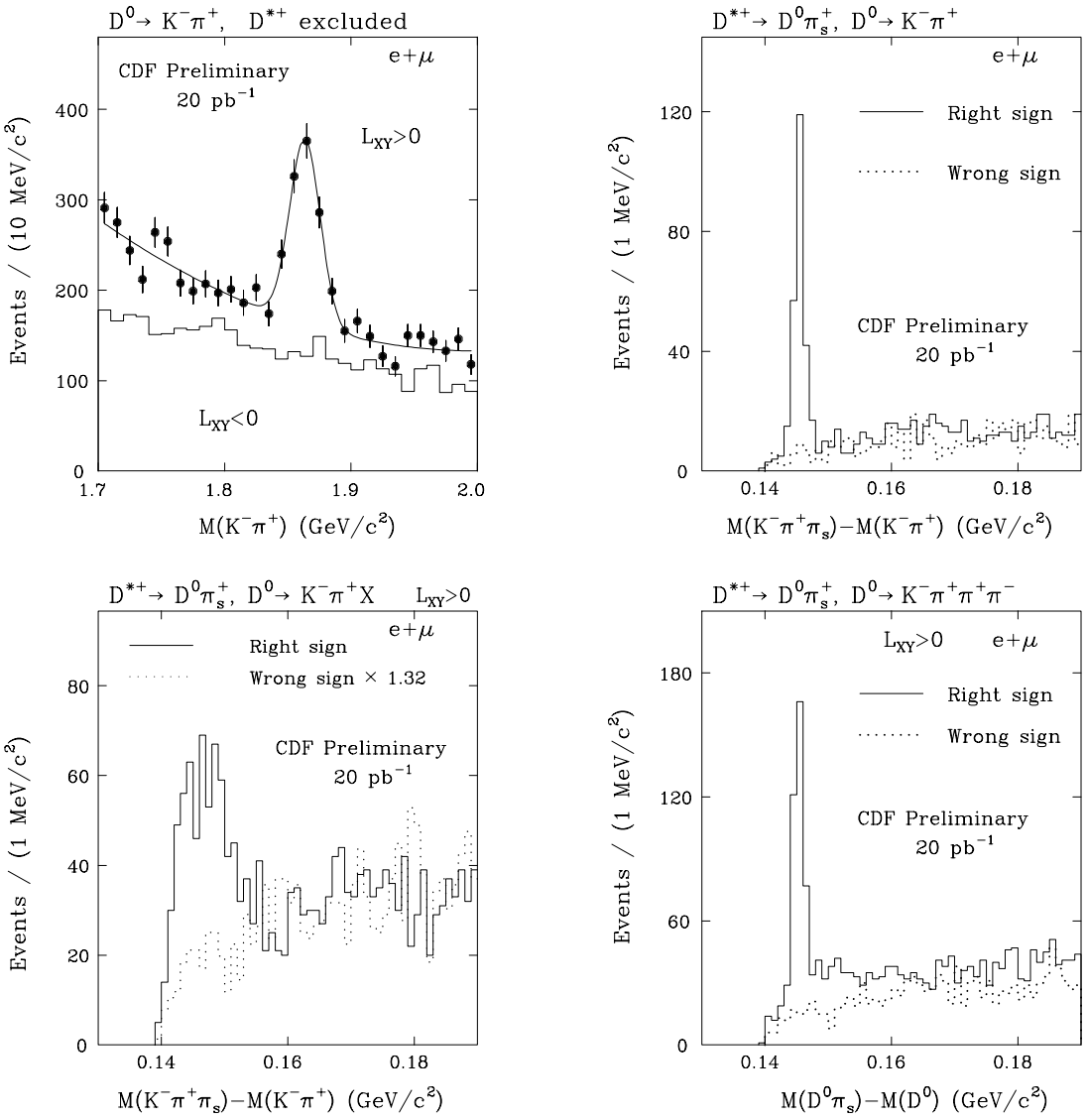

Figure 29: Various charm signals reconstructed in association with a high-P_T lepton.
Top left: Signal for $B^- \to \ell^- D^0 \bar{\nu}; D^0 \to K^- \pi^+$
Top right: Signal for $\bar{B}^0 \to \ell^- D^{*+} \bar{\nu}; D^{*+} \to D^0 \pi^+; D^0 \to K^- \pi^+$
Bottom left: Signal for $\bar{B}^0 \to \ell^- D^{*+} \bar{\nu}; D^{*+} \to D^0 \pi^+; D^0 \to K^- \pi^+ X$
Bottom right: Signal for $\bar{B}^0 \to \ell^- D^{*+} \bar{\nu}; D^{*+} \to D^0 \pi^+; D^0 \to K^- \pi^+ \pi^- \pi^+;$
L_{xy} is the two-dimensional distance between the beamspot and the reconstructed D vertex.

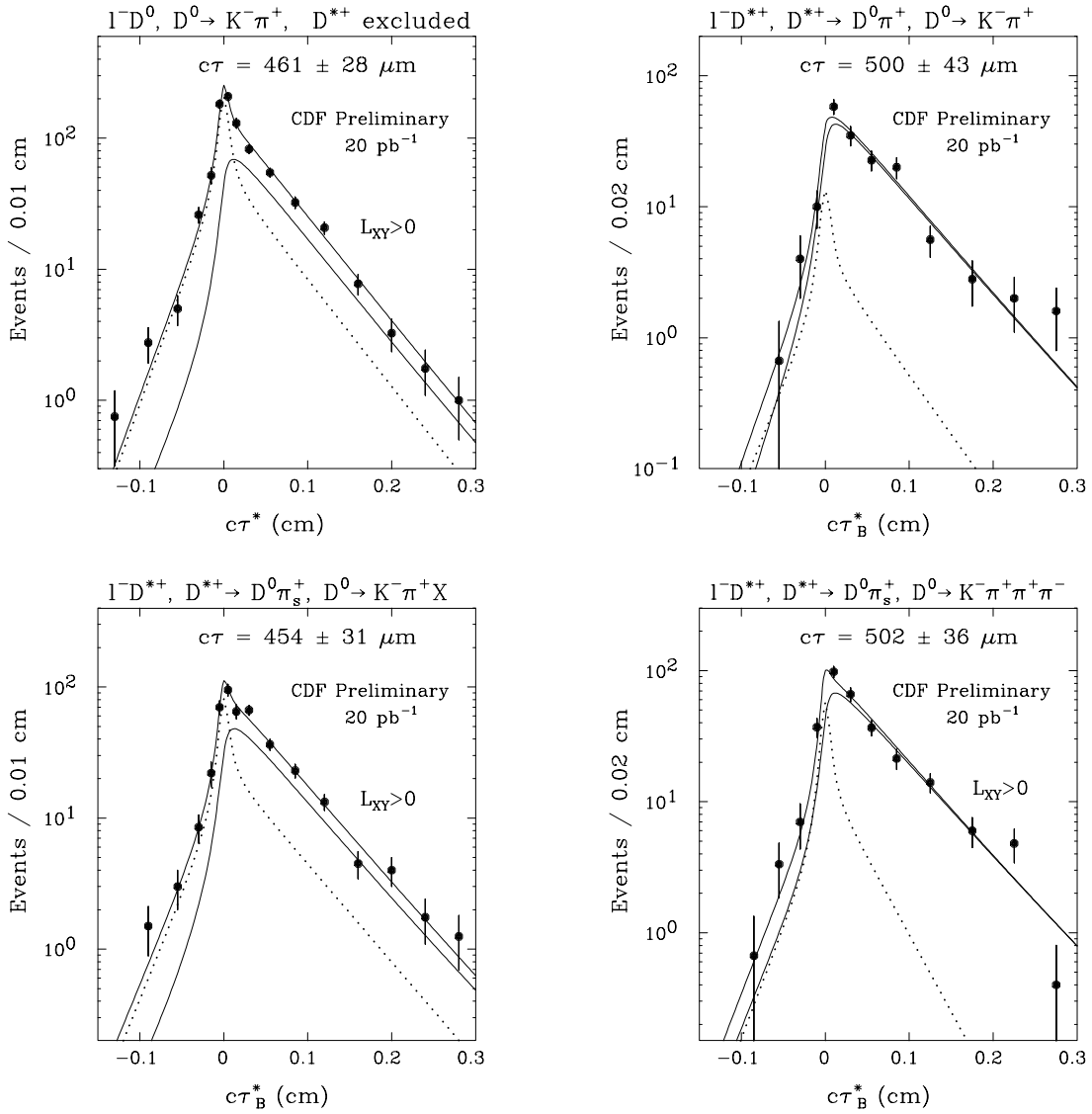

Figure 30: B meson lifetimes, $c\tau$, from lepton + "D" signals. In all plots, the dotted line is the background; the lower solid line is $c\tau$ distribution of the signal; the upper solid line is the sum of the signal and background distributions.
Top left: Proper lifetime distribution for $B^- \to \ell^- D^0 \bar{\nu}; D^0 \to K^- \pi^+$
Top right: Proper lifetime distribution for $\bar{B}^0 \to \ell^- D^{*+} \bar{\nu}; D^{*+} \to D^0 \pi^+; D^0 \to K^- \pi^+$
Bottom left: Proper lifetime distribution for $\bar{B}^0 \to \ell^- D^{*+} \bar{\nu}; D^{*+} \to D^0 \pi^+; D^0 \to K^- \pi^+ X$
Bottom right: Proper lifetime distribution for $\bar{B}^0 \to \ell^- D^{*+} \bar{\nu}; D^{*+} \to D^0 \pi^+; D^0 \to K^- \pi^+ \pi^- \pi^+$
L_{xy} is the two-dimensional distance between the beamspot and the reconstructed D vertex.

5.2 CP Violation in the B system

5.2.1 CP Asymmetry in $B_d \to J/\psi K_s$: $\sin(2\beta)$

By far the most important goal of our Run II B physics program is the observation of CP violation in the B system. The decay mode most frequently cited in the literature is $B_d \to J/\psi K_s$. CDF has already collected the world's largest sample of these decays: in the first 60 pb^{-1} of Run I, as shown in Figure 31, we have observed 140 $B^0 \to J/\psi K_s$ events with signal-to-noise better than 1:1. We obtained this sample with a dimuon trigger that required both muons to have transverse momentum (P_T) greater than 2.0 GeV. For this analysis, we have not required that the events be in the SVX fiducial region, although we used SVX information if available.

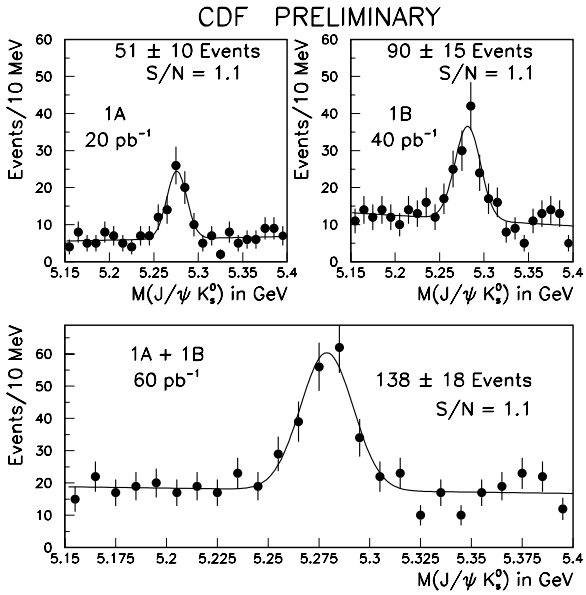

Figure 31: $B_d \to J/\psi K_s$ signal. The number of signal events is the result of a fit.

Our goal for Run II is to improve the trigger efficiency to the point that we reconstruct 10 $B^0 \to J/\psi K_s$ events per pb^{-1}. We expect to achieve this by using $J/\psi \to e^+e^-$ as well as $J/\psi \to \mu^+\mu^-$ decays, by improving the coverage for lepton identification, and by lowering the P_T threshold to 1.5 GeV. We are preparing a special set of triggers to test these changes during Run I. We also expect to achieve much improved signal-to-noise by using the improved capability and coverage of the SVX II, but have conservatively assumed S/N =2:1.

In addition to the above basic expectation of 20,000 $B^0 \to J/\psi K_s$ events in 2 fb^{-1}, the $B^0 \to J/\psi K_s$ yield can increase by employing (a) the increased tracking coverage and (b) new ways of triggering using the SVT upgrade [47]:

(a) Using tracks at higher pseudorapidity we can reconstruct $\approx 50\%$ more events with good mass resolution.

(b) Simulations of the SVT indicate that it may be possible to trigger requiring one lepton and one additional track with large impact parameter. In the offline analysis, the second lepton is found primarily using tracking information. Attaining good signal-to-noise will be a challenge. However, if this turns out to be feasible with the upgraded detector and improvements to the offline analysis, we may attain an additional factor of four or more in the number of reconstructed $B^0 \to J/\psi K_s$ events.

To obtain the CP asymmetry we must tag the flavor of the B meson at the time at which it was produced. At this point, the flavor tagging efficiency is more uncertain than the $B^0 \to J/\psi K_s$ yield. As shown in Table 5.2.1, we are investigating many flavor tagging methods. Work is under way to use a combination of Run I data and Monte Carlo to establish the "effective tagging efficiency" (ϵD^2)[1] for each possible method. These techniques will be applied to Run I analyses as well as Run II projections.

Tagging Method	ϵD^2 (%) (measured)	ϵD^2 (%) (expected)	Relevant Run II Upgrade
Jet Charge	1.0 ± 0.3	4.0	SVX II. Fiber tracker
Central Muon	0.7 ± 0.2	0.7	Completed CMX coverage
Non-Central Muon		0.3	Move FMU. Fiber tracking
Electron		1.0	Plug calorimeter. Fiber tracking
Same-side pion		2.0	
Opposite-side Kaon		3.0	Time of Flight

Table 5: Flavor tagging methods currently under consideration, the effective tagging efficiency, ϵD^2, for the two algorithms from Run I data the expected ϵD^2 in Run II, and the list of detector upgrades that will improve ϵD^2.

We currently have results for two methods, Jet Charge [48] and Lepton tagging (using central muons [49]) for a total efficiency of $\approx 2\%$. We expect a large improvement in the total efficiency from the following sources:

- A total of 2% from lepton tagging, using electrons as well as muons and the additional coverage planned for lepton identification in Run II.

[1]For a flavor tagging method with efficiency ϵ and "dilution" D, the uncertainty on the CP asymmetry, δA_{CP}, is given by $\delta A_{CP}^2 \approx 1/\epsilon D^2 N$ where N is the total number of signal events prior to flavor tagging. The dilution is defined as $D = (N_R - N_W)/(N_R + N_W)$ where N_R and N_W are the number of events with right and wrong tags respectively.

- $\approx$ 2% from Same-Side tagging, which exploits the charge correlation of the pions produced in the fragmentation process along with the B meson[50].
- As much as 3% from kaon tagging, using tracks with high impact parameter identified as kaons in the time-of-flight system [51].
- $\approx$ 3% gain from adding to our jet charge algorithm the information on whether tracks originate from a primary or secondary vertex. The 3D nature of the SVX II and stand-alone tracking abilities of the SVX II and Intermediate Fiber Tracker help make this a powerful technique [52].

In Table 5.2.1 we list all the tagging methods we expect to exploit, the measured effective tagging efficiency where available, and the Run II upgrades that impact these algorithms. We believe that a reasonable assumption is that we will achieve a total flavor tagging efficiency of 8% (even though the sum above equals 11%).

We thus present three estimates of the uncertainty in our $\sin(2\beta)$ measurement:

1. A conservative extrapolation, based on (a) our current $J/\psi K_s$ signal, and modest dilepton trigger improvements (expected signal of 20,000 $B^0 \to J/\psi K_s$ events) and (b) our currently established flavor tagging techniques ($\epsilon D^2 = 2\%$). This results in an uncertainty on $\sin(2\beta)$, $\delta[\sin(2\beta)]$, of 0.14.
2. An extrapolation assuming the same $B^0 \to J/\psi K_s$ yield and a total effective flavor tagging efficiency $\epsilon D^2 = 8\%$. This results in $\delta[\sin(2\beta)] = 0.07$.
3. An extrapolation assuming $\epsilon D^2 = 8\%$ and an increased yield $B^0 \to J/\psi K_s$ signal from (a) the extended the rapidity region from the SVX II and the fiber tracker, and (b) the employment of SVT triggering. This results in an expectation of $\delta[\sin(2\beta)] = 0.03$.

The current Standard Model predictions for $\sin(2\beta)$ are $\sin(2\beta) > 0.17$[53] and $\sin(2\beta) = 0.65 \pm 0.12$ [54]. Thus, even in the most conservative case, with $\delta[\sin(2\beta)] = 0.14$, we will have a very interesting measurement of $\sin(2\beta)$ that will probaby result in the observation of CP violation. It is likely that we will do much better than the conservative case. Finally, as we gain experience, additional triggering and reconstruction techniques may allow an even more precise measurement that will tightly constrain the parameters of the Standard Model.

5.2.2 CP Asymmetry in $B^0 \to \pi^+\pi^-$: $\sin(2\alpha)$

A measurement of $\sin(2\alpha)$ in conjunction with $\sin(2\beta)$ provides powerful constraints on the unitarity triangle [55]. The greatest challenge in this measurement is the trigger requirement at a luminosity of $1 \times 10^{32}\text{cm}^{-2}\text{sec}^{-1}$. Our plan (described in detail in[56]) consists of

1. At Level-1: Use the XFT (the fast trigger processor which finds tracks with $P_T > 2$ GeV with $\delta P_T/P_T^2 < 0.04$ GeV^{-1}). Imposing $\Delta\phi$ cuts on opposite sign track pairs yields (using Run I data) an expected Level-1 accept rate of 15 kHz.

2. At Level-2: Use the SVT (the fast trigger processor capable of extrapolating the XFT tracks in the SVX II detector and determining their impact parameter, d, with resolution $\sigma_d \approx 25\mu$m). Demanding $d > 100$ μm yields an expected Level-2 accept rate of 200 Hz. We are currently studying additional trigger requirements which may allow this rate to be reduced by an additional factor of 10.

3. At Level-3: Here the full event information is available. We expect to be able to reduce the rate out of Level-3 to about 10 Hz.

With these trigger requirements we expect ≈ 5 $B^0 \to \pi^+\pi^-$ events per pb^{-1}. Since these events pass the SVT requirement, they have a proper lifetime distribution starting at ≈ 1.5 lifetimes. Therefore, the dilution of the CP asymmetry due to mixing of the signal B before it decays will be 0.82, rather than 0.47 as we assumed for $\sin(2\beta)$.

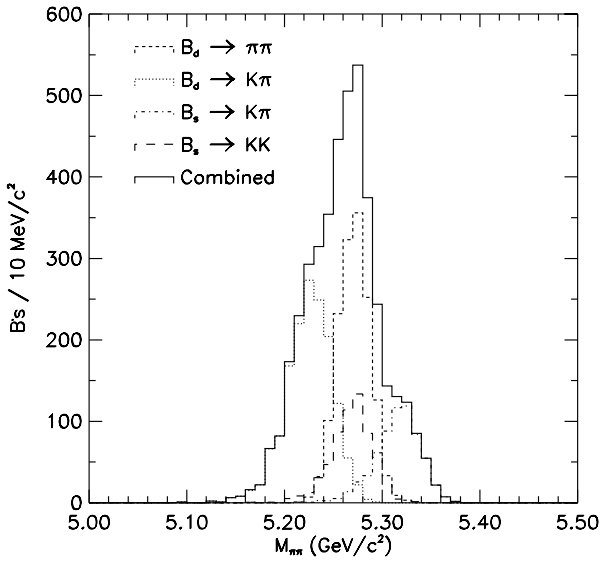

Figure 32: Mass distribution for the combination $B^0 \to \pi^+\pi^-$, $B_d \to K\pi$, $B_s \to K\pi$ and $B_s \to KK$ assuming all K's to be π's.

To measure the CP asymmetry in $B^0 \to \pi^+\pi^-$ events one needs to extract the backgrounds from $B_d \to K\pi$, $B_s \to K\pi$ and $B_s \to KK$ decays. Figure 32 displays the expected mass distribution for the combination of the above four signals, assuming all K's to be π's[56]. The $B_d \to \pi\pi$ and $B_d \to K\pi$ peaks are separated by 40 MeV/c^2. The mass resolution used for this study is $\sigma_m \approx 20$ MeV/c^2. A simulation of the upgraded detector, including the intermediate fiber tracker and SVX II indicates that the resolution at $P_T(B) \approx 6$ GeV will be slightly worse, $\sigma_m \approx 28$ MeV/c^2.

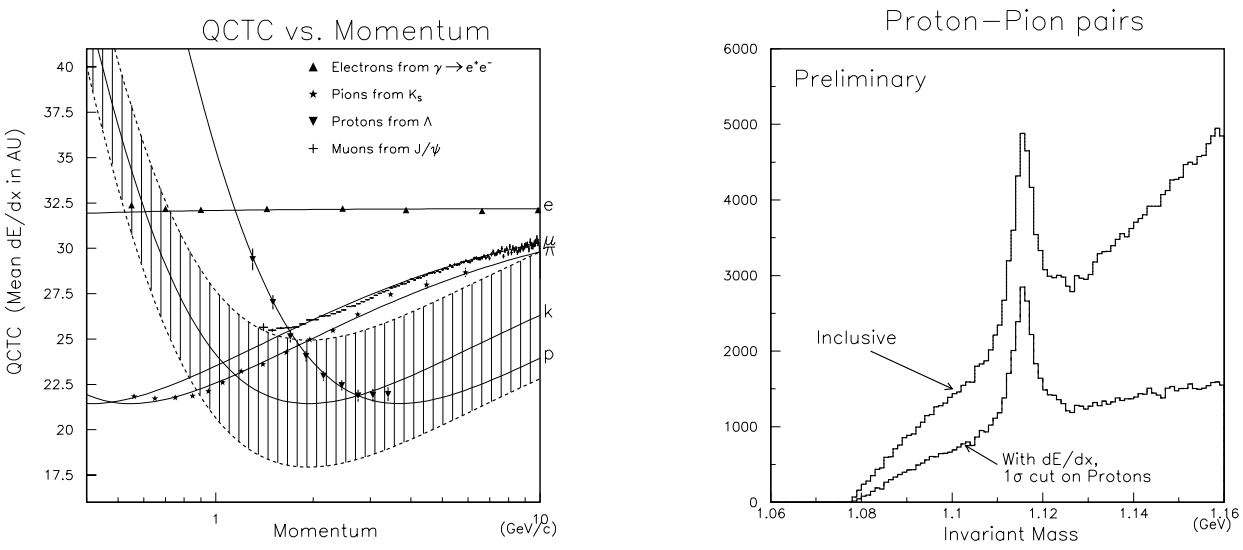

Figure 33: The CDF dE/dx system: mean energy loss for different particle species as measured in Run Ib data and application to $\Lambda \to p\pi$ decays in the J/ψ sample.

The extraction of the $\pi\pi$ signal will benefit greatly from the dE/dx system. Figure 33 (left) shows the mean energy loss as a function of momentum, extracted from the Run I data, for different particle species. The shaded band is the 1σ band around the kaon average value. It can be seen that we maintain a 1σ separation between the K and π signals for momenta > 2 GeV. The utility of the dE/dx system can be further seen in Figure 33 (right) where the invariant mass distribution for proton-pion pairs around the Λ^o mass is shown without dE/dx information (taking all track pairs and assigning them the p and π mass) and with a 1σ cut around the proton band. A clear improvement in the Λ signal can be seen. With the dE/dx information and the mass distribution we can extract the $B_d \to \pi\pi$ component from the total invariant mass distribution.

Another issue for this analysis is the combinatorial background under the B peak. Although in the Run Ia data we expect only a fraction of a signal event, we can estimate the background level for the Run I detector using the inclusive electron data sample. Using standard cuts on the decay vertex and the isolation of the two-track combination, we obtain an observed background, N, comparable to the expected signal, S, for $P_T > 4$ GeV on each track: $S/N \approx 1:1$. Lowering the P_T threshold to 2 GeV will allow us to double our efficiency. We expect to do this with the Run II detector while maintaining S/N better than 1:1 by exploiting the 3D information from the SVX II and optimizing cuts.

The final issue related to the extraction of the angle α from the measured CP asymmetry in $B_d \to \pi\pi$ is the extraction of possible penguin contributions in addition to the tree diagram which is expected to dominate this decay mode. We can estimate this penguin contamination, and thus extract α, from a combination of experimental measurements and theoretical inputs. In particular, a time-dependent analysis yields a measurement of the amplitude as well as the phase of the CP asymmetry, which oscillates with the mixing frequency. This latter phase would be zero in the absence of a penguin contribution. In addition, we use the average branching ratio $\left(Br(B^0 \to \pi^+\pi^-) + Br(\bar{B}^0 \to \pi^+\pi^-)\right)/2$. This quantity can be extracted

from untagged $B_d \to \pi\pi$ decays and will therefore have a very small error. Other ingredients are the value of $Br(B \to \pi\ell\nu)$ (which will be available from CLEO and possibly CDF as well) and some theoretical input such as the magnitude of the tree diagram given $Br(B \to \pi\ell\nu)$. As an example, if the penguin amplitude, A_p, is small compared to the tree amplitude, A_t, (say, $A_p/A_t = 0.07$ as predicted by Deshpande *et. al.* [57]) the extraction of α is relatively easy, and the theoretical constraints can be relatively crude. If $A_p/A_t \approx 0.2$, this becomes more challenging, but feasible. A detailed analysis can be found in reference [58].

In conclusion, modulo the uncertainty in extracting α from the CP asymmetry, assuming a flavor-tagging efficiency of 8% as in the $J/\psi K_s$ case, and a conservative $S/N = 1/4$, we expect an overall uncertainty on $\sin(2\alpha)$ of ± 0.10.

5.2.3 CP Asymmetry in $B_s \to J/\psi\phi$

While the CP asymmetry in $B_d \to J/\psi K_s$ measures the weak phase of the CKM matrix element V_{td}, the CP asymmetry in $B_s \to J/\psi\phi$ measures the weak phase of the CKM matrix element V_{ts}. This latter asymmetry is very small in the Standard Model, but in the context of testing the Standard Model has the same fundamental importance as measuring the more familiar CP asymmetries. This measurement is unique to experiments at a hadron collider.

Our Run Ia B_s mass analysis indicates that our yield of reconstructed $B_s \to J/\psi\phi$ events is 60% that of $B_d \to J/\psi K_s$. Since the modest trigger improvements for $B_d \to J/\psi K_s$ ($\approx 20{,}000$ events) apply equally to $B_s \to J/\psi\phi$, we can expect ≈ 12000 events for this decay mode in Run II.

The flavor tagging techniques described for the B_d case apply also to the B_s with one exception: The fragmentation track correlated with the B_s meson is a kaon instead of a pion. A PYTHIA study indicates that a time-of-flight system, by identifying kaons, would allow us to increase the efficiency of the same-side algorithm from 2% to 5%[51]. Thus, we assume a total flavor tagging efficiency for B_s mesons of 11%.

The magnitude of a CP asymmetry in $B_s \to J/\psi\phi$ decays would be modulated by the frequency of B_s oscillations. Thus, for a meaningful limit, we must be able to resolve B_s oscillations. If we neglect resolution effects, we can expect a precision on the asymmetry of ± 0.09. However, resolution effects smear the oscillations and produce an additional dilution. For our Run I data, if we determine the primary vertex event-by-event, the proper lifetime resolution for fully reconstructed B decays is $\approx 30\mu$m[59]. We expect that the proper lifetime resolution for the SVX II will be $\approx 10\%$ better than that for the Run I detector[60]. Figure 34 shows our expected precision on the asymmetry as a function of x_s.

5.2.4 Feasibility of measuring γ

Measuring the third angle, γ, in the CP triangle completes the test of the unitarity of the CKM matrix. The angle gamma can be probed[61] via the decays

1. $B_s^0 \to D_s^- K^+$ and $D_s^+ K^-$

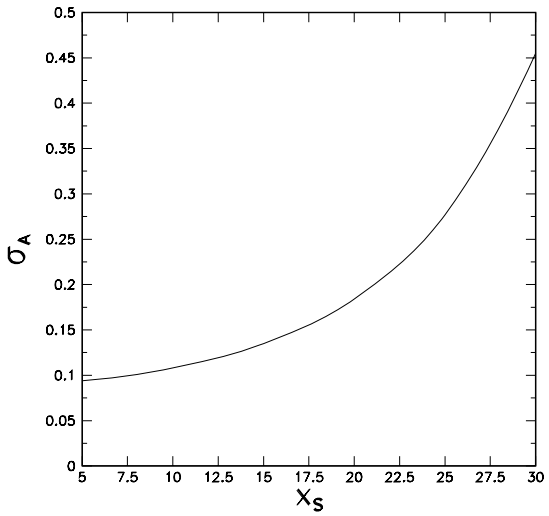

Figure 34: The uncertainty on the CP asymmetry for $B_s \to J/\psi\phi$ as a function of the B_s mixing parameter x_s

2. $B^+ \to \bar{D}^0 K^+$, $B^+ \to D^0 K^+$, and $B^+ \to D^0_{CP+} K^+$,

where D_{CP+} refers to the even CP state $(|D^0\rangle + |\bar{D}^0\rangle)/\sqrt{2}$.

These decay modes have been considered in reference[62]. As with the $B^0 \to \pi^+\pi^-$ decay mode, this analysis must trigger on all-hadronic decay modes. Assuming a Level-1 trigger of two tracks with opposite sign and $P_T > 2$ GeV, and a Level-2 trigger cut of 100μm on the impact parameter, we expect an overall efficiency times acceptance $\approx 3 \times 10^{-4}$ for the B_s and $B^\pm$ decay modes above.

Unfortunately, the decay mode $B^0_s \to D^-_s K^+$ and $D^+_s K^-$ involves a time-dependent analysis and therefore its utility depends on the B_s mixing parameter, x_s. Moreover, the results in reference [62] indicate that a very small tagged signal is expected.

The charged B modes are more interesting since the observation of an asymmetry between B^+ and B^- would indicate the presence of direct CP violation. Experimentally, measurement of the asymmetry involves only time-integrated quantities; the decays are also self-tagging. The uncertainty on the observed CP asymmetry is now a function of (a) the angle γ and (b) the strong phase difference, δ. In the most favorable case, $\gamma = \pi/2$ and $\delta = \pi/2$. Then the CP asymmetry, A_{CP}, and the uncertainty on it, δA_{CP}, are $A_{CP} = 0.2$ and $\delta A_{CP} = 0.05$ respectively. The detailed discussion of the uncertainty on A_{CP} is contained in[62].

5.3 Determination of $|\frac{V_{td}}{V_{ts}}|$

Within the CKM model, $|\frac{V_{td}}{V_{ts}}|$ is constrained at 95% confidence level to lie in the range[53]:

$$0.11 \leq \left|\frac{V_{td}}{V_{ts}}\right| \leq 0.36 \tag{1}$$

Experiments operating on the $\Upsilon(4S)$ can determine $|\frac{V_{td}}{V_{ts}}|$ by measuring the ratio of decay rates of radiative B decays $B(B \to \rho\gamma)/B(B \to K^*\gamma)$[63]. However, recent studies [64] have shown that such decays have potentially large long-distance contributions, making extraction of $|\frac{V_{td}}{V_{ts}}|$ difficult.

In contrast, experiments at hadron colliders can also use B_s mesons, which are amply produced, and determine $|\frac{V_{td}}{V_{ts}}|$ using several independent techniques, including some with quite small theoretical uncertainties as discussed below. Combining these techniques, CDF should, with 2 fb^{-1} of data, not only be able to constrain $|\frac{V_{td}}{V_{ts}}|$, but also *measure* its value over the full range permitted by the Standard Model.

5.3.1 B_s Mixing

Mixing in the B system has been discussed extensively in the literature[53]. In the Standard Model, this mixing occurs dominantly through top contributions to the electroweak box diagram. The size of the mixing is expressed in terms of the mixing parameter $x \equiv \Delta m/\Gamma$ where Δm is the difference in mass between the heavy and light B meson states and Γ is the average lifetime of the states. The value of x depends on the top quark mass, the B decay constant, the QCD bag parameter and corrections due to the breaking of SU(3) flavor symmetry. Theoretical uncertainties in the determination of the CKM parameters can be greatly reduced by considering the ratio of x_s to x_d:

$$\frac{x_s}{x_d} = \frac{(m_{B_s}\eta_{QCD}^{B_s} B f_{B_s}^2)}{(m_{B_d}\eta_{QCD}^{B_d} B f_{B_d}^2)} \left|\frac{V_{ts}}{V_{td}}\right|^2 \tag{2}$$

In the limit of SU(3) symmetry, the factors in front of the ratio of CKM elements would be unity. Lattice Gauge theory determines the value of these factors to be 1.3 ± 0.2[65]. Since x_d/x_s depends on $|\frac{V_{td}}{V_{ts}}|^2$, the theoretical uncertainty on $|\frac{V_{td}}{V_{ts}}|$ is $\sim 10\%$.

Because x_s is large, it must be determined by fitting the time-dependent oscillation

$$Prob(B_s \to \overline{B_s}) = \frac{1}{2} e^{-t/\tau} \left(1 - \cos(x_s t/\tau)\right) \tag{3}$$

The quality of the measurement depends upon the experimental proper decay time resolution and its ability to tag the flavor of the B at production time. CDF has already performed a measurement of x_d (see Figure 35), demonstrating that flavor tagging is possible in the

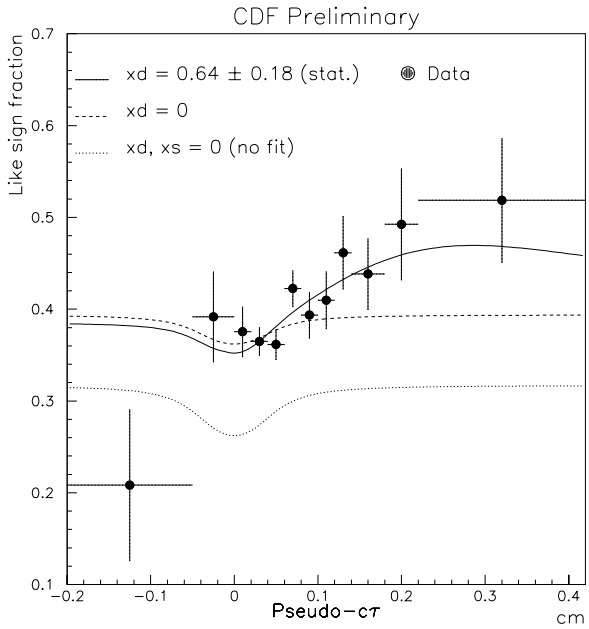

Figure 35: Results of a fit to the like-sign fraction vs proper lifetime in Run Ia dimuon events. For this fit, maximal x_s mixing is assumed. Overlaid are also the fits obtained if x_d is set to zero.

hadron collider environment. Because B_s oscillations are rapid, an x_s measurement will place stringent demands on the experiment's ability to determine the proper time of the decay.

Vertexing requirements for the x_s measurement are discussed in detail in Reference [66]. In general, the proper time resolution can be parameterized in terms of two constants

$$\sigma_t = \sqrt{a^2 + b^2 t^2} \tag{4}$$

Here a is determined from the resolution on the primary and secondary vertex positions and b depends on the accuracy with which the momentum of the B is known. The decay time t and its uncertainty σ_t are measured in units of proper time, relative to one B lifetime.

For the Run Ia B_s lifetime measurement[67], CDF reconstructed 70 $B_s \to D_s \ell\nu$ events. For Run II, triggering and reconstruction of this channel with very high statistics is straightforward, and our x_s reach will be limited by our proper lifetime resolution. Simulation studies of the SVX II detector[60] have determined that for semileptonic decays $a = 0.11$ and $b = 0.15$, thus knowledge of the B momentum limits the measurement to values of $x_s <\sim 11$. However, improvements in the analysis technique may result in an improved momentum resolution. For example, 3D vertexing allows a determination of the four-momentum of the missing neutrino, although with a quadratic ambiguity.

For fully reconstructed decays $a = 0.06$ and $b = 0.036$[68]. This value of a is based on our Run I proper lifetime resolution using fully reconstructed B events for which we determine

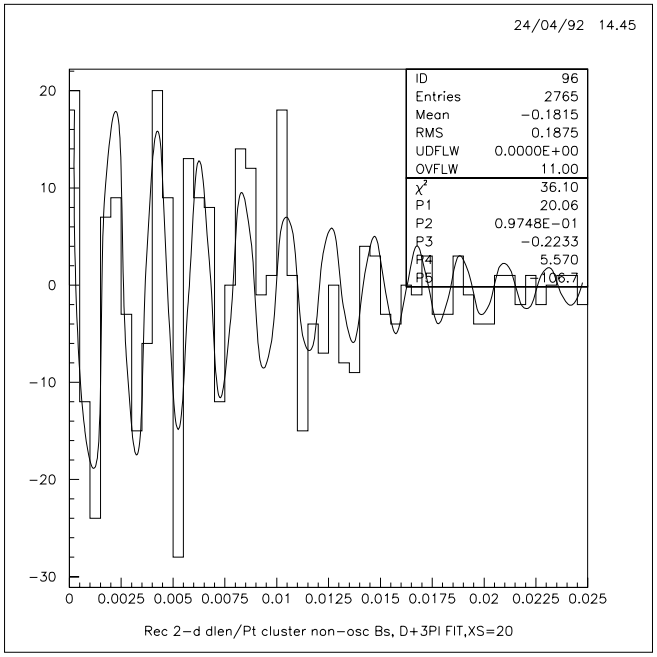

Figure 36: A Monte Carlo simulation of the reconstructed B_s mixing signal for a Run II sample with the upgraded CDF detector. The units of the abscissa are cm/GeV/c.

the primary vertex event by event, as in the section on the CP asymmetry in $B_s \to J/\psi\phi$. Thus, the ultimate x_s reach for fully reconstructed decays is set by the vertex resolution. Figure 36 shows that oscillations can still be clearly resolved in the SVX II for $x_s = 20$.

In order to determine the flavor of the B_s at the time of the decay this measurement requires events of the type $B_s \to D_s n\pi$. The challenge for CDF is to trigger on, and isolate from background, signals of this type. We note that the presence of a Time-of-flight system in CDF should significantly improve the reconstruction efficiency by allowing efficient selection of kaons and rejection of pions at low P_T, where the backgrounds are largest.

One strategy is to trigger on a single lepton (e or μ), which will serve as the flavor tag and then reconstruct B_s decays in this sample [66]. For a 6 GeV lepton threshold in Run II, there will be $\sim 2 \times 10^3$ B_s mesons that have decayed within the CDF fiducial volume to the modes $B_s \to D_s + \pi$ and $B_s \to D_s + 3\pi$ with $D_s \to \phi\pi$ or $D_s \to K^{*\pm}K^{\mp}$. It is not yet known how many of these may be reconstructed with good signal-to-noise. It is likely that the lepton trigger threshold will be lower, and also that some of the decay products of the B_s will be included in the trigger requirement as well.

Another strategy is to use a fully hadronic trigger, as for $B \to \pi^+\pi^-$, in which case all tagging techniques may be applied. The final states of the B_s we are trying to reconstruct are produced an order of magnitude more frequently than $B \to \pi^+\pi^-$. More work is needed to design such a trigger; one possibility is a two-track trigger optimized for $\phi \to K^+K^-$.

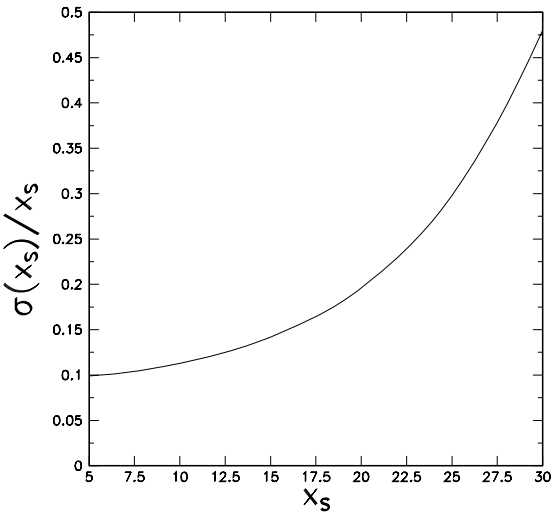

Figure 37: Relative uncertainty on x_s for fully reconstructed B_s decays.

Although we do not have a solid projection of how many events we will reconstruct, we show in Figure 37 our precision on x_s if we succeed in reconstructing 2000 events from fully hadronic triggers, with an effective tagging efficiency of 11%, or equivalently, 800 events recontructed in events with a lepton trigger.

5.3.2 $\Delta\Gamma_s/\Gamma_s$

The calculation of x_s depends upon the evaluation of the real part of the mass matrix element. The imaginary part of the same matrix describes the decay widths of the two mass eigenstates B_s^H and B_s^L. Within the Standard Model it is possible to calculate the ratio $\Delta\Gamma_{B_s}/\Delta m_{B_s}$[69]:

$$\Delta\Gamma_{B_s}/\Delta m_{B_s} = -\frac{3}{2}\pi\frac{m_b^2}{m_t^2}\frac{\eta_{QCD}^{\Delta\Gamma_{B_s}}}{\eta_{QCD}^{\Delta m_{B_s}}} \tag{5}$$

where the ratio of the QCD factors in the numerator and denominator is expected to be of order unity. This ratio does not depend on CKM parameters. Thus, a measurement of $\Delta\Gamma_{B_s}$ determines Δm_{B_s} up to QCD uncertainties. Moreover, the larger Δm_{B_s} becomes the larger $\Delta\Gamma_{B_s}$ is. Thus, as it becomes more difficult to measure x_s, $\Delta\Gamma$ becomes more accessible. Using the above expression, Browder *et al.* [70] show that if $x_s = 15$, a 7% difference in lifetime is expected.[2] They estimate that the uncertainties in calculating $\Delta\Gamma/\Delta m$ contribute

[2]This large $\Delta\Gamma_{B_s}$ is possible because there are large branching fraction common decay modes available to the B_s and $\overline{B_s}$ (eg $D_s^{(*)+}D_s^{(*)-}$).

an uncertainty of $\sim 30\%$ on $|\frac{V_{td}}{V_{ts}}|^2$ (*i.e.* a 15% uncertainty on $|\frac{V_{td}}{V_{ts}}|$). This contribution is in addition to the 10% uncertainty discussed in the previous section.

Several techniques can be used to determine $\Delta\Gamma_{B_s}$[71]. First, the proper time distribution of a flavor-specific B_s mode (*eg.* $B_s \to D_s \ell\nu$) can be fit to the sum of two exponentials. Second, the average lifetime of such a flavor specific mode can be compared to the lifetime of a mode that is dominated by a single CP state (it is expected that $B_s \to J/\psi\phi$ will be such a mode)[72]. Finally, a decay such as $B_s \to J/\psi\phi$ can be decomposed into its two CP components (via a helicity analysis) fitting a separate lifetime for each component.

The smallest systematic uncertainties on the lifetime difference will, however, certainly come from the study of $B_s \to J/\psi\phi$ decays. Using Run Ia data, CDF has measured the helicity structure of the decays $B \to J/\psi K^*$ and $B \to J/\psi\phi$ [73]. The preliminary results are $\Gamma_L/\Gamma = 0.64 \pm 0.10 \pm 0.04$ for $B \to J/\psi K^*$. Moreover, these measurements show that the physics of decays can be studied in a hadron collider environment.

The statistical uncertainty on the B_s lifetime from semileptonic B decays in Run II will be well below 1%. CDF reconstructed ~ 35 $B_s \to J/\psi\phi$ events in Run Ia. The Run II expectation, including only the modest set of trigger improvements described in section 5.2.1, is therefore $\sim$ 12000 events. Thus the $B_s \to J/\psi\phi$ helicity structure should be known to about 1% [3]. Using the current CDF number for the $B_s \to J/\psi\phi$ helicity structure, then in 2 fb^{-1}, the lifetime difference could be determined to $2-3\%$. Including current theoretical uncertainties of 18%, this determination of $\Delta\Gamma_{b_s}$ would either measure $|\frac{V_{td}}{V_{ts}}|$ or set an *upper* bound on $x_s \leq 15$.

5.3.3 Radiative B Decays

In the absence of long distance effects, radiative B decays provide an alternative approach for measuring $|\frac{V_{td}}{V_{ts}}|$.

$$\frac{B(B^- \to \rho^-\gamma)}{B(B^- \to K^{*-}\gamma)} = \frac{B(B^0 \to \rho^0\gamma) + B(B^0 \to \omega\gamma)}{B(B^- \to K^{*0}\gamma)} = \left|\frac{V_{td}}{V_{ts}}\right|^2 \xi\Omega \qquad (6)$$

where Ω is a phase space correction and ξ is a model dependent factor in the range 0.58 - 0.81[63]. The relative rates for $\rho^0\gamma$ and $\omega\gamma$ decays are equal in the quark model. Based upon a 2 pb^{-1} sample containing 13 $K^*\gamma$ candidates (with an estimated background of 1.9) and 2 $\rho\gamma + \omega\gamma$ candidates (with an estimated background of 4.1), CLEO has used this technique to set a bound on $|\frac{V_{td}}{V_{ts}}|$ in the range 0.64 - 0.76 depending upon theoretical model[74].

CDF has already installed a trigger to collect radiative penguin decays (see Reference [75] for details). The limited bandwidth available in the current trigger and data acquisition system require the trigger to have quite high thresholds (10 GeV photon plus two 2 GeV

[3] The systematic uncertainties in the polarization measurements are dominated by the estimate of the size and helicity of the background under the B mass peak. These systematic uncertainties should scale with the square root of the number of events in the sample.

tracks). The expected yield with this trigger is $\approx 20\ \gamma K^*$ events per 100 pb^{-1}. In Run II, we expect to lower the photon E_t threshold to 5 GeV and the track P_t threshold to 1.5 GeV, with a resulting yield of ~ 135 events per 100 pb^{-1} or ~ 2700 for 2 fb^{-1}.

The mass resolution of the reconstructed B is dominated by the resolution on the photon energy and is ~ 140 MeV. We have studied our ability to reject combinatorial background using Run 1A photon data and have studied with Monte Carlo the discrimination against $B \to K^*\pi^0$ and $\rho\pi^0$ and from higher multiplicity penguin decays[75]. These backgrounds are manageable. However, the offline cuts to remove background are expected to reduce the signal by about a factor of 2. The mass resolution is not adequate to separate $\gamma\rho$ from γK^* on an event-by-event basis (see Figure 38); however, a statistical separation is possible. In addition, the CTC dE/dx system should provide 1σ K-π separation in the momentum range of interest.

These radiative B decays can also be observed using converted photons. The probability for a photon to convert ($\sim 5\%$) will be offset by a lower photon E_t threshold. Also, the mass resolution is ~ 5 times better than for the signals with unconverted photons, allowing a cleaner separation between $B \to \gamma K^*$ and $B \to \gamma\rho$.

At the Tevatron it is possible to study B_s penguin decays as well. Information on $|\frac{V_{td}}{V_{ts}}|$ can be obtained in the same manner as above from studying the ratio of $B(B_s \to \gamma K^*)/B(B_s \to \gamma\phi)$. The size of the B_s penguin sample is expected to be 1/2 to 1/3 the size of the B_d sample. Comparison of the two results would help constrain the size of the long distance contributions to the decays.

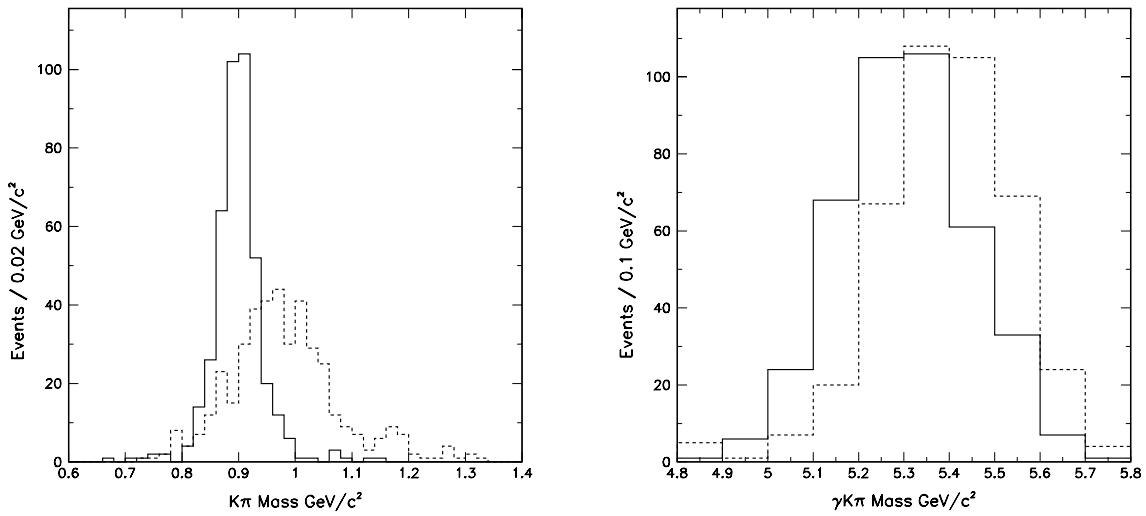

Figure 38: A Monte Carlo simulation for $B \to K^*\gamma$ (solid) and $B \to \rho\gamma$ (dashed) reconstructed as $B \to K^*\gamma$.

5.4 Rare B decays

Rare B decays provide a stringent test of the Standard Model for possible new physics effects, such as an anomalous magnetic moment of the W and the presence of a charged Higgs. Experimentally, these rare decays are accessible via the dimuon trigger. Using these triggers, CDF has performed a search for the decay modes $B^{\pm} \to \mu^+\mu^- K^{\pm}, B^0 \to \mu^+\mu^- K^{*o}$ and $B_{d,s} \to \mu^+\mu^-$, with competitive results. The Standard Model predictions[76] for the branching ratio for these decay modes, together with the CDF expected sensitivity in Run II, are listed in table 6. The projections for $B^{\pm} \to \mu^+\mu^- K^{\pm}$ and $B^0 \to \mu^+\mu^- K^{*0}$ conservatively assume the same signal-to-noise ($\sim 1:10$) as obtained for the Run Ia searches. We expect that a Run II analysis will easily achieve much improved signal-to-noise.

B Decay Mode	Standard Model	CDF Run II
$\mu^+\mu^- K^+$	0.6×10^{-6}	1.1×10^{-7}
$\mu^+\mu^- K^{*o}$	2.9×10^{-6}	3.4×10^{-7}
$B_d \to \mu^+\mu^-$	8.0×10^{-11}	1.0×10^{-8}
$B_s \to \mu^+\mu^-$	1.8×10^{-9}	4.0×10^{-8}

Table 6: Rare B decay modes, the predictions of the Standard Model for their Branching ratios, and the CDF sensitivity for Run II.

Assuming the Standard Model Branching ratios for $B^+ \to \mu^+\mu^- K^+$ and $B^0 \to \mu^+\mu^- K^{*o}$, we expect to have visible signals for these decays. In particular, we expect ≈ 400 $B^+ \to \mu^+\mu^- K^+$ and ≈ 650 $B^0 \to \mu^+\mu^- K^{*o}$ events. This will enable us to study both (a) the invariant mass distribution of the dimuon pair and (b) the forward-backward charge asymmetry in the decay. Both of these distributions are sensitive to physics beyond the Standard Model, e.g. the presence of a charged Higgs or charginos[77], [78].

We also expect to oberve the decays $B^{\pm} \to e^+e^- K^{\pm}$ and $B^0 \to e^+e^- K^{*0}$. The decays $B^{\pm} \to \ell^+\ell^+\pi^{\pm}$ and $B^0 \to \ell^+\ell^-\rho^0$ are suppressed by an order of magnitude, but will be observable if we can achieve a high enough level of signal-to-noise. An observation of these decay modes would provide another determination of $|V_{td}/V_{ts}|$.

5.5 V_{ub} and V_{cb}

As shown in Figure 29 CDF has cleanly reconstructed exclusive semileptonic decays in several channels in Run Ia. By the end of Run I, we expect several thousands of these events. In Run II, 3D vertexing will allow reconstruction of the four-momentum of the neutrino to within a quadratic ambiguity, thus making possible detailed studies of the dynamics of these semileptonic decays.

Currently, the theoretically most precise determination[70] of the CKM matrix element V_{cb} is obtained by comparing measurements of the rate for $B \to D^* \ell\nu$ decays, at the point of zero D^* recoil, with predictions from Heavy Quark Effective Theory (HQET). Although V_{cb} will be quite well known by Run II, CDF may be able to make a substantial contribution by performing the analysis with $\Lambda_b \to \Lambda_c \ell\nu$ decays. This provides a check of HQET in a different system. Also, the Λ_b may provide the most precise result, as the higher order corrections to HQET are simpler and smaller in magnitude for this system[79].

The CKM matrix element V_{ub} may be studied via exclusive semileptonic decays such as $B \to \rho\ell\nu$ and $B \to \pi\ell\nu$. For Run II, high statistics observations should be possible. The challenges will be to isolate the exclusive modes from combinatorial background and decays with additional π^0s. A study with Run Ia electron triggers[80] shows that signal-to-noise of 1/2 or better can be attained, and an observation may be feasible by the end of Run I.

5.6 B_c Physics

The $B_c \equiv (\bar{b}c)$ meson is a deeply bound state of two heavy quarks for which non-relativistic potential models should reliably apply [81]. Since its constituents cannot annihilate into gluons, there is a rich spectroscopy of narrow states below BD threshold. Using a subset of Run I data CDF has searched for the decay mode $B_c \to J/\psi\pi$. The resulting 95% CL limit on the cross-section times Branching ratio relative to that for $B^+ \to J/\psi K^+$ using 75 pb^{-1} of data is shown in Figure 39. Assuming the predicted lifetime of 1.35 ± 0.15 ps, we are within an order of magnitude of the expected rate (although the predictions on the fraction for $b \to B_c$ are highly uncertain).

In Run II, with the modest set of improvements to the dilepton triggers discussed in the section on $\sin(2\beta)$, we will observe 800 $B_c \to J/\psi\pi$ events assuming the expected rate and lifetime. This will allow a precise measurement of the mass and lifetime of the B_c. There is also a possibility of studying the spectroscopy of excited states using the techniques CDF has used to reconstruct $\chi_c \to J/\psi\gamma$. We also expect a sizable signal in the $B_c \to J/\psi\ell\nu$ decay mode.

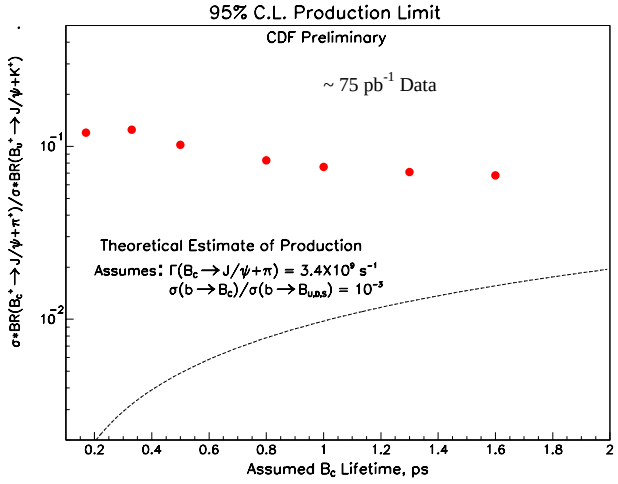

Figure 39: 95% CL limit on the production of $B_c^+ \to J/\psi\pi^+$ relative to $B^+ \to J/\psi K^+$. The dashed line is the theoretical prediction assuming a relative production ratio of 10^{-3} and a fixed width $\Gamma(B_c^+ \to J/\psi\pi^+) = 3.4 \times 10^6$ ps^{-1}.

6 Exotic Physics

6.1 Introduction

The Standard Model has continued to agree well with increasingly precise experimental results from the Tevatron, LEP, and elsewhere. However, it is not complete because it does not answer several fundamental questions: it does not predict the masses of the particles or the number of generations; it does not explain the symmetry breaking energy scales; it has a proliferation of arbitrary parameters; and it does not address the question of grand unification. There are many alternate theories which address these issues, for example Supersymmetry, Technicolor, Compositeness, and various schemes of Grand Unification. All of the new theories predict new particles and interactions. The prediction of these new theories must be tested with experiment. The Tevatron is one of the best places to explore physics beyond the Standard Model and will continue to be during the Main Injector era. To date, most of the highest limits in direct searches for physics beyond the Standard Model come from CDF. In Run II, with the luminosity increase and the proposed detector upgrades, CDF's reach will be extended even further. We will discuss the progress which CDF has made in the search for new physics and how it will improve with luminosity and the proposed detector upgrades. Our extrapolations assume the proposed detector upgrades, which are necessary to maintain our capability of detecting high E_T jets, photons, and isolated leptons with high efficiency in the future high luminosity environment. All quoted limits are at 95% confidence level, and for simplicity we define mass reach as the largest excluded mass at 95% CL [82, 83].

6.2 New Gauge Bosons W' and Z'

Heavy W bosons, W', occur in the left-right symmetric model [84] of electroweak interactions $SU(2)_R \times SU(2)_L \times U(1)_Y$. CDF has searched for $W' \rightarrow l\nu$ in the electron and muon channels [85, 86]. The analysis of Run Ia electron data yielded the world's best limit of $M_{W'} > 652$ GeV/c^2, assuming Standard Model couplings, and is shown in Figure 40a. Extrapolating to a Run II luminosity of $2fb^{-1}$ we predict that the mass reach can be extended to 990 GeV/c^2 in the $W' \rightarrow e\nu$ mode. See Figure 43a. We have also performed a new search for W' decaying to WZ [87] and set bounds of $205 < M_{W'} < 400$ GeV/c^2, as shown in Figure 40b.

Heavy neutral gauge bosons in addition to the Z^0, generically denoted as Z', occur in any extension of the Standard Model that contains an extra U(1) after symmetry breaking. For example, in one model with E_6 as the grand unified gauge group [88] there exists a Z_ψ from the symmetry breaking $E_6 \rightarrow SO(10) \times U(1)_\psi$ and a Z_χ from the symmetry breaking $SO(10) \rightarrow SU(5) \times U(1)_\chi$. Finally the SU(5) symmetry breaks to recover the Standard Model: $SU(5) \rightarrow SU(3)_C \times SU(2)_L \times U(1)_Y$. In superstring inspired E_6 models there exists a Z_η which is the linear combination $Z_\eta = \sqrt{3/8}Z_\chi + \sqrt{5/8}Z_\psi$. In each running period (88/89,

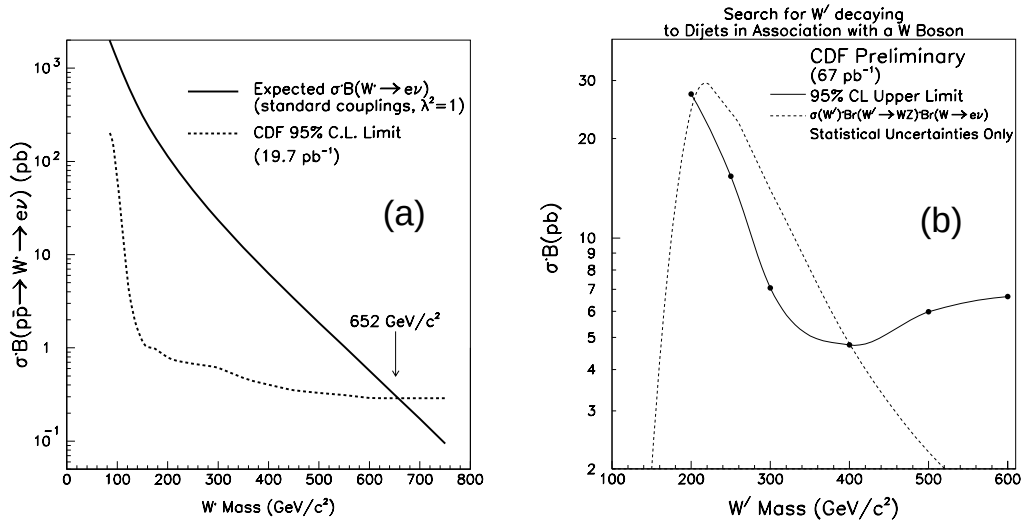

Figure 40: Limits are shown for (a) $W' \to e\nu$ and for (b) $W' \to WZ \to e\nu + dijet$.

Run Ia, and Run Ib), we have searched for $Z' \to ll$ and set the world's best mass limit. Most recently, we have analysed 70 pb^{-1} of Run Ia and Ib data in both dimuon and dielectron decay modes. Figure 41 shows the invariant mass distributions of dimuons and dielectrons in the Z' search data sample and the comparison of data with background predictions. From this analysis, we set the current best limit of $M_{Z'} > 650$ GeV/c^2 for Standard Model couplings. This experimental limit can be applied to compare with many specific models. For example, in Run Ia we set the lower mass limits for Z_ψ, Z_η, Z_χ, Z_I, Z_{LR} and $Z_{\rm ALRM}$ to be 415, 440, 425, 400, 445, and 420 GeV/c^2. Extrapolating to Run II we predict that the mass reach can be extended to 900 GeV/c^2, assuming Standard Model couplings and to about 800 GeV/c^2 for the specific cases mentioned above, assuming $\sqrt{s} = 1.8$ TeV. (Extrapolated mass limits are higher by approximately 100 GeV/c^2 if we assume $\sqrt{s} = 2.0$ TeV.) See Figure 43a.

6.3 New Particles decaying to Dijets

Many theories predict particles which decay to dijets. These would appear as bumps in the dijet mass spectrum. The existence of a larger chiral color group, $SU(3)_L \times SU(3)_R$, would lead to massive color-octet axial vector gluons, axigluons, which would be produced and decay strongly giving a very large cross section times branching ratio to dijets [89, 90]. A recent technicolor model [91, 92] predicts a color octet technirho (ρ_T) which couples to $q\bar{q}$ and gg via a gluon. Superstring inspired E_6 models predict the existence of many new particles [93] including a color triplet scalar diquark $D(D^c)$ with charge $-(+)\frac{1}{3}$ which couples to $\bar{u}\bar{d}(ud)$. Continuing our Run Ia search [94], in Run Ib we have searched for resonance and set limits on these theories. At high mass, the data are consistently higher than the QCD monte carlo prediction. This issue is discussed in more detail in the QCD section of this document. See section 4.2. To search for high mass resonances, we compare the data with a curve obtained from a fit to the data. Figure 42a shows the fractional difference between the data and the fit (see Figure 44 for the form of the fitting function). We observe some excess

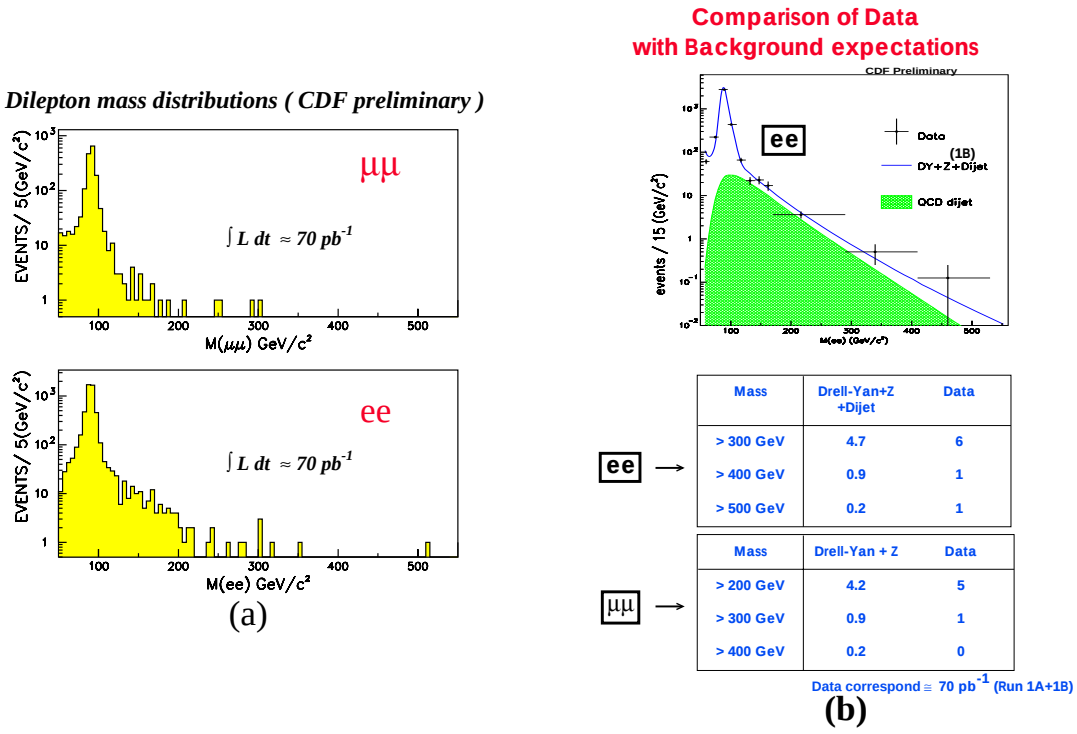

Figure 41: (a) The dimuon and dielectron invariant mass distributions for the Z' search data sample are shown. (b) The data are compared to background predictions.

events in the mass region around 550 GeV/c^2, but it is not statistically significant. The cross section times branching ratio limits which we derive are shown as a function of dijet mass in Figure 42b along with the resulting limits for various specific models. The predictions for Run II are shown in Figure 43b and listed in Figure 50.

6.4 Topcolor Theory and b tagged dijet Search

The large mass of the top quark suggests that the third generation may be special. This has motivated the Topcolor model [95, 96, 19] which assumes that the top mass is large mainly because of a dynamical $t\bar{t}$ condensate generated by a new strong dynamics coupling to the third generation. It predicts massive color octet bosons, topgluons B, and a new gauge boson, Z'_{TopC}, from an additional $U(1)$ symmetry. Both of these new particles couple largely to $b\bar{b}$ and $t\bar{t}$. Using CDF's b-tagging capabilities we have searched for topgluons B and Z'_{TopC} in the $b\bar{b}$ channel. Figure 44 shows the invariant mass distribution of b tagged dijets and limits on Z'_{TopC} and topgluons of various widths. A search is also underway in the $t\bar{t}$ mass distribution. See section 2.6.

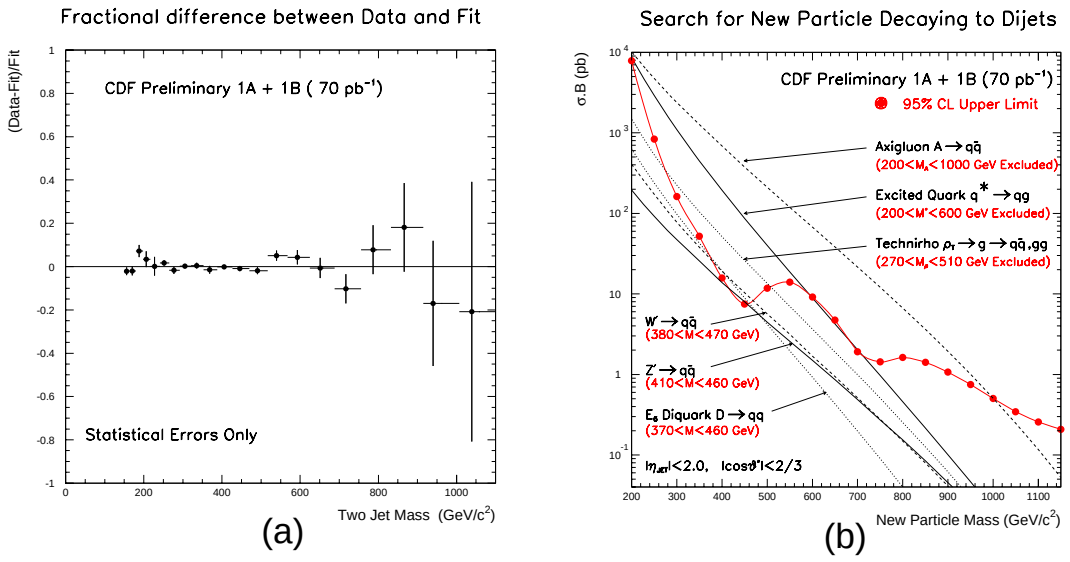

Figure 42: Fractional difference between the dijet mass data and a fit to the data are shown in (a), and the resulting mass limits are shown in (b).

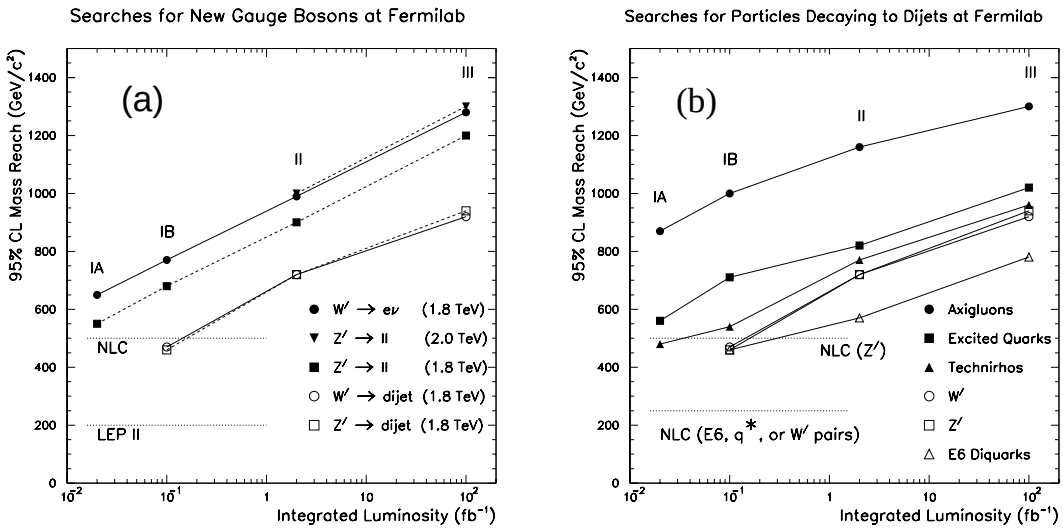

Figure 43: The expected mass reach, defined as the 95% CL lower limit on the mass, is plotted vs. integrated luminosity at the Tevatron. The maximum mass reach of other accelerators is shown for comparison. Searches for new gauge bosons are shown in (a), and searches for new particles decaying to dijets are shown in (b).

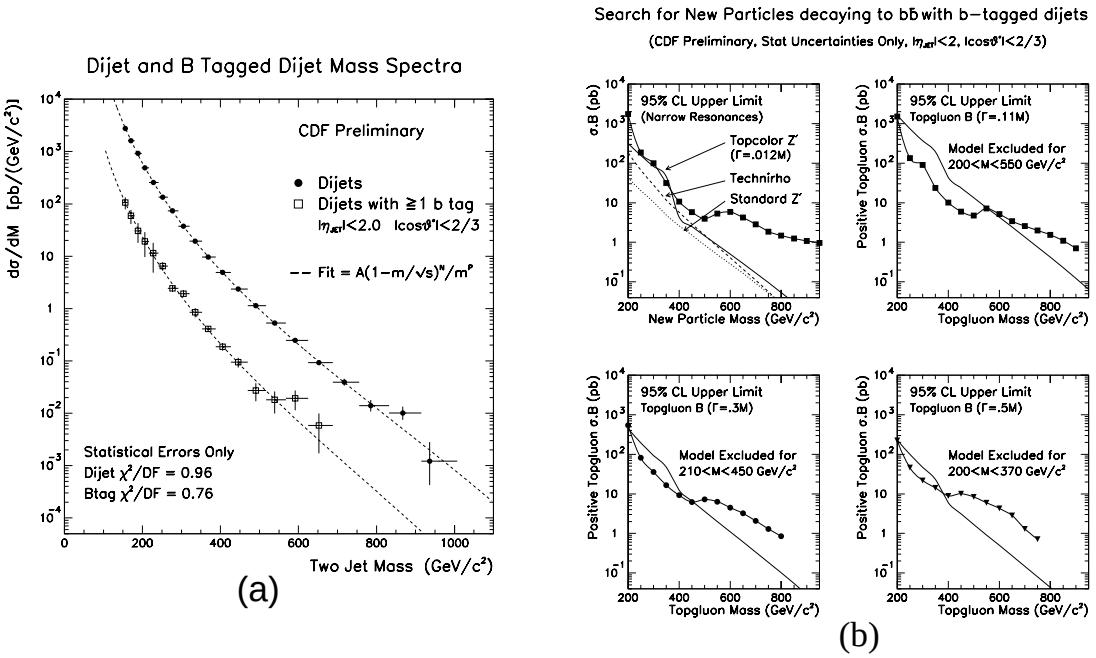

Figure 44: The invariant mass distribution of b tagged dijets is shown in (a), and the resulting limits on Z'_{TopC} and topgluons of various widths are shown in (b). Data used are from Run Ia.

6.5 Leptoquarks

Leptoquarks, color triplet particles coupling to a lepton and quark, appear in many extensions of the Standard Model [97, 93]. Leptoquarks are generally assumed to link, through an unknown coupling strength, quark and lepton multiplets of the same generation in order to prevent violation of bounds on rare decays of mesons and bounds on flavor changing neutral currents [97, 98]. We have searched for pair production of scalar leptoquarks. In the 88/89 run, we set the best first generation leptoquark mass limit of $M_{LQ1} > 113$ GeV/c^2 for $\beta = 100\%$ and $M_{LQ1} > 80$ GeV/c^2 for $\beta = 50\%$, where β is the branching ratio for a leptoquark decaying to a charged lepton and quark. Since then, HERA has improved the first generation limits. In Run Ia we set the world's best limit on second generation leptoquarks and have subsequently improved it with Run Ib data. The current best limit is $M_{LQ2} > 180$ GeV/c^2 for $\beta = 100\%$ and $M_{LQ2} > 140$ GeV/c^2 for $\beta = 50\%$. Figure 45 shows the limit on $\sigma \cdot \beta^2$ as a function of LQ2 mass and limits on β as a function of LQ2 mass. Extrapolating to Run II, we expect to extend the second generation mass reach to 300 GeV/c^2. We are also beginning the difficult but challenging search for third generation leptoquarks. As a first promising step in the analysis, we have identified $Z^0 \to \tau^+\tau^-$ decays where one of the τ decays leptonically and the other decays hadronically.

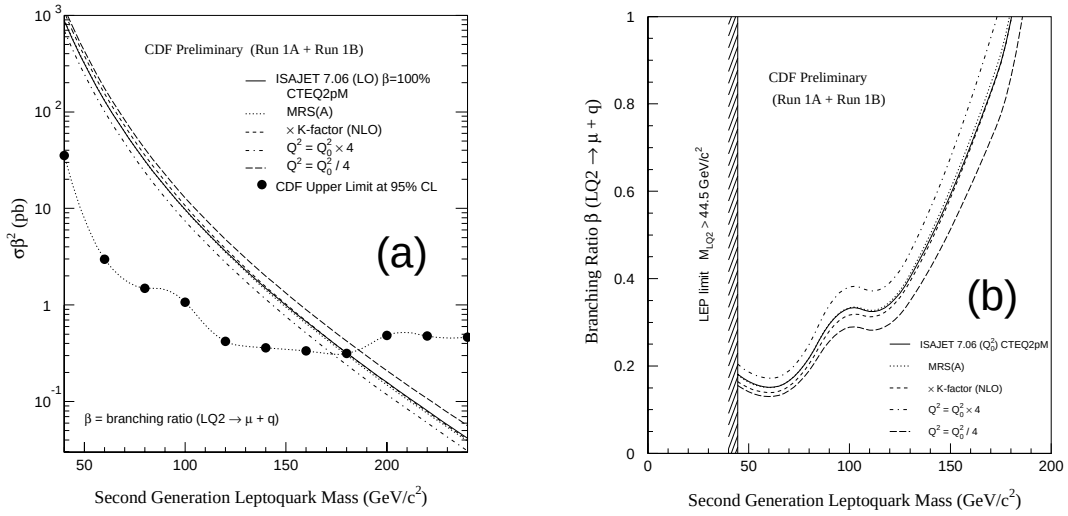

Figure 45: The limit on $\sigma \cdot \beta^2$ is shown as a function of LQ2 mass in (a), and the limit on β as a function of LQ2 mass is shown in (b). β values above the curves are excluded at 95 % C.L.

6.6 Compositeness

The standard model has a large number of parameters and particles. The possibility that these parameters and particles are composed of a smaller and simpler set is appealing. If quarks and leptons are composite particles we expect four-fermion contact interactions [99] to modify the quark and lepton production cross sections at high transverse momentum. Excited states [100] would also be expected and can be searched for in the invariant mass spectrum.

We have searched for an excess of events in the inclusive jet cross section which could result from the four quark contact interaction. As discussed in section 4.2 an excess of events is observed and is under investigation.

If quarks and leptons are both composite and share constituents, then effective contact interactions arise between them at low energies [99]. We have searched for the quark-lepton contact interaction in the dielectron [101] and dimuon [102, 103] channels by looking for an excess of high mass dileptons compared to the Drell-Yan prediction. We set limits on the lepton-quark compositeness scale of $\Lambda^- > 2.2$ TeV and $\Lambda^+ > 1.7$ TeV for electrons, where -(+) corresponds to the constructive (destructive) interference with the dominant up-quark contribution to the cross section. In the muon channel, the limits are $\Lambda^- > 1.6$ TeV and $\Lambda^+ > 1.4$ TeV. In Run II we expect to extend these to around 5 TeV.

Excited states of composite quarks, denoted q^*, have been searched for at UA2 [104] and CDF [105]. They would be produced singly by quark gluon fusion and could decay to a common quark and any gauge boson (g, γ, W or Z) [100]. Using the photon + jet and W + jet channels in the Run Ia data, we have excluded the mass region below 540 GeV/c^2 for the

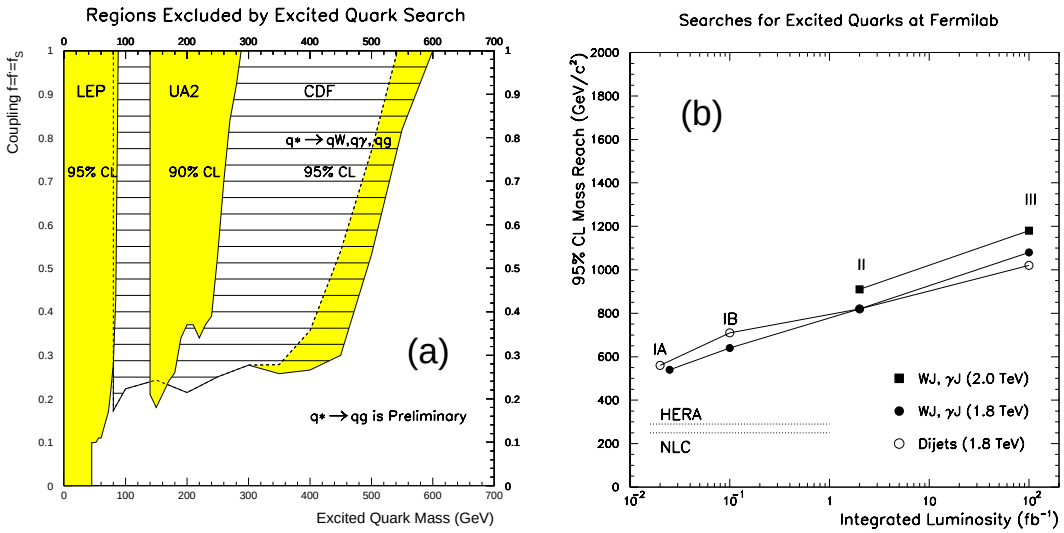

Figure 46: The mass regions currently excluded are shown in (a). The expected mass reach, defined as the 95% CL lower limit on the mass, is plotted vs. integrated luminosity at the Tevatron in (b). The maximum mass reach of other accelerators is shown for comparison.

simplest model of q^*[105]. We have also searched for q^* decaying into a dijet mode ($q^* \rightarrow qg$) with 70 pb^{-1} of Run Ia and Ib data, and we have excluded the mass range between 200 and 600 GeV/c^2 for the simplest model of q^* (Figure 42b). Extrapolating to a Run II luminosity of $2fb^{-1}$ we predict that the q^* mass reach can be extended to 820 GeV/c^2 in each of these decay modes. See Figures 46 and 50.

Currently the best limit for excited states of composite leptons, l^*, is set by a LEP experiment. The lower limit is 45 GeV/c^2 for pair production and 90 GeV/c^2 for single production. Recently, we have started an analysis searching for l^*. We expect that we will set a mass limit of several hundred GeV with the current data, and as for the q^* search, the mass reach will be substantially extended in Run II.

6.7 Massive Stable Particles

Massive stable particles are possible features of several theories for physics beyond the standard model including supersymmetry, mirror fermions, technicolor, and compositeness. We have searched in the 88/89 data for heavy stable charged particles [106, 107] based upon their expected high transverse momenta, relatively low velocities (via time of flight), and muon-like penetration of matter. We obtained upper limits on the cross-section for the production of heavy stable particles as a function of their mass. This can be translated into a mass limit from the cross-section for any particular theory and varies from about 140 GeV/c^2 for color triplets to 255 GeV/c^2 for color decuplets as shown in Figure 47b. This analysis is currently being extended using Run I data. In addition to time of flight, it will take advantage of the large ionization depositions, $\frac{dE}{dx}$, expected for massive particles. For example, see Figure 47a.

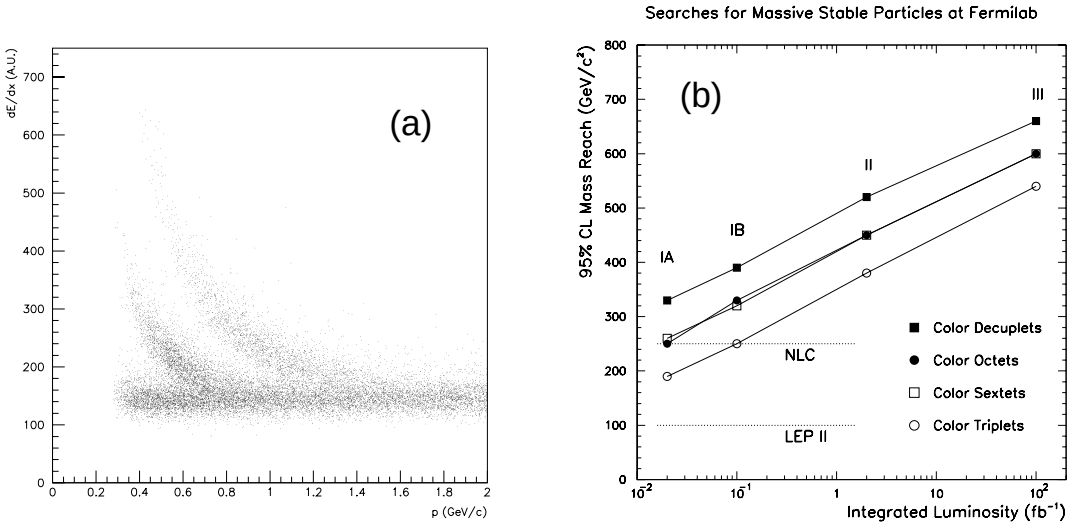

Figure 47: (a) A scatter plot of the $\frac{dE}{dx}$ vs momentum is shown for the Run Ib silicon detector after a cut has been applied on the $\frac{dE}{dx}$ from the main tracking chamber. Known particles (kaons and protons) can be clearly distinguished for $p < 1.2m$, i.e. $\beta < 0.6$. New massive particles would look similar but at higher momentum. (b) The expected mass reach is plotted vs. integrated luminosity at the Tevatron. The maximum mass reach of other accelerators is shown for comparison.

The extrapolations to Run II are shown in Figure 47b. The proposed time of flight system and the improvements in $\frac{dE}{dx}$ from the silicon upgrade could improve these results significantly by providing extra background rejection and allowing detection of massive particles out to even higher β.

6.8 Supersymmetry

Supersymmetric theories which solve the hierarchy problem of grand unified theories predict the existence of new supersymmetric particles having masses below 1 TeV/c^2. The Tevatron can explore a significant portion of the theoretical phase space of these theories, using several possible signatures. Using Run Ia data, two of the signatures have been searched for and are described below. One signature is tri-lepton events coming from chargino-neutralino ($\tilde{\chi}_1^{\pm}\tilde{\chi}_2^0$) pair production with the subsequent leptonic decays ($\tilde{\chi}_1^{\pm} \rightarrow \ell\nu\tilde{\chi}^0$ and $\tilde{\chi}_2^0 \rightarrow \mathrm{l\bar{l}}\tilde{\chi}^0$). The other signature is squark and gluino ($\tilde{q}$ and $\tilde{g}$) production followed by decays into $\not\!\!E_T$ plus multijets. Other searches underway within CDF are for the supersymmetric partner of the top quark ($\tilde{t}$ or stop) in both the single and dilepton modes, and for $\tilde{q}$ and $\tilde{g}$ production with decays to like-sign leptons.

6.8.1 Trilepton Search

The Run Ia CDF search for trilepton events from SUSY follows the straightforward path of requiring three well-identified and isolated electrons or muons, with removal of events

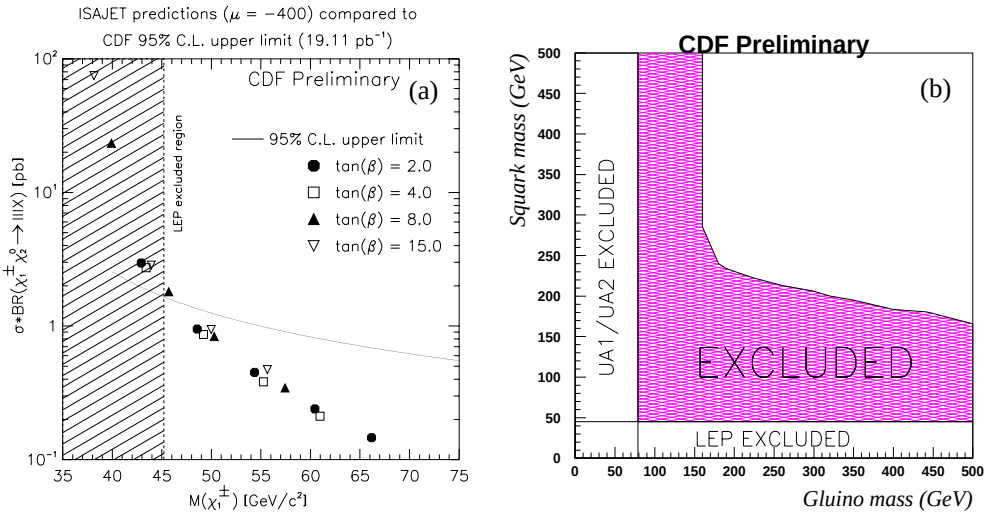

Figure 48: Illustrations of CDF limits on SUSY in a) trilepton, and b) jets plus $\not\!\!E_T$ channels: a) 95% confidence level upper limit on $\sigma \cdot BR(\tilde{\chi}_1^{\pm}\tilde{\chi}_2^0 \to 3\ell X)$ vs. $M(\tilde{\chi}_1^{\pm})$, where $BR(\tilde{\chi}_1^{\pm}\tilde{\chi}_2^0 \to 3\ell X)$ is the branching ratio for a single trilepton mode. The points are the predictions of ISAJET. The shaded region corresponds to the LEP limit [109]. b) Squark vs gluino mass space showing the region excluded at 95% by the current CDF Run Ia search. SUSY parameters are $\tan\beta = 4$, $\mu = -400$, slepton mass = 350 GeV/c^2. Also shown are the regions excluded by UA1/UA2 and LEP.

containing pairs of leptons which could come from J/Ψ, Υ, or Z decays[108]. No trilepton events were observed in 19.1 pb^{-1} of data. To turn this non-observation into a limit on SUSY models, an upper limit on production cross-section, $\sigma \cdot BR(\tilde{\chi}_1^{\pm}\tilde{\chi}_2^0 \to 3\ell X)$, is compared with predicted ISAJET cross-sections, as in Figure 48a. This figure shows the predictions from several different $\tan\beta$ values at $\mu = -400$ GeV. It is apparent that $M(\tilde{\chi}_1^{\pm}) < 46$ GeV/c^2 is excluded. This limit is comparable to the LEP results [109], which exclude chargino/neutralino masses below $M_Z/2$. Because of strong correlations between SUSY particle masses, the $\tilde{g}$ mass values which correspond to $M(\tilde{\chi}_1^{\pm}) = 46$ GeV/c^2 are 131, 149, 161, and 167 GeV/c^2 at $\tan\beta = 2$, 4, 8, and 15, respectively.

With larger data samples of 0.1-2.0 fb^{-1}, background estimates have shown that additional cuts are likely to be required to reduce backgrounds, particularly from $b\bar{b} + X$ semileptonic decays and from Drell-Yan+X or $Z + X$ events with misidentification of jets as leptons. Tighter lepton identification cuts are one possibility, or a $\not\!\!E_T$ cut can be employed.

Extrapolations of the chargino/neutralino search using the trilepton channel to higher integrated luminosities have been made by three groups [110, 111, 112]. The analyses in Refs. [110] and [112] are optimized for the search without a $\not\!\!E_T$ cut. It appears that the current limit of about 46 GeV/c^2 can be extended to 60 GeV/c^2 with 0.1 fb^{-1} of data (Run Ib), and to 105 GeV/c^2 with 2.0 fb^{-1} of data in Run II.

6.8.2 Multi-jet Plus $\not\!\!E_T$ Search

The Run Ia CDF search for multijet plus $\not\!\!E_T$ events from SUSY requires 3 or more jets and > 60 GeV of $\not\!\!E_T$. Additional cuts are imposed to reduce detector-related, cosmic ray, mismeasured QCD multijet, and W/Z plus jets backgrounds to a reasonable level. The removal of W/Z plus jets backgrounds requires rejection of events with electrons or muons. The final data sample of 36 events is comparable to a background estimate of 28.7 events which does not include any contribution from standard QCD multijet production. The background estimate contains W and Z leptonic, and top semileptonic decays. The W and Z backgrounds (lepton not observed) are normalized directly to the data, using multijet events in which a lepton is observed. We conclude that no significant excess is observed and set a conservative upper limit on potential SUSY contributions by assuming a zero background contribution from QCD mismeasurement. The current CDF preliminary limits are shown as an excluded region on the squark versus gluino masses plane in Figure 48b. The limits most comparable to LEP limits are on gluino mass. The present limits can be quoted as $M_{\tilde{g}} > 160$ GeV/c^2 for all $M_{\tilde{q}}$ and $M_{\tilde{g}} > 220$ GeV/c^2 when $M_{\tilde{g}} = M_{\tilde{q}}$.

The larger data samples of Run Ib and Run II will allow proportionally better determination of the backgrounds. However, since the analysis is background dominated, better limits will be obtained by tightening analysis cuts and perhaps fitting the shape of the $\not\!\!E_T$ spectrum. A first attempt to estimate the future improvement in this analysis by making a higher $\not\!\!E_T$ cut of 80 GeV and requiring 4 or more jets shows that with 0.1 fb^{-1} we can extend the search region to 250 GeV/c^2 for the case of equal squark and gluino masses. Previous extrapolations[113] have shown that an additional 30% can be gained in mass reach with 2 fb^{-1} over the limits with 0.1 fb^{-1}, i.e. we can search up to about 330 GeV/c^2 (equal squark/gluino masses) with such a data sample. Some help from theorists may be forthcoming when recent NLO calculations of squark pair production, showing cross-sections approximately double those of the leading order calculations, get extended to squark/gluino and gluino/gluino production.

6.8.3 Other SUSY Channels

Several other potential signatures for SUSY at the Tevatron are worth mentioning. First, the 'classic' jets plus $\not\!\!E_T$ analysis vetoes leptons to reduce W/Z/$t\bar{t}$ backgrounds. However, SUSY models predict that many squark and gluino decays occur through cascade decays to intermediate charginos and neutralinos, which can subsequently decay leptonically. Such decays are preferentially excluded from the current analysis, but can be isolated and separated from most backgrounds by demanding same-sign leptons. An analysis is well underway in CDF to discover or place limits on such SUSY decays using Run Ia data. Preliminary results of this search will appear soon.

Secondly, the SUSY partner of the top quark may have a mass significantly lower than other squarks. Although the production rate of stop quark pairs is an order of magnitude

smaller than the production of 'ordinary' top quark pairs for equal masses, it is still possible that the mass of stop is much lower than the top quark mass.

Third, slepton pairs can be produced in quark-antiquark collisions via virtual photons or Z's. Although the production cross-sections are typically low, there may be discovery potential just above the $M_Z/2$ mass limits from LEP.

These SUSY channels benefit greatly from large data samples. Unfortunately, in most SUSY models the squarks and gluinos are among the heaviest of SUSY particles. Because of this, relatively low-mass limits from LEP on charginos and neutralinos have in the past supplied the most stringent limits on SUSY models. Only with the Run Ia data has the Tevatron data begun to explore these models beyond LEP limits. With Ib data, we have a modest region of discovery potential. With 2 fb^{-1} from Run II, we can expect an interesting competition between improved SUSY searches from the Tevatron and the higher mass reach which will be accessed by LEP II at that time.

6.9 Summary

CDF has produced most of the current highest limits in direct searches for physics beyond the Standard Model. This experience allows us to make realistic predictions of how the additional luminosity obtained in Run II will substantially extend our reach for new physics, as summarized in Figures 49 and 50. These predictions require the proposed detector upgrades which are essential to maintain CDF's excellent capabilities for studying high p_T physics in the high luminosity environment of Run II. The prospects of exploring the regions opened to us in Run II are exciting.

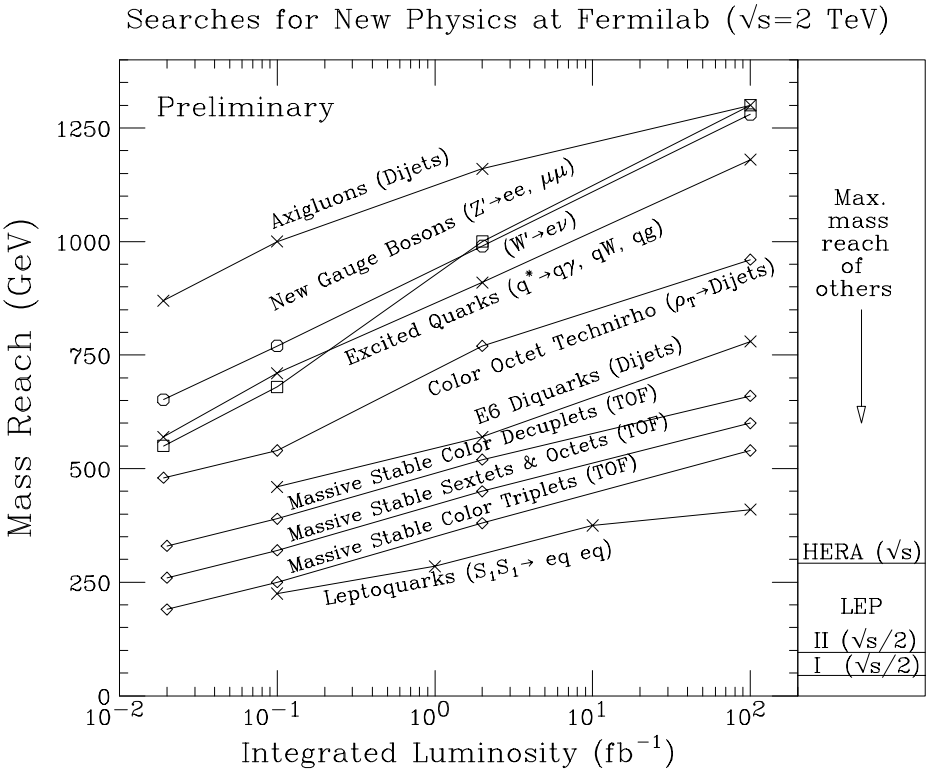

Figure 49: The mass reach, defined as the 95% CL lower limit on the mass, is plotted as a function of integrated luminosity at the Tevatron. The maximum mass reach of other accelerators is shown for selected processes.

CDF Exotic Particle Searches: Results and Run II Prospects

Searches	current limit (Gev) set by CDF		data set	run II (GeV) with 2 fb^{-1}
W'→ eν(SM)	< 652	*	1a (20 pb-1)	< 990
W'→ WZ	205<M<400	*	1a + 1b (70 pb-1)	
Z'→ *ll* (SM)	< 650	*	1a + 1b (70 pb-1)	< 900
$Z\psi, Z\eta, Z\chi, Z_I$	< 415,440,425,400	*	1a (20 pb-1)	< 800
Z_{LR}, Z_{ALRM}	< 445,420	*	1a (20 pb-1)	< 800
Axigluon→ qq	200<M<1000	*	1a + 1b (70 pb-1)	< 1160
Techniro →dijet	270<M<510	*	1a + 1b (70 pb-1)	200<M<770
W'→ qq (SM)	380<M<470	+	1a + 1b (70 pb-1)	200<M<720
Z'→ qq (SM)	410<M<460	+	1a + 1b (70 pb-1)	290<M<720
E_6 Diquark→ qq	370<M<460	*	1a + 1b (70 pb-1)	200<M<570
topgluon Γ=.1M	200<M<550	*	1a (20 pb-1)	
topgluon Γ=.3M	210<M<450	*	1a (20 pb-1)	
topgluon Γ=.5M	200<M<370	*	1a (20 pb-1)	
Leptoquark (μq)	< 180, (β=1)	*	1a + 1b (70 pb-1)	< 300
Composit. Scale (qqqq)	< 1800	*	1a + 1b (70 pb-1)	< 2200
Composit. Scale (qq*ll*)	2200, 1700 (ee) 1600, 1400 (μμ)	*	'88-89 (4pb-1)	< 5000
q* (W+jet, γ+jet)	< 540	*	1a (20 pb-1)	< 820
q*→ dijet	200<M<600	*	1a + 1b (70 pb-1)	<820
massive stable ptl.,	< 140 to < 255	*	'88-89 (4pb-1)	<350/<520
susy particles	see figures in the susy section	#	1a (20 pb-1)	

* Current world best limit in direct search mode for the model.

\+ CDF has the world best limit in another decay mode.

\# Same as *, but D0 also has comparable limits.

Figure 50: A summary is given of the CDF's searches for physics beyond the standard model along with the prospects for Run II.

7 Conclusions

The Tevatron Collider is the world's highest energy machine, the only source of the top quark, the most prolific (until LEP200 the unique) source of W bosons, the most copious producer of B hadrons, and the best opportunity we have of discovering something beyond the Standard Model. The CDF detector has, in over 90 publications, established that in each of these areas we can make world-class measurements.

We have described above a rich and exciting program for Run II based on the present measurements. These provide a solid basis for a conservative extrapolation of our capabilities. As we gain experience we find that new techniques and ideas present themselves– there are still large factors to be gained in many areas. The study of hadron interactions is detector-limited in that the triggering and detection efficiencies still are not near unity in general – there are significant improvements to be made by clever instrumentation and experimenting.

The Tevatron is unique in its opportunities in studying the top system, exploring the electroweak interaction, making precision measurements in B physics, and in looking for the clue that will finally take us beyond the standard model. We look forward with great enthusiasm to upgrading the CDF detector to be capable of fully exploiting the Main Injector, and to the wealth of data expected in Run II.

References

[1] F. Abe *et. al.* (CDF Collaboration), Phys. Rev. D **50**, 2966 (1994); F. Abe *et. al.* (CDF Collaboration), Phys. Rev. Lett. **73**, 225 (1994).

[2] F. Abe *et. al.* (CDF Collaboration), Phys. Rev. Lett. **74**, 2626 (1995).

[3] F. Abe *et al.*(CDF), Accepted for publication in Phys. Rev., FERMILAB-PUB-95/033-E.

[4] F. Abe *et. al.* (CDF Collaboration), The CDF Upgrade, CDF note 3171.

[5] S. Abachi *et. al.* (D0 Collaboration), Phys. Rev. Lett. **74**, 2632 (1995).

[6] An ee dilepton candidate has been recorded in data collected subsequent to the 67 pb^{-1} data sample reported.

[7] F. Abe *et. al.* (CDF Collaboration), Submitted to Phys. Rev. Lett., FERMILAB–PUB–95/083–E.

[8] CDF Collaboration, *Study of $t\bar{t}$ Production in $p\bar{p}$ Collisions Using Total Transverse Energy*, CDF Note 3110, in preparation for publication.

[9] R. Hughes, B. Winer, T. Liss, *Combining the SVX, SLT, and Dilepton $t\bar{t}$ Cross Sections*, CDF Note 3111.

[10] E. Laenen, J. Smith, W.L. van Neerven, Phys. Lett. **321B**, 254 (1994).

[11] T. LeCompte, M. Roser,*Measurement of $BF(t \rightarrow Wb)$ and the CKM Matrix Element $|V_{tb}|$ in Top Decays*, CDF Note 3056.

[12] E. Laenen,D. Amidei, private communication.

[13] D. Amidei, private communication, TeV2000 Working Group Studies, CDF Note in preparation.

[14] D. Atwood, A. Kagan, T.G. Rizzo *Constraining Anomalous Top Quark Couplings at the Tevatron*, SLAC-PUB-6580, July 1994.

[15] G. Kane, C.-P. Yuan, and D. Ladinsky, Phys. Rev. D **45**, 124, (1992); D. Atwood, A. Aeppli, and A. Soni, Phys. Rev. Lett. **69**, 2754, (1992); R.S. Chivukula, S.B. Selipsky, E.H. Simmons, Phys. Rev. Lett. **69**, 575, (1992); M.Peskin, talk presented at the *Second International Workshop on Physics and Experiments at a Linear e+e- Collider*, Waikoloa, HI, April 1993; M.Peskin and P. Zerwas, talks presented at the *First International Workshop on Physics and Experiments at a Linear e+e- Collider*, Saariselka, Finland, September 1991.

[16] D. Winn, D. Amidei, *Study of the $t \to Wb$ Vertex at CDF*, CDF Note 2914.

[17] D.O.Carlson, C.-P. Yuan, Phys. Lett. **306B**, 386 (1993).

[18] T. Stelzer, S. Willenbrock, *Single-Top-Quark Production via $q\bar{q} \to t\bar{b}$*, DTP/95/40, ILL-(TH)-95-30 (1995).

[19] C. Hill, *Topcolor Assisted Technicolor*, Fermilab-Pub-94/395-T

[20] K. Lane, *Top Quarks and Flavor Physics*, BUHEP–95–2.

[21] C. T. Hill, Physics Lett. **266B**, 419 (1991).

[22] K. Lane, E. Eichten, Phys. Lett. **222B**, 274 (1989); K. Lane and M.V. Ramana, Phys. Rev. D **44**, 2678, (1991).

[23] S. L. Glashow, Nucl. Phys. **22**, 579 (1961); S. Weinberg, Phys. Rev. Lett. **19**, 1264 (1967); A. Salam, in *Elementary Particle Theory: Relativistic Groups and Analyticity*, ed. N. Svartholm (Almqvist and Wiksell, Stockholm, 1968), p. 367.

[24] F. S. Merritt, H. Montgomery, A. Sirlin and M. Swartz, DPF report on Precision Tests of Electroweak Physics, CDF Note 3154.

[25] D. Schaile, presented at 10th International Workshow on [$\bar{p}$ Interactions, Fermilab 1995.

[26] F. Abe *et al.*(CDF), Phys. Rev. **D43**, 2070 (1991).

[27] The curves are calculated using a FORTRAN program from F. Halzen and B.A. Kniehl (private communication), described in Nucl. Phys. **B353**, 567 (1990). See Ref. 4 for details.

[28] F. Abe *et al.*(CDF), Phys. Rev. Lett. **73**, 220 (1994).

[29] Particle Data Group, Phys. Rev. **D50**, p 1173 (1994).

[30] W. Badgett (CDF), proc. DPF Abaquerque (1994), FERMILAB-CONF-95/258-E.

[31] F. Abe *et al.*(CDF), Phys. Rev. **D50**, 5550 (1994).

[32] F. Abe *et al.*(CDF), Phys. Rev. Lett. **74**, 341 (1995).

[33] F. Abe *et al.*(CDF), subm. Phys. Rev., FERMILAB-PUB-94/244-E; F. Abe *et al.*(CDF), Phys. Rev. Lett. **74**, 1936 (1995).

[34] F. Abe *et al.*(CDF), Phys. Rev. Lett. **74**, 1941 (1995).

[35] F. Abe *et al.*(CDF), subm. Phys. Rev. Lett., FERMILAB-PUB-95/036-E.

[36] For Electroweak symmetry breaking beyond the standard model DPF study, H. Aihara *et al.*, FERMILAB-PUB-95/031

[37] Liqun Zhang, WW Search Update II, CDF note 3093.

[38] J. Ohnemus, Phys. Rev. **D44**, 1403 (1994).

[39] F. Abe *et al.*(CDF), Phys. Rev. Lett. **74**, 850 (1995).

[40] F. Abe *et al.*(CDF), Phys. Rev. **D49**, R1 (1994).

[41] S. Ellis, Z. Kunszt and D. Soper, Phys. Rev. **D40** 2188 (1989); U. of Oregon Preprint OITS 436 (1990).

[42] E. Eichten, G. Kane and M. Peskin, Phys. Rev. Lett. **50**, 133 (1983).

[43] P. Arnold and M.H. Reno, FERMILAB-Pub-88/168 (1988).

[44] E. Eichten and K. Lane, Phys. Lett. **222** 274 (1989).

[45] W.T. Giele and E.W.N. Glover, Moriond 95.

[46] F. Abe *et al.*(CDF), Phys. Rev. Lett. **74**, 855 (1995).

[47] S. Belforte *et al.*, *Silicon Vertex Tracker (SVT) Technical Design Report*, CDF note 3108.

[48] O. Long and J. Kroll, *A Jet Charge B-Tagging Method*, CDF note 3069.

[49] M. D. Peters *et al.*, *A Study of B-Flavor Tagging Using Soft Muons*, CDF note 3098.

[50] M. Gronau and J.L. Rosner, Phys. Rev. **D49**, (1994) 254.

[51] The CDF Collaboration, *A Time of Flight System for CDF* Proposal submitted to the FNAL PAC, 28 March 1995.

[52] F. DeJongh, *A Generator Level Study of Charged-Vertex Tagging*, CDF note 2629.

[53] A. Ali and D. London, CERN-TH.7398/94.

[54] M. Ciuchini *et. al.*, CERN-TH.7514/94.

[55] M.E. Lautenbacher, Proceedings of the 27th Int. Conf. on High Energy Physics, Glasgow, Scotland, 20-27 Jul 1994.

[56] J. Mueller and P. Wilson, *A 2 Track $B \to \pi\pi$ Trigger for Run II*, CDF note 2665; see also J.D.Lewis, J.Muller, J.Spalding and P.Wilson in "Proceedings of the Workshop on B physics at Hadron Accelerators", Snowmass, Colorado, June 21-July 2, 1993, eds. P.McBride and C.S.Mishra, p. 217.

[57] N.G. Deshpande and X.G. He, Phys. Rev. Lett. **74**, 26 (1995).

[58] F. DeJongh and P. Sphicas, *Extracting α from the CP Asymmetry in $B^0 \to \pi^+\pi^-$ Decays*, CDF note 3045.

[59] A. Spies and O. Schneider, *A Measurement of the B^+ and B^0 Lifetimes using Exclusive Decay Channels*, CDF note 2345.

[60] The CDF Collaboration, *SVXII Simulation Study and Upgrade Proposal*, CDF Note 1922, (see in particular Table 13).

[61] R. Aleksan, B.Kayser and P.Sphicas, in "Proceedings of the Workshop on B physics at Hadron Accelerators", Snowmass, Colorado, June 21-July 2, 1993, eds. P.McBride and C.S.Mishra, p. 291.

[62] E.Blucher, J.Cunningham, J.Kroll, F.Snider and P.Sphicas in "Proceedings of the Workshop on B physics at Hadron Accelerators", Snowmass, Colorado, June 21-July 2, 1993, eds. P.McBride and C.S.Mishra, p.309.

[63] A. Ali, V.M. Braun and H. Simma, Z. Phys. **C63**, 437 (1994); J.M. Soares, Phys. Rev. **D49**, 283 (1994); S. Narison, Phys. Lett. **B327** 354 (1994).

[64] E. Golowich and S. Pakvasa, UH-511-800-94; H. Y. Cheng, Academica Sinica preprint IP-ASTP-23-94; D. Atwood, B. Blok and A. Soni, SLAC-PUB-6635.

[65] For a recent review, see J. Shigemitsu, *Lattice Gauge Theory: Status Report 1994* Proceedings of the XXVII International Conference on High Energy Physics, Glasgow, Scotland (1994).

[66] D.J. Ritchie, J.E. Skarha and A. Zieminski, *Report of the Mixing Sub-Group of the δ Working Group*, Proceedings of the Workshop on B Physics at Hadron Accelerators, Snowmass, Colorado (1993); J. Skarha and A. B. Wicklund *Prospects for Measuring B_s Mixing at CDF*, Proceedings of the Workshop on B Physics at Hadron Accelerators, Snowmass, Colorado (1993).

[67] The CDF Collaboration, F. Abe *et al.*, FERMILAB-PUB-94/420-E. submitted to Phys. Rev. Lett.

[68] CDF SVX-II Upgrade Proposal, CDF Note No. 1922 (1993).

[69] J. Hagelin, Nucl. Phys. **B193** (1981) 123; M.B. Voloshin *et. al* Sov. J. Nucl. Phys. **46**, 112, (1987).

[70] T.E. Browder and S. Pakvasa, UH 511-814-95.

[71] I. Dunietz, FERMILAB-PUB-94/361-T.

[72] I. Bigi *et al.* in "B Physics", 2nd edition, S. Stone editor.

[73] R. Hans *et al.*, *Helicity Analysis of* $B^0 \to J/\psi K^\star$, CDF Note 2941.

[74] The CLEO Collaboration, CLEO CONF 94-2.

[75] F. DeJongh and M. Shapiro, *A Proposal for Observing Radiative B Decays at CDF*, CDF Note 2570.

[76] A.Ali, C.Greub, T.Mannel, *Proceedings of the ECFA Workshop on the Physics of the European B Meson Factory* (1993), 155.

[77] A.Ali, T.Mannel and T.Morozumi, Phys. Lett. **B273**, 473 (1991); B.Grinstein, M.J.Savage and M.B.Wise, Nucl. Phys. **B319**, 271 (1989); W.Jaus and D.Wyler, Phys. Rev. **D41**, 3405 (1991).

[78] A.Ali, G.Giudice and T.Mannel, *Towards a Model Independent Analysis of Rare B Decays*, Proceedings of the XXVII International Conference on High Energy Physics, Glasgow, Scotland (1994).

[79] Adam F. Falk and Matthias Neubert, Phys. Rev. **D47**, 2982 (1993).

[80] F. DeJongh, *On the Feasibility of Observing Exclusive* $b \to u$ *Semileptonic Decays at CDF*, CDF note 2543.

[81] C. Quigg, in "Proceedings of the Workshop on B physics at Hadron Accelerators", Snowmass, Colorado, June 21-July 2, 1993, eds. P.McBride and C.S.Mishra, p. 439.

[82] In all of the new particle searches discussed here, except for the dijet and b-tagged dijet searches, there are almost no events in the mass region where the limits are set. To obtain a number for the run II extrapolation, we assume this will remain the case so that the cross section limit will roughly scale inversely with luminosity. In the dijet and b tagged dijet mass searches, there are significant backgrounds in the search region so the cross section limit will scale inversely with the square root of the luminosity.

[83] R. Harris, K. Maeshima, D. Norman, Sacha Kopp, M. Gold, and Alvin Laasanen, Prospects for Exotic Physics at the Tevatron (TEV2000 Working Group Studies) CDF Note 2900. T. Kamon, et al., Prospects for SUSY at the Tevatron (TEV2000 Working Group Studies). CDF Note in preparation.

[84] For a review and original references see R. N. Mohapatra, *Unification and Supersymmetry* (Springer, New York, 1986).

[85] (CDF Collaboration) F. Abe et al., Phys. Rev. Lett. **67**, 2609 (1991).

[86] (CDF Collaboration) F. Abe et al., Fermilab-PUB-94/268-E, submitted to Phys. Rev. Lett.

[87] G. Altarelli, B.Mele and M. Ruiz-Altaba, Searching for new Heavy Vector Bosons in $p\bar{p}$ colliders, P.Ramond, Ann. Rev. Nucl. Part. Sci. 33 (1983) 31.

[88] See F. del Aguila, M. Quiros, and F. Zwirner, Nucl. Phys. **B287**, 457 (1987) and references therein.

[89] P. Frampton and S. Glashow, Phys. Lett. **B190**, 157 (1987).

[90] (UA1 Collaboration), C. Albajar et al., Phys. Lett. **B209**, 127 (1988).

[91] K. Lane and M. V. Ramana, Phys. Rev. **D44**, 2678 (1991).

[92] E. Eichten and K. Lane, Phys. Lett. **B327**, 129 (1994).

[93] J. Hewett and T. Rizzo, Phys. Rep. **C183**, 193 (1989).

[94] F. Abe et al, Phys. Rev. Lett. 74, 3538 (1995).

[95] C. Hill and S. Parke, Phys. Rev. **D49**, 4454 (1994).

[96] C. Hill and X. Zang, Fermilab-PUB-94/231-T (1994).

[97] J. Hewett and S. Pakvasa, Phys. Rev. **D37**, 3165 (1988).

[98] W. Buckmüller and D. Wyler, Phys. Lett. B *177*, 377 (1986).

[99] E. Eichten, K. Lane, and M. Peskin, Phys. Rev. Lett. **50**, 811 (1983).

[100] U. Baur, I. Hinchliffe, and D. Zeppenfeld, Int. J. Mod. Phys. **A2**, 1285 (1987); U. Baur, M. Spira and P. Zerwas, Phys. Rev. **D37**, 1188 (1988).

[101] (CDF Collaboration) F. Abe et al., Phys. Rev. Lett. **67**, 2418 (1991).

[102] (CDF Collaboration) F. Abe et al., Phys. Rev. Lett. **68**, 1462 (1992).

[103] (CDF Collaboration) F. Abe et al., Fermilab-PUB-94/198-E, submitted to Phys. Rev. Lett.

[104] (UA2 Collaboration) J. Alitti et al., Nucl. Phys. **B400**, 3 (1993).

[105] (CDF Collaboration) F. Abe et al., Phys. Rev. Lett. **72**, 3004 (1994).

[106] (CDF Collaboration) F. Abe et al., Phys. Rev. Lett. **63**, 1447 (1989).

[107] (CDF Collaboration) F. Abe et al., Phys. Rev. **D46**, 1889 (1992).

[108] CDF Collaboration, "Search for Supersymmetry at CDF," *for the 27th International Conference on High Energy Physics* (Glasgow, Scotland, July 20-27, 1994), Fermilab-CONF-94/148-E (1994).

[109] ALEPH Collaboration, Phys. Lett. B **244**, 541 (1990) and Phys. Rep. **216C**, 253 (1992); DELPHI Collaboration, Phys. Lett. B **247**, 157 (1990); L3 Collaboration, Phys. Lett. B **233**, 530 (1989) and Phys. Rep. **236**, 1 (1993); OPAL Collaboration, Phys. Lett. B **240**, 261 (1990) and Phys. Lett. **B248**, 211 (1990). For review, see G. Giacomelli and P. Giacomelli, Riv. Nuovo Cim. **16**, 1 (1993).

[110] T. Kamon, J.L. Lopez, P. McIntyre, and J.T. White, Phys. Rev. D **50**, 5676 (1994).

[111] H. Baer, C.-H. Chen, C. Kao, and X. Tata, "Supersymmetry Reach of an Upgraded Tevatron Collider," hep-ph/9504234, FSU-HEP-950301, UR-1411, UH-511-826-95 (1995).

[112] S. Mrenna, G.L. Kane, G.D. Kribs, and J.D. Wells, "Possible Signals of Constrained Minimal Supersymmetry at a High Luminosity Fermilab Tevatron Collider," hep-ph/9505245, CIT 68-1986, UM-TH-95-14 (1995).

[113] (D0 collaboration) M. Paterno, private communication.